ALMA MATER STUDIORUM · UNIVERSITY OF BOLOGNA

Ph.D. in Industrial and Information Engineering – XXVI

Department of Electrical, Electronic and Information Engineering
"Guglielmo Marconi"

Ph.D. Thesis

# Aging of nuclear power plant cables: in search of non-destructive diagnostic quantities

**Luca Verardi**

Tutor
Prof. Gian Carlo Montanari
Dr. Davide Fabiani

Ph.D. Coordinator
Prof. Domenico Casadei

Academic year 2012-2013

*La cattiveria, l'ignoranza e l'ipocrisia*
*da cui siamo circondati rendono la vita*
*difficile per chi è stato allevato in base*
*ai principi di onestà (anche intellettuale)*
*e di coerenza.*
*La mia famiglia mi ha fatto un grande*
*regalo crescendomi così, rendendomi nello*
*stesso tempo l'esistenza complessa.*

# Summary

The safety systems of nuclear power plants rely on low-voltage power, instrumentation and control cables. Inside the containment area, cables operate in harsh environments, characterized by relatively high temperature and gamma-irradiation. Several stresses can lead to insulation aging: the degradation causes polymers to become more and more brittle, thus no more useful as cable electrical insulation which requires good thermal, mechanical and electrical properties. As these cables are related to fundamental safety systems, they must be able to withstand unexpected accident conditions and, therefore, their condition assessment is of utmost importance as plants age and lifetime extensions are required.

Nowadays, the integrity and functionality of these cables are monitored mainly through insulation resistance, voltage withstand tests and mechanical properties. Among the mechanical properties, elongation at break is generally considered one of the best aging indicators, but the assessment of mechanical properties is a destructive tes,t which requires specific laboratory. Other techniques based on thermal analysis, such as oxidation induction time, thermogravimetric analysis and differential scanning calorimetry are commonly used. These techniques require small amounts of material, but they are able to assess the cable condition only locally and sometimes are not sensitive to aging.

The investigation of electrical aging markers which can provide information about the state of the cable by non-destructive testing methods would improve significantly the present diagnostic techniques. Literature regarding the effect of aging on electrical properties of low-voltage insulation is still lacking and the long-term relation between physical/chemical degradation mechanisms and electrical property variations have not been studied in detail for low-voltage cable materials. Some techniques like capacitance and dielectric loss tangent measurements, usually performed at power frequency and 0.1 Hz, are currently used. However, it is believed that the variation of cable electrical properties occurs only when the cable is already in a state of advanced and unacceptable degradation.

This work has been made within the framework of the ADVANCE (Aging Diagnostic and Prognostics of Low-Voltage I&C Cables) project, a FP7 European

program. This Ph.D. thesis aims at studying the impact of aging on cable electrical parameters, in order to understand the evolution of the electrical properties associated with cable degradation. The identification of suitable aging markers requires the comparison of the electrical property variation with the physical/chemical degradation mechanisms of polymers for different insulating materials and compositions. The feasibility of non-destructive electrical condition monitoring techniques as potential substitutes for destructive methods will be finally discussed studying the correlation between electrical and mechanical properties.

In this work, the electrical properties of cable insulators are monitored and characterized mainly by dielectric spectroscopy, polarization/depolarization current analysis and space charge distribution. These techniques have been developed mainly for high-voltage and medium-voltage cables to study their performance and aging. The assumption is that the effect of radiation and thermal stresses could be revealed independently of the voltage level applied to the insulation. Among these techniques, dielectric spectroscopy showed the most promising results; by means of dielectric spectroscopy is possible to identify the frequency range where the properties are more sensitive to aging. In particular, the imaginary part of permittivity at high frequency, which is related to oxidation, has been identified as the most suitable aging marker based on electrical quantities.

# Table of contents

# Chapter 1

# Introduction to nuclear power plant cable aging management

Low-voltage electrical cables are extensively used throughout nuclear power plants (NPPs, Fig.1.1) for power transmission, control of equipment and instrumentation, communication of signals and data. Depending on their location and application, these cables are exposed to a wide range of environmental conditions and stresses, involving temperature, radiation, humidity and bending; environmental conditions could become particularly harsh inside the containment area.

Cable function often consists in directly supporting the safe operation of the facility; therefore, unanticipated or premature cable aging could lead to unavailability of equipment important to safety or could cause plant transients and shutdowns. Since an accident at a NPP can have catastrophic consequences, it is of critical importance for the nuclear power industry that all components associated with the safe operation and shutdown of the plant perform their functions during postulated accidents, even in an aged condition.

Among the safety related cables, LOCA cables[1] need to be qualified to perform their functions both under their normal operating conditions and under a design-basis event[2] (DBE) and post-DBE conditions occurring at the end of their installed life. Furthermore, the assessment of the condition of these cables is of increasing

[1]Most reactor cooling circuits use water as their cooling fluid. One of the most severe accident scenarios involves a leak in the primary cooling circuit and is defined as Loss-Of-Coolant Accident. During a LOCA, large quantities of radioactive water at high temperature are released within the reactor containment, resulting in high pressure, radiation and temperature. Cables qualified to 1E LOCA ensure power is delivered to the equipment and instrument readings are fed back to the control room under these conditions.

[2]DBE: a postulated event used in the design to establish the acceptable performance requirements of the structures, systems, and components.

importance as plants age and lifetime extensions are now under discussion. Extending the lifetime of NPPs to 60 (possibly even 80) years is one of the most important concerns in the global nuclear industry. As electrical cables are one of the long life items that have not been considered for replacement during the design life of NPPs, typically 40 years, assessing their degradation state and predicting their remaining lifetime are very critical issues. Finally, as new reactors are being constructed and many others are planned for the near future, the initial cable choice and the use of effective condition monitoring (CM) techniques to follow cable condition indicators from the beginning, can result to be very valuable at a later time for an effective cable lifetime management.

Cable insulation and jackets are made of polymer-based compounds, whose degradation state is traditionally assessed through destructive methods, like tensile testing or thermal analysis. The prediction of long-term aging performance has been practiced for years by accelerated aging tests; however, the relationship between artificial and natural aging is still under discussion. The use of accelerated thermal aging based on the Arrhenius theory has many limitations and the effect of the dose-rate on accelerated radiation aging has been examined extensively. Accelerated testing conditions are often unrealistic, leading to a wrong evaluation of cable remaining life which could cause expensive and unnecessary replacements.

NPP cable aging has been studied for the last two decades. Researchers have faced the challenge of simulating the environmental and operational conditions of low-voltage cables located inside and outside the containment and predicting the degradation processes caused by these stressors. The challenge is even more difficult considering that each cable manufacturer uses proprietary formulations, including

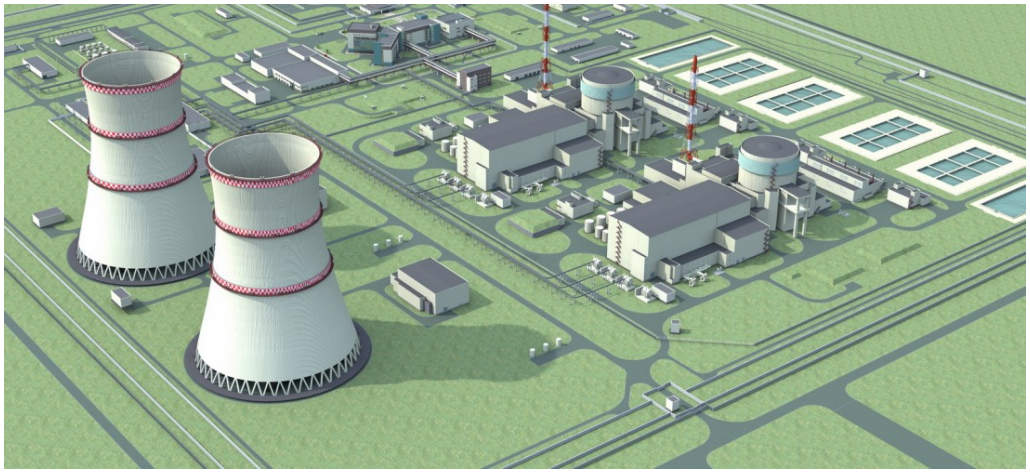

Figure 1.1. Render image of a nuclear power plant.

many additives (antioxidants, flame retardants, dyes, fillers, curing agents, plasticizers and other chemicals for thermal and radiation stability) to the base polymer. Additives strongly affect the aging characteristics of insulation or jacket compounds. Furthermore, geometry and design of the cables, as well as the fabrication procedures, can affect the overall aging characteristics. Lastly, synergistic effects due to combined radiation and thermal aging have complicated the understanding of this topic even further.

## 1.1 NPP low-voltage cables overview

Three basic types of low-voltage ($\leq$ 1 kV) cables are used for safety functions (Class 1E[3]) in nuclear power plants [1, 2]:

- power cables,
- control cables,
- instrument cables.

Designs and materials used for power and control cables overlap, but the current levels in control cable applications normally are much lower than in power cables. Power cables usually interconnect low-voltage electrical equipment, such as switchgear, motors, motor control centers and batteries. Typical control cables are used to interconnect the control components of a system, such as solenoid operated valves, relays, limit switches and control switches. They typically provide the feedback signal path for component status indication, e.g. "motor running" or "valve closed" [3]. Shielded control cables are used for protection against interference. Also instrument cables are shielded; mechanically, the presence of a shield or tape barrier between the inner conductor and jacket may prevent cracks or other physical damage in the jacket from propagating into and through the conductor insulation. Instrument cables include thermocouples and present different configuration like twisted pair, coaxial, twinaxial, triaxial and multipolar cables with conductors arranged in concentric layers.

A typical boiling water reactor (BWR) requires approximately 95 km of power cables, 80 km of control cables and 400 km of instrument cables. Almost 1600 km of cables could be installed in the containment building of a pressurized water reactor (PWR). The predominant type is a low-voltage, unshielded, multipolar cable. The

[3]Class 1E is the safety classification of the electric equipment and systems that are essential to emergency reactor shutdown, containment isolation, reactor core cooling and containment, and reactor heat removal or otherwise are essential in preventing significant release of radioactive material to the environment.

lack of a shield is a significant impediment to electrical testing of the insulation because there is not a fixed ground reference. Typically, cables are contained in raceways, usually metallic conduits or cable trays, which are not generally sealed from the environment [3]. Most of the LOCA cables (Fig.1.2) are instrumentation and control cables with average length of $100 - 150$ m.

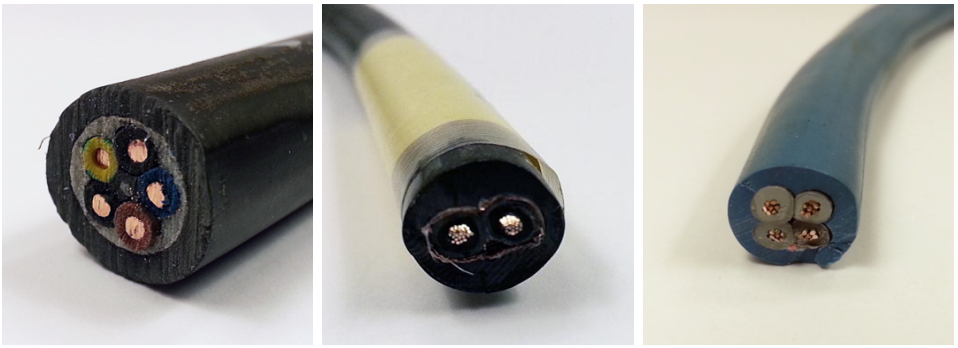

Figure 1.2. Examples of nuclear power plant LOCA cable design.

Metal conductors are usually made up of strands, to facilitate flexibility during installation. Copper, particularly annealed copper, is the most widely used conductor material. It is often coated with tin, tin-lead alloy, pure lead, nickel, or silver to minimize oxidation, enhance solderability and allow operation at higher conductor temperatures. Fillers enhance the roundness of multi-conductor cables. Jackets protect the cable from plant stressors like (see section 1.2):

- mechanical damage during installation;
- moisture and chemical contaminants during operation;
- fire, steam and chemical attacks in case of accident.

Electrical cables use organic polymers as insulation and jacket. The most commonly used insulation base materials include:

- polyethylene (PE),
- silicone rubber (SR),
- ethylene-propylene copolymer and terpolymer (EPR, EPDM),
- ethylene-vinyl acetate (EVA),

and relative blends. Jacket materials include:

- chlorosulfonated polyethylene (CSPE, also known as Hypalon),

- polychloroprene (CR, also known as Neoprene)
- polyvinylchloride (PVC),

and again, EVA-based polymer blends. In order to minimize the release of halogens in the event of fire, PVC jackets are no longer used in the design of cables for NPPs. In most cases, the polymers used in nuclear applications are crosslinked by radiation or heat (vulcanized). They are manufactured by mixing the raw polymer with selected chemicals, fillers, plasticizers, accelerators and vulcanizing agents to enhance their electrical and physical properties [3, 4].

Flame retardants are the most abundant additives and can contribute to more than 50% of the material weight. Due to their hygroscopic nature, they may significantly affect electrical properties, especially if reactions involving flame retardant materials are activated by radiation. Flame retardant wire and cable materials are divided into non-halogen and halogen-containing flame retardants. In general:

- inorganic flame retardants include metal hydroxides, like aluminum hydroxide (usually indicated as ATH) and magnesium hydroxide. Other compounds like zinc borate are sometimes involved;
- phosphorus based flame retardants comprises mainly organic and inorganic phosphorus compounds with different oxidation states;
- nitrogen-based flame retardants are typically melamine and melamine derivatives used in combination with phosphorus-based flame retardants.

Brominated flame retardants are represented by a wide range of brominated components added to materials to inhibit their ignition and to slow their rate of combustion. The fillers are usually $Al(OH)_3$ or $Mg(OH)_2$ with high specific surface area; they efficiently contribute in heat and radiation energy dissipation, thus reducing their effect on plastics.

Antioxidants are compounds that can act at different stages of the oxidation process. Combination of two types of antioxidants, playing the role of radical trap and hydroperoxide decomposer, is commonly used to inhibit the oxidative process at more than one step. Hindered amines and phenols are examples of alkoxy and peroxy radical trap antioxidants. During aging, antioxidants are "consumed" and no longer protect the polymer. Combinations of phenolic antioxidants with phosphites and thiosynergists (are often used. The phosphite antioxidant reacting with hydroperoxide becomes oxidized to phosphate while the peroxide is reduced to alcohol or other harmless functional group. In addition, peroxide decomposing antioxidants are thought to be capable of reacting with the consumed phenolic antioxidant to regenerate its protective action. This explains how a combination of two antioxidants can improve antioxidant effectiveness and provide longer service lifetimes.

Lubricants are composed by metal stearates, fatty acids, acid esters or alcohols, esters, paraffin waxes, amides or a combination of these components. They are added to reduce the shear rate during the manufacturing process, particularly if inorganic fillers are present.

Plasticizers are added to improve flexibility and softness of wires and cables. They are chemically and thermally stable; their addition also enhances the material stability and reduces the degradation of the host polymer.

The color of wires and cables is given by organic or inorganic pigments; dyes are available in the form of powder, liquid as well as concentrate resins. Usually, a mixture of several dyes is required, comprising titanium dioxide or iron oxide.

In addition to the above specified components, other additives are also used, like stabilizers, initiators, curing agents, etc; thus, the chemical composition of insulation and jacket comprises a lot of constituents of various nature and concentrations. Cable manufacturers might choose the most suitable compounds from many products, taking into consideration their character, compatibility, stability and last but not least, their cost. The composition of insulation and sheath materials usually remains trade secret and is undisclosed by cable manufacturers.

Among all the sub-components of low-voltage cables used inside the containment at NPPs, insulation and jacket materials exhibit the most significant degradation. Indeed, insulation and jacket materials are directly vulnerable to thermal and radiation aging and to self-heating. In addition, they could be exposed to accident conditions (e.g. radiation, steam, temperature, pressure, moisture, chemical spray and submergence).

## 1.2 Stressors

As previously mentioned, nuclear power plant LOCA cables are exposed to a wide range of environmental conditions and stresses, depending on their location and application. Environmental stresses are particularly harsh inside the containment area, where LOCA cables operate. The main stresses causing age-related degradation of polymer-based cable materials are [5, 6]:

- temperature (ambient room temperature, localized high temperature or radiant heat, i.e. hot spots, ohmic heating for power cables);
- radiation dose rate and total dose (low dose rate gamma-irradiation during normal operations, high dose rate gamma and beta radiation during accidents);
- oxygen;
- moisture;

- mechanical stress or manipulation;
- ozone;
- contaminating chemicals;

Among these, the dominant stresses are temperature, radiation and the presence of oxygen for the majority of reactor systems; for BWR systems moisture may also be significant. Generally, material aging leads to embrittlement, increasing the probability of cracking under mechanical stresses. In practice, this loss of mechanical integrity is the prime cause of failure of low-voltage cables, resulting in the loss of electrical integrity.

Thermal aging results from the exposure of cable materials to normal and abnormal thermal environments [6]. The normal ambient room temperature in most plant areas results in very slow degradation of cable insulation and jacket materials. However, localized elevated temperature or radiant heat from sources such as adjacent process lines, or inadequate ventilation (dead air spaces), can produce severe damage relatively rapidly. Generally, the damage is limited to one portion of the cable. Elevated temperatures resulting from thermal stratification in the ambient air volume can age large sections of cable that are located at higher elevations within an enclosed space. Aging of insulation can also result from ohmic losses of cable conductors, especially when the combination of ambient temperature and ohmic heating is not properly considered for the application. Furthermore, cables are sometimes sprayed with flame retardant solutions, which can prevent cables from dissipating internal heat, thus resulting in higher service temperatures. Plant areas that are known to have high localized temperatures include:

- main steam isolation valves (MSIVs),
- pressurizer compartments,
- main steam pipe tunnels,
- compartments under turbines in BWRs,
- electrical cabinets,
- high-power, incandescent lighting fixtures.

The absorbed dose of the ionizing radiation is practically the measure of the energy transmitted by the radiation field to the material. Its SI unit is the gray (1 Gy = 1 J/kg), while the older unit is the rad (1 Gy = 100 rad). To study the kinetics of degradation of polymer materials under ionizing radiation, it is necessary to make

reference to the absorbed dose rate which is the variation of the absorbed dose with respect to the time, $DR = dD/dt$. Dose rate SI unit is the gray per second.

The radiation tolerance of an individual material will vary depending on the general type of material and its chemical structure and formulation. Organic materials commonly used in nuclear plant cable applications vary widely in their radiation resistance. Changes in the material mechanical properties (such as elongation-at-break, tensile strength, and hardness) and electrical properties (such as dielectric strength and conductivity) can result from exposure to radiation. Cable materials exposed to a total gamma dose of less than approximately $10^3$ Gy will experience little or no aging effect caused by radiation exposure. The most commonly used cable materials tend to harden with irradiation except for butyl rubber, which softens [6].

The dose rate distribution in the NPP should be known, in order to identify the places within the plant characterized by higher dose rates. Radiation zone maps are established when a plant is constructed, but for older plants they are not always available. Furthermore, certain areas might have become more radioactive since the map was established, making more difficult the evaluation of the total dose absorbed by cable materials. Updated radiological maps and the ongoing experience can help to determine if there are areas containing cables where normal radiation levels will exceed $10^3$ Gy during the design life of the plant.

The manipulation of cables can also result in cracking and, possibly, the exposure of bare conductors in cables that have embrittled insulation or jacket from severe thermal and/or radiation aging. Cable bending also should be taken into account. As the cable is bent, the outer edge is subject to tensile stresses, dependent on the diameter of the cable, whereas the inner section is under compressive stress. If the bend is of a sufficiently small radius, the elongation capability of the aged material can be exceeded and cracks can be initiated. The jacket can age more rapidly than the underlying insulation, thereby more readily breaking under sufficient bending stress [5, 6, 7, 8].

Ozone chemical-attack significantly affects only polymers containing high proportions of double bonds in the molecular chain. Of the polymers commonly used in cables, only some of the EPR materials which are diene-containing terpolymers (i.e., EPDM) are likely to show such effects. Moisture is another potential stressor that has not been adequately studied in its effects on degradation of low-voltage NPP cables. High humidity and the design of cable trunking and conduits will often expose cables to excessive moisture. Its presence within the cable insulation can have a significant effect on the electrical properties of the cables, but little is known of its effects on changes in the mechanical properties [5].

It should be emphasized that real service conditions usually involve synergistic effects between two or more of the listed stressors. In particular, dose rate effects can be a major factor in the degradation of cables in plants. In many polymers the

dose required to reach a specific level of degradation (Dose to Equivalent Damage, DED) is significantly lower when irradiation is carried out at low dose rates (e.g. at 1 Gy/h) [5].

The thermal rating (i.e. the maximum continuous temperature that the wire can withstand during its lifetime) of the insulation is typically 90°C. Common service conditions [3] are bounded by 35°C-65°C ambient temperature, and total integrated doses of $20 - 1000$ kGy. In certain high elevations in the drywell of a BWR, and close to the pressurizer electric heaters in a PWR, components such as continuously energized solenoids experience both radiation and high temperatures (2000 kGy and 75°C-100°C). Stress factors are usually continuous in time, but may vary in intensity depending on external events (e.g. climatic changes, plant events or hazards). For many of the polymers of interest in cables, oxidation is the main degradation mechanism (see section 1.4). The initiation of this phenomenon can either be temperature or radiation but the combination of both is synergistic [8].

## 1.3 Cable qualification

The first part of the qualification process is the development of a detailed qualification plan, which contains the chosen condition indicators and acceptance criteria, and describes the limiting service environment, the chosen target service life as well as the methodology used.

The acceptance criteria [9] are usually the limiting values of properties beyond which the degree of deterioration is considered to reduce the ability of the cable to withstand stresses encountered in normal service, and during and following accidents. During qualification, a number of functional properties are tested. The extent of the measured properties and their acceptance criteria may vary and are generally based on the specific cable application at the NPP. The most frequently tested parameters are insulation resistance (IR), voltage withstand tests and mechanical properties. Other properties (e.g. capacitance, attenuation and/or signal propagation) can also be measured. Some recommended functional properties, which are typically measured during cable qualification, and their acceptance values are described in Fig.1.3 [10].

Mechanical properties (such as elongation at break or a mandrel bend test) are very important parameters. They have no direct influence on the functionality of the cable but demonstrate the retention of a degree of flexibility and ability to withstand mechanical stress and vibration during normal operation, as well as during postulated accidents. A typical recommended threshold value of elongation at break (EaB) after pre-aging is not less than 50% absolute. However, for some cables, a lower value than 50% absolute may be appropriate. Concerning the electrical properties, voltage withstand tests are performed on a cable coiled around a mandrel

| Technique | Cable type | Acceptance criterion | | |
|---|---|---|---|---|
| | | New cable | After pre-ageing | During and after DBA |
| Elongation at break | All types | Should meet cable technical specification | >50% absolute | Not measured |
| Mandrel bend test | All types | No insulator cracks | No insulator cracks | No insulator cracks |
| Voltage withstand test | All types | Pass the test | Pass the test | Pass the test |
| Insulation resistance/volume resistivity | All types | Should meet cable technical specification or should meet the values given in the respective design. Volume resistivity $\geq 10^8$ Ωm | Should meet the value in technical specification decreased by one order or should meet the values given in the respective design. Volume resistivity $\geq 10^8$ Ωm | Should meet the value in technical specification decreased by four orders; the functionality must be maintained or should meet the values given in the respective design. Volume resistivity $\geq 10^8$ Ωm |
| Capacitance | Communication coaxial | No changes relative to the technical specification | No changes relative to the technical specification | No changes relative to the technical specification |
| Attenuation | Coaxial | No changes relative to the technical specification | No changes relative to the technical specification | No changes relative to the technical specification |
| Characteristic impedance | | | | |
| Noise rejection | | | | |
| Signal propagation | | | | |
| Other | | Depend on the specific cable application (e.g. no fluid or steam inside the cable under the DBA test) | | |

Figure 1.3. List of the most commonly used acceptance criteria [10].

that has a diameter between 9 and 40 times the diameter of the cable (dependent on the standard applied). The insulation resistance of a cable needs to be sufficiently high to exclude the possibility of activation of the current protection systems at the NPP for the specific installation.

Qualification may be accomplished in several ways, like type testing, operating experience and analysis. These may be used individually or in any combination depending upon the particular situation [3, 10, 11]:

- in a type test, cable samples are exposed to test conditions in order to simulate degradation during the qualified life period and design-basis events. Based on acceptance criteria, it is verified whether the cable is capable of performing expected safety function at the time of a DBE, even after their in-service period. As a type test, a cable environmental qualification (EQ) test is generally performed.

- Operating experience on cables that were actually capable of performing their expected safety functions under specific operating conditions is available for environmental qualification. In general, the operating experience on cables

consists of data obtained during normal operation. Therefore, when applying environmental qualification by operating experience, a DBE test taking must be performed using a test cable.

- Environmental qualification by analysis uses a theoretical approach based on physical principles, such as the physical properties of cable insulation. Environmental qualification only by analysis is not acceptable, but must be conducted in combination with type test data or operating experience.

The preferred method of qualification is type testing, which is described in various standards, national requirements or recommendations [1, 2, 3, 10, 11, 12]. The IEEE Std. 323 for qualifying Class 1E equipment for nuclear power generating stations [13, 14, 15] describes basic requirements for the qualification of safety-related electrical equipment. This standard describes principles, methods and procedures used for qualifying equipment and maintaining, extending as well as updating qualification. The standard provides references related to equipment qualification, but does not provide environmental stress level and performance requirements, such as radiation levels or LOCA parameters.

The IEEE Std. 383 for qualifying Class 1E electric cables and field splices for nuclear power generating stations provides general requirements, directions and methods for qualifying Class 1E electrical cables, field splices and factory splices in NPPs. It addresses power, control and instrumentation cables, including those used for communication and signals. The purpose of this standard is to provide specific directions for the implementation of IEEE Std. 323. The IEEE Std. 383 requires that safety-related cables and splices meet or exceed specified performance requirements throughout their installed life, and be subjected to a quality assurance program which includes design, qualification and production quality control [16, 17]. The standard specifies methods of qualification applicable to various types of NPP. The equipment shall be subjected to the significant type of radiation equivalent to or greater than that expected in service, therefore, parameters like radiation levels and LOCA profile depend on plant and reactor type.

Initial qualification of Class 1E cables includes in-laboratory accelerated aging by means of high temperature. The Arrhenius model gives a law to extrapolate expected lifetime at lower temperature. A minimum of three data points, at least 10°C apart, shall be used. As a rough approximation, the degradation rate will increase by approximately 2 times for a 10°C rise in temperature, considering the values of activation energy typically found for cable materials. Oven conditions can vary within the chamber by $5 - 7$°C. The corresponding error in the reaction rate would be almost 100%. Furthermore, since the Arrhenius equation presents the pseudo-first-order reactions to simplify the calculations and most thermal aging of polymers can be second-order, the presence of oxygen at a constant concentration in the oven chamber may dominate other reactants to exhibit a single degradation

mechanism. A high rate of ventilation is therefore suggested to avoid stagnation within the oven chamber and the consequent variations in temperature [3]. For non LOCA cables, lifetime evaluation stops after thermal aging. For LOCA cables, the initial qualification includes also radiation aging, LOCA and post-LOCA simulation tests. The accelerated aging procedures before LOCA-simulation tests are also called "pre-aging", as reported in Fig.1.3.

Only a few test laboratories are able to carry out simultaneous radiation and thermal aging for cable qualification accelerated tests. Therefore, in many cases, such tests are carried out by using sequential aging, either thermal followed by radiation, or vice versa. The sequence of aging that gives the worst degradation to the cable insulation should be chosen. Indeed, the sequence of thermal prior to radiation exposure, as stated by IEEE Std. 383, is not essential and may therefore be reversed, as may be desired by the qualifying agency for purposes of addressing potential synergistic effects or, absent these, ease of completing the aging process. In many cases, radiation aging first is more severe for polymeric materials [10].

The present status regarding application of acceleration factors varies from country to country. As an example, the dose rate used for accelerated testing varies from 500 Gy/h to 10 kGy/h and the total dose applied, including accident dose, varies from 250 kGy to 2 MGy. The high temperatures and dose rates used for initial qualification are likely to give unreliable results. The use of high acceleration factors and sequential aging can introduce considerable uncertainties in determining what is an appropriate test sequence for each type of cable material. The activation energy of degradation can change over the temperature frame and over the composition of the insulating material; the Arrhenius model (see section 1.5) cannot be applied across a physical transition of the material or even if the degradation mechanism changes, involving different reactions, additives migration or diffusion. Finally, qualification procedures take into account radiation and thermal degradation of cable materials but do not take into account other degradation mechanisms, like the effect of moisture on cable materials filled with hygroscopic compounds which become more susceptible to the effects of long term exposure to high humidity [5, 10].

Condition-based qualification (CBQ) is an improved method of environmental qualification that provides improved confidence in equipment performance, since it requires CM techniques to be utilized following each step in the qualification process, e.g., at intervals during the accelerated aging used to simulate operating conditions. CM activities measure and record the level of cable degradation to keep track of the rate of degradation of the cable being tested. At the end of the accelerated aging, another measurement is performed. If the samples pass the DBA test, this last point with additional margin determines the Qualified Level of Degradation (QLD) against which aging is managed. This will be the value with which future CM measurements on installed cable are compared to confirm whether the condition of the equipment remains within qualification limits [10].

In some plants, cable deposits were installed during the installation of new cables. The deposit cables are often used in a program for periodically monitoring the condition of the installed cables and revising the qualified life. Samples are taken out from the deposit at predetermined intervals and subjected to accelerated laboratory aging and DBE testing. If this testing shows that the cables still retain their required dielectric and other characteristics in DBE after the accelerated aging, a revised qualified life is established for the installed cables. The procedure may then be repeated well before the end of the revised qualified life, for a further extension. Activities performed after the initial environmental qualification which aim at extending qualification for an additional period of time are commonly referred to as "ongoing qualification". Instead of deposit cables, installed cables that are removed and replaced with cables from the storage may be used for testing [2, 5, 10].

The aging of cables in such programs is dependent on the source of sample and can be in-situ or at the laboratory. A "pace cable", is a cable specimen placed in a very severe natural environment where its aging occurs quickly enough to permit early, but more reliable, life estimates. It may even be possible to find a location (pace site) where the ambient temperature is also similar to the design temperature (generally of the order of 50−60°C). Experience has shown that the loop line between the reactor pressure vessel and the steam generator is suitable for this purpose in pressurized water reactors and the reactor water cleanup system is suitable in boiling water reactors. In PWRs, the dose rate at this position is 1.3 to 1.5 times higher than the values prevailing at the most exposed cable positions. The design of the deposit can be easily adapted to the local conditions in the power plant. The methodology is mainly suitable for new power plants or for new cable installations in older power plants. It can also be applied to older plants, provided that installed cables can be removed for testing and replaced by identical, unaged ones. Ongoing qualification needs not affect plant operation since samples are required for testing at relatively long time intervals which can be scheduled into normal maintenance periods. The timing should be such that the qualified life of the cables being tested covers the next planned maintenance so that any cable which fails the extended test can be replaced within its qualified life [18].

## 1.4 Degradation Mechanisms

Material aging is the irreversible change of at least one of the properties of a material submitted to its environment during its operational life. It has to be distinguished from the transient change due to a temporary external stress. Aging always results from a change in the physico-chemical structure. The degradation of the polymer chains is the most important aging mechanism because it has a direct influence on the service performance of the material.

Polymer degradation is the result of two main causes. The first is chemical degradation due to changes in the chemical structure of the polymer sample. The second cause of degradation is associated with physical changes in the polymer, e.g. changes in composition due to the diffusion of low-molecular-weight components, such as plasticizer or water, out of the amorphous regions [4, 10, 19, 20]. The main chemical aging mechanisms are:

- scission of macromolecular chains, when two shorter chains are created by the breaking up of one. It is usually a scission of alkoxy or peroxide radicals. The effect is usually a mechanical weakening of the polymer.
- Cross-linking reactions, which corresponds to the formation of a covalent link of two adjacent macromolecules. The increment of crosslink density forms a three dimensional network. With the increase of the density of those bonds, material stiffness usually increases too. Prolonged cross-linking causes embrittlement.
- Oxidation, which is the main cause of degradation in the ambient atmosphere, and is accelerated by increased temperatures and by ionizing radiation. Without radiation or other means of producing free radicals, the rate of oxidation at ambient temperature is small.

The chemical reactions of oxidation (Fig.1.4) occurring in polyolefin polymers, due both thermal and radiation aging, are [21]:

$$\text{Polymer (RH)} \rightarrow R\bullet \text{ (polymer radical)} + H\bullet \text{ (proton)} \tag{1.1}$$

$$R\bullet + O_2 \rightarrow R-O-O\bullet \text{ (peroxy radical)} \tag{1.2}$$

$$R-O-O\bullet + RH \rightarrow R-O-OH \text{ (hydro-peroxide)} + R\bullet \tag{1.3}$$

$$R-O-OH \rightarrow RO\bullet + \bullet OH \text{ (thermal decomposition)} \tag{1.4}$$

$$RO\bullet \rightarrow \text{Chain Scission (carbonyl, alcohol)} \tag{1.5}$$

$$R-O-O\bullet\,(RO\bullet) + AX \text{ (antioxidant)} \rightarrow R-O-OX(R-OX) + AY \tag{1.6}$$

The initiation step is the radical formation on polymer chain (1.1) by thermal or radiation energy. The radical (1.2) reacts with oxygen to form peroxy radical, which abstracts hydrogen from the neighbor polymer (1.3) to form the same radical of (1.1) on polymer and hydro-peroxide. Hydro-peroxide decomposes (1.4) to poly-oxy radical and hydro-oxy radical: poly-oxy radical decomposes (1.5) to chain scission and oxidation products (carbonyl groups, alcohols). The antioxidant (1.6) reacts with radicals to terminate the oxidation reactions. The combination of (1.2) and (1.3) produces the cycle reaction, i.e. the chain reaction of oxidation until the radicals are recombined. Antioxidant stops the chain reaction by the quench of free radicals.

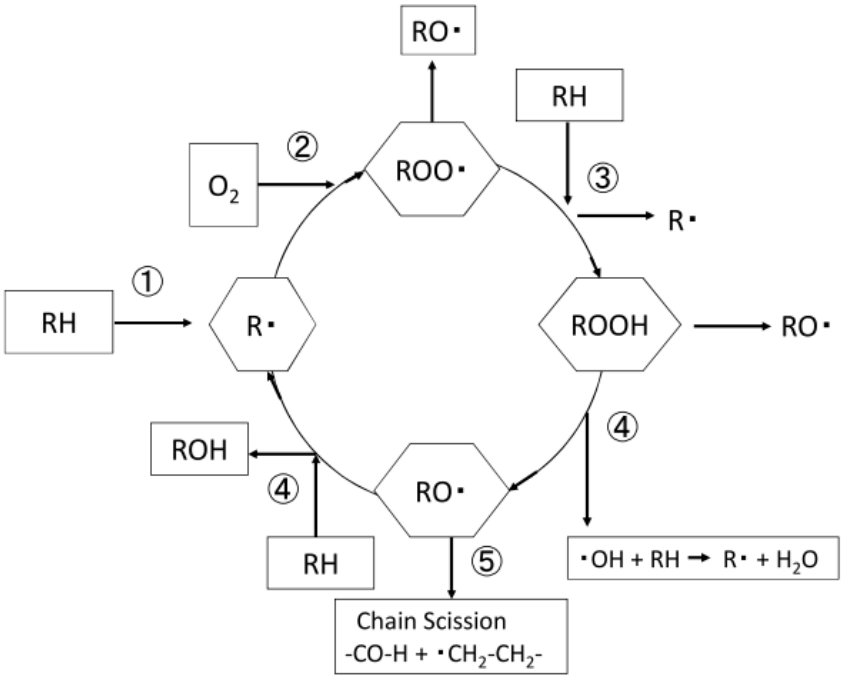


Figure 1.4. Chemical reactions involved in polymer oxidation [21].

The radio-oxidation reactions include both chain scission and cross-linking, depending on the detailed kinetics of the individual steps in the oxidation chain reaction. These kinetics are strongly dependent on the type of radiation and additives present in the polymeric compound and will therefore vary with the detailed formulation of the material.

The use of antioxidants is widely common in cable manufacturing. It has been proved that antioxidants provide significant radiation stability. It has also been shown that antioxidants which are effective for thermal stability are effective for radiation stability as well. The protection of antioxidant is not linear, even if the stabilization against radiation aging increases at large doses, as the amount of antioxidant is increased. Studies have shown that a minimum concentration of antioxidant is required to have a significant protection of the material. On the other hand, an excess content of antioxidant does not contribute to reducing more the degradation rate. If the aging temperature is higher than a specific threshold, the antioxidant can evaporate from the polymer matrix resulting in decrease of its concentration and accelerated degradation [4, 21, 22].

The effects of scission and cross-linking combined with oxidation vary according to several factors, and are not easily predicted. Chain scission without oxidation results in a net decrease in polymer molecular weight and is evidenced by reduced

tensile strength, hardness and Young's modulus (increased elasticity). Crosslinking without oxidation usually results in increased tensile strength, hardness and Young's modulus. Oxidation generally reduces the molecular weight of the polymers and introduces oxygen containing functional groups. It is often characterized by brittleness and cracking. Some results also indicated that polymers with higher initial crosslinking density present less oxidative degradation induced by irradiation [3].

### 1.4.1 Dose Rate Effects

The radiation response of polymeric materials depends on both the total dose and the dose rate. For a given polymer, dose rate effects will differ based on macromolecular structure, formulation, and environmental conditions. Dose rate effects have an impact through both physical and chemical mechanisms. Physical dose rate effects result from oxygen diffusion into the irradiated polymer. Atmospheric oxygen penetrates the molecular structure and interacts with the radicals created when the polymer molecules are excited by the ionizing radiation. Chemical dose rate effects result from time dependent oxidation reactions.

For irradiation in vacuum or inert gas environments, it is usually assumed that there is no dose rate effect. However, if the rate of energy absorption is greater than the rate of dissipation, this will no more be true because there will be a significant heating of the material. This temperature increment will accelerate the chemical reactions but also modify the mobility of the polymer chains and thus increase the physical mechanisms like diffusion (especially near the glass transition temperature).

For certain materials, if the irradiation takes place in air or oxygen environment, the degradation is more severe at lower dose rate. At very low dose rates, there is apparently a region where, for some polymers, the dose rate effect does not exist. On the other hand, at very high dose rates, irradiation in air or in the absence of oxygen gives similar results, since within the short time of irradiation, oxygen cannot diffuse inside the polymer. In the transition region between these two limits, irradiation causes either the formation of peroxy radicals or diffusion-limited oxidation, which may give rise to dose-rate effects. The dose rate dependency of the degradation for radiation aging was derived in principle from chain reactions (1.2) and (1.3). The other dose rate effects are caused by the oxygen diffusion rate into polymer materials during irradiation at relatively high dose rate [21].

Figure 1.5 offers a convenient schematic format for discussing aging effects under combined radiation and thermal conditions [19]. The dose to equivalent damage (DED) for some specified degradation property is plotted against the dose rate at a constant temperature, $T_1$, for both inert and air aging conditions. The DED might represent, for example, the dose required to decrease the elongation at break to the 50% absolute. The present figure schematically represents a material where

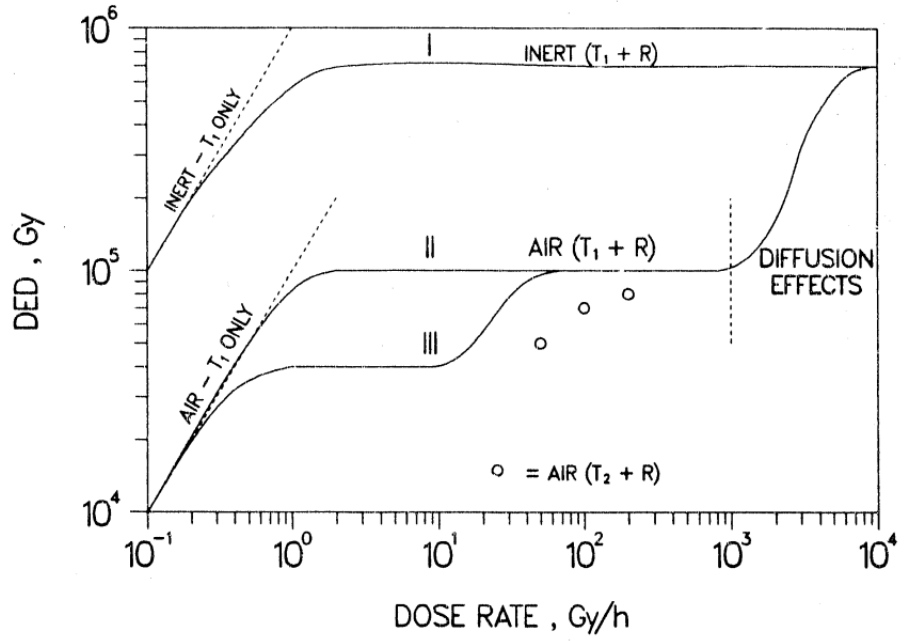


Figure 1.5. Different types of dose-rate effects which can occur in radiation-aged polymeric materials [19].

degradation occurs slower in inert environments than in air, a common but not universal situation. For dose-rate regions where neither chemical nor physical dose-rate effects occur for a given material, the DED would be independent of dose rate and therefore be expressed as a horizontal line.

In air environments, diffusion-limited oxidation will become important above a certain dose rate. For many materials, the resulting reduction in oxidation at the higher dose rates leads to reductions in the degradation rate. In such cases the DED will increase with increasing dose rate, as indicated by the upward curvature of curve `II` toward the right hand side of the figure. Eventually, at high enough dose rates, oxidation will be confined to a small region near the sample surface. This small amount of oxidation can often be insignificant compared to the bulk of the sample, whose degradation occurs without oxygen contribution; therefore, the DED will then approach curve `I`, as indicated. The dividing line between homogeneous oxidation and heterogeneous diffusion-limited oxidation, which is indicated schematically in Fig.1.5, can be estimated using theoretical expressions or by profiling experiments directly on the aged samples [23, 24, 25].

Deviations from the horizontal behavior shown for lines `I` and `II` must also occur on the low-dose-rate side of Fig.1.5 because the dose rates eventually become small enough such that thermal aging effects alone will dominate the deterioration. In this low dose-rate limit, the time for a certain amount of degradation will be a

constant determined only by the time required for thermal degradation at $T_1$, i.e. the applied temperature. In terms of the log-log plot used in Fig.1.5, the constant time condition is represented by a straight line (isochrone) with slope equal to unity. Similar arguments hold for the inert aging case (line `I`) at low dose rates.

Considering the interaction between thermal and radiation degradation, the drop-off at low dose rates represents a true chemical dose-rate effect. For air environments, there are other types of chemical dose-rate effects. These will occur whenever an important rate-limiting step in the oxidation chemistry occurs on a timescale similar to the experimental timescale. The result will be a third class of dose-rate effects (i.e., regions of non-horizontal behavior), yielding situations represented schematically by the intermediate drop-off region of curve `III`. This kind of situation can be given for example by the slow reactions of long lived radicals, such as those trapped in the crystalline regions of partially crystalline polymers.

In general, raising the exposure temperature at a given dose rate will accelerate the degradation. Hypothetical data of samples aged at $T_2 (> T_1)$ with dose rates equal to 50, 100 and 200 Gy/h are plotted as the three circles in Fig.1.5. Clearly, the asymptotic isocrone at $T_2$ will be shifted to the right by the thermo-oxidative acceleration factor which depends on the difference between the two aging temperatures.

As already mentioned, temperature and radiation have synergistic effects. Depending on the conditions, there will be a predominant degradation process which will predict the behavior of the material. A predominance chart showing the dominant process in function of the dose rate and the temperature can be used [26]:

- Zone I: Thermo-oxidation controlled by oxygen diffusion
- Zone II: Thermo-oxidation non-controlled by oxygen diffusion
- Zone III: Radio-oxidation non-controlled by oxygen diffusion
- Zone IV: Radio-oxidation controlled by oxygen diffusion
- Curve B: Limit between thermo-oxidation and radio-oxidation
- Curve C: Limit between oxygen controlled and non-controlled radio-oxidation

Using the chart of Fig.1.6, a critical limit value can be predicted for the irradiation dose rate after which the oxidation of the polymer is no more homogeneous due to oxygen diffusion. When the temperature-dose rate combination is located in zone I or IV, it simply means that the oxidation is not homogeneous within the material.

Concerning the oxygen diffusion, this effect is controlled by the permeation coefficient of the polymer and the material thickness. Oxygen diffusion can become rate determinant if the oxygen present in the material bulk is consumed by reaction with

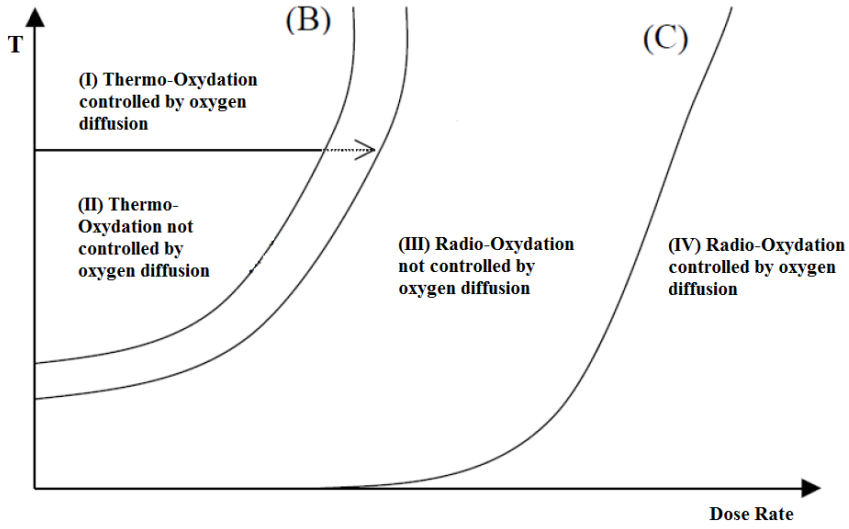


Figure 1.6. Predominance diagram for the mechanisms of degradation during radiation and thermal ageing in radiation environment [26].

free radicals (generated by the irradiation) faster than the oxygen that is replaced by diffusion from the atmosphere. If this effect is important, the degradation of the material becomes heterogeneous: high oxidation takes place at the surface of the cable and less oxidation (or no oxidation) occurs in the bulk. At lower irradiation rates, the oxygen has more time to diffuse through the material and the oxidized zone is deeper. This phenomenon is the major explanation of the dose rate sensitivity of polymers showing larger damage for a given absorbed dose if the irradiation rate is low [27, 28].

An estimate of the sample thickness $L$ at which diffusion limited oxidation is insignificant can be made using the relation [19]:

$$L \propto \frac{pP_{ox}}{\phi} \tag{1.7}$$

where $p$ is the partial pressure of oxygen surrounding the sample, $P_{ox}$ is the oxygen permeation rate and $\phi$ is the oxygen consumption rate in the material. The consumption rate and the permeability will also be functions of temperature and/or radiation dose rate. The solution of this equation for a given material of thickness $L$ provides the determination of line C (Fig.1.6). Line B separates zone (II) and (III), where oxidation reactions are promoted by thermal degradation and irradiation, respectively.

## 1.5 Modeling

The goal of extrapolated predictions is to take accelerated radiation-aging data at various dose rates and temperatures and use these data to generate predictions at the operating temperature, under much lower dose rate conditions. This will first entail the separation between heterogeneously and homogeneously-oxidized samples, in order to apply the appropriate model.

Several methods are used for the prediction of thermal and radiation aging behavior of polymeric materials through accelerated laboratory testing. As already mentioned in section 1.3, the most commonly used method for accelerated thermal aging is the application of the Arrhenius equation, which describes the relationship between rate of degradation, aging temperature and duration of exposure. According to this model, the logarithm of the lifetime is a linear function of the inverse absolute temperature; the slope corresponds to the activation energy $E_a$ for the oxidation reaction:

$$Life\ time = Ae^{\frac{E_a}{kT}}, \tag{1.8}$$

where $k$ is the Boltzmann constant and $A$ is called pre-exponential factor.

Laboratory aging aims at reproducing the type of degradation observed in operation. Conditions of testing therefore need to be carefully chosen to ensure that the degradation mechanisms occurring in the accelerated tests are similar to those which occur in service. In particular, the effect of oxygen on the degradation process must be taken into account. The Arrhenius equation also cannot be applied across

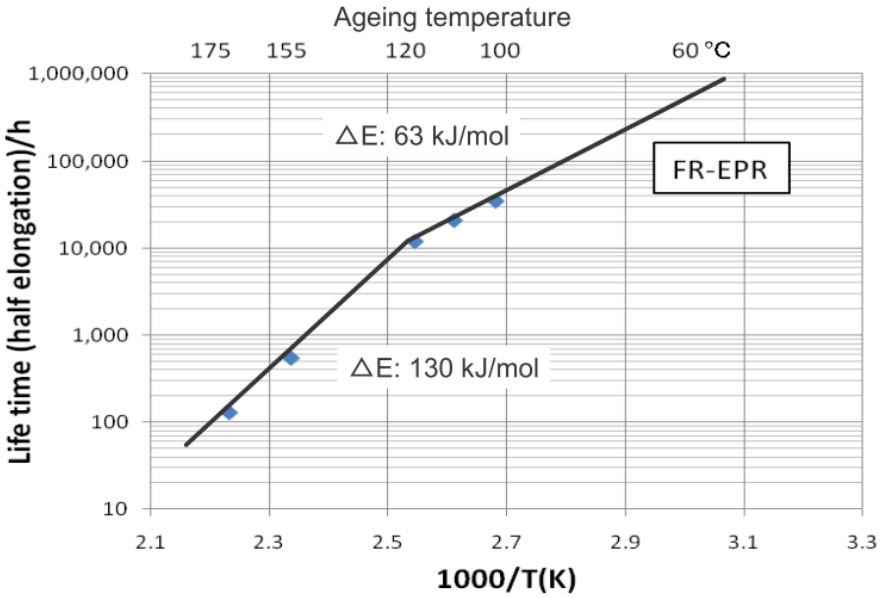


Figure 1.7. Arrhenius plot for a semicrystalline cable material [10, 11]

a physical transition of the material (Fig.1.7). For example, in semi-crystalline materials such as XLPE, there is a crystalline melting point in the temperature range $90 - 120°C$. In service conditions, such materials would normally be used at a temperature below this melting point. However, accelerated aging is often carried out at temperatures above 120°C where the material would be amorphous rather than semi-crystalline, and the use of such activation energies will lead to the wrong estimation of real service life. Differential Scanning Calorimetry (DSC) can be used to assess suitable temperature regimes for accelerated testing [10, 11, 29].

Turning to aging by radiation, four basic methods of predicting the radiation aging behavior of cable materials have been developed in the last two decades, based on laboratory aging test [5, 10]. These are:

- the power law extrapolation method (Fig.1.8);
- the superposition of time dependent data;
- the superposition of dose to equivalent damage (DED) data (Fig.1.10);
- the kinetic model.

All these methods use elongation at break as a function of aging time under accelerated test conditions. In each of the methods, it is emphasized that care must be taken to ensure homogeneous oxidation conditions when assessing the results. The methods differ mainly in the amount of data required for predicting the behavior of cable materials and in the way the test data are extrapolated to the service conditions.

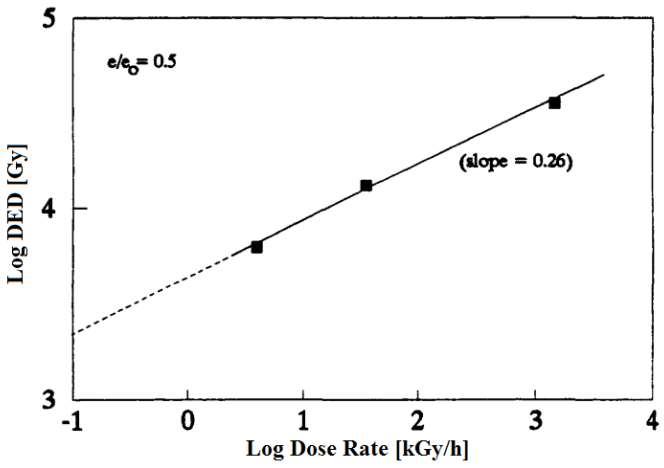


Figure 1.8. Power law extrapolation method [5].

The power law extrapolation method utilizes data obtained at a single temperature over several dose rates. The DED values are assessed at each of the test conditions and reported as a function of the dose rate in a log-log plot. Typical DED values for evaluation could be $EaB/EaB_0 = 0.5$ or $EaB = 50\%$ absolute. This plot is linear in a number of polymers, particularly polyolefins, allowing the extrapolation of the DED to lower dose rates. The power law extrapolation method can only be safely used for those service conditions where thermal degradation is insignificant compared with radiation-induced degradation. The method has been demonstrated so far to work satisfactorily on some polyolefins, but it may have wider applications [5, 30].

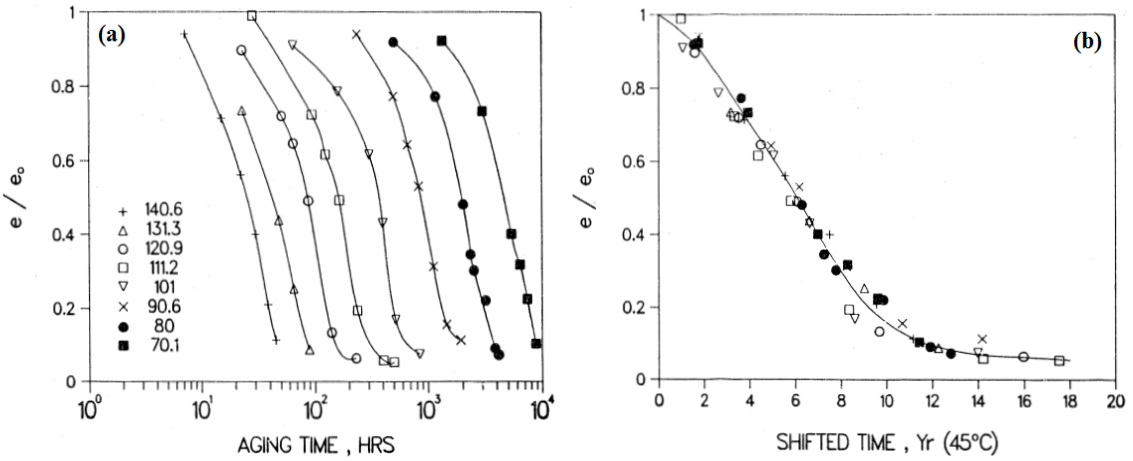


Figure 1.9. Time-Temperature superposition for thermal aging [19]; (a) elongation at break vs. time, (b) master curve.

The method based on superposition of time dependent data, also known as time-temperature-dose rate superposition [19], uses data on elongation at break as a function of time in a range of combined temperature/dose rate conditions. The method uses the superposition principle, which has been used extensively for thermal aging (time-temperature superposition, Fig.1.9): the data of the elongation against the logarithm of time are superposed, to yield a master curve [19, 30]. The shift parameters required to form this master curve are found to be related to the test temperature and dose rate by a semi-empirical equation which has been verified for a number of cable materials. The equation can then be used to calculate the shift factors for the master curve of elongation against time at temperatures and dose rates appropriate to service conditions. The superposition of time dependent data is only possible where the general shape of the elongation versus log time curve does not vary with changes in temperature and dose rate. This implies that all of the degradation mechanisms are equally accelerated by an increase in temperature or

dose rate. This is generally the case when the degradation is dominated by a single mechanism (e.g. oxidation), as occurs case with many of the commonly used cable materials. If more than one degradation process is significant in the temperature and dose rate range tested, then the curve shapes will not be the same and the data cannot be superposed. The method has been successfully applied to a range of polymers, including EVA, XLPE and EPR [5, 30].

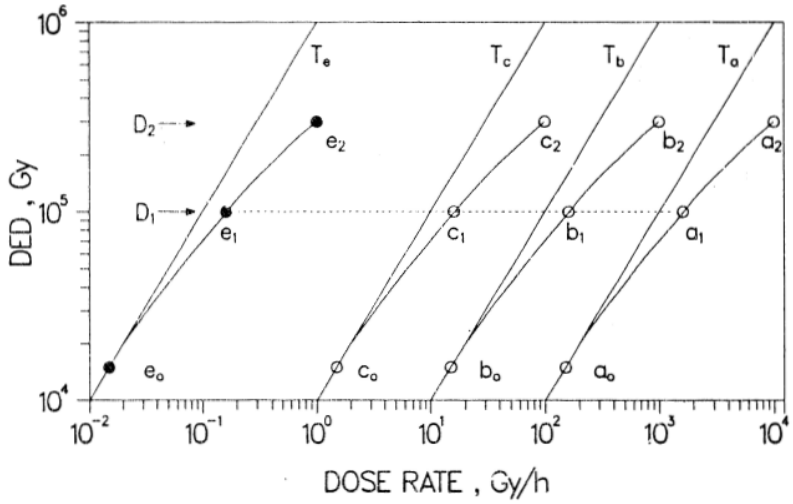


Figure 1.10. Time-Temperature-Dose Rate superposition using DED data as a function of the dose rate [19].

The method based on superposition of DED data also comes from the time-temperature-dose rate superposition. DED values are reported against dose rate in a log-log plot, and the data are superposed using a shift factor determined by the Arrhenius relationship. In many cable materials, a single value of activation energy can be used in the Arrhenius equation to superpose all of the DED data. The superposition of DED data can be used even for those polymers which do not have one dominant degradation mechanism. The method does however require a large data set to obtain sufficient DED values for superposition to be carried out. It is not very successful in those materials which show little or no dose rate effect, but can generally be used on a wide range of materials [5, 19, 30].

The kinetic modeling method based on Dakin's law also utilizes elongation data obtained in a range of temperature and dose rate conditions. Superposition of the data is obtained using equations based on the chemical kinetics of the degradation. The analysis of the different rate constants (radiation, thermal, pressure etc.) allows to draw up a predominance diagram for the material. The combination of these approaches is useful in defining accelerated test procedures. The kinetic model can be applied to a range of materials, including EPR and EVA. The main limitation in its wider application is the extensive matrix of test data required [5].

All of the methods are dependent on data being obtained at dose rates low enough for homogeneous oxidation to occur in the test samples and assume that the temperatures used do not span any physical transitions of the polymer, such as crystalline melting or glass transition. At present, the laboratory aging methods are aimed at predicting age-related degradation of cables arising from their normal operating conditions. These test programs are not aimed at predicting the ability of the cables to survive a DBE test. Survivability in a DBE would need to be demonstrated by additional specific DBE testing after laboratory aging.

It must be kept in mind that the degradation of a cable material can be quite different depending on its formulation. For example, even an XLPE insulation produced by the same manufacturer, using similar raw materials, additives and curing process can show very different deterioration characteristics. The manufacturer may use the same manufacturing procedure, but the formulations in the supplied raw materials may have changed, altering the chemical composition of the cable insulation. Therefore, the same manufacturer may not duplicate the cable previously supplied to a NPP. Some manufacturers have either sold or closed their businesses. Consequently, it is difficult to develop a list with manufacturing details for tracing the original compositions of cable material. This poses problems in comparing the results from simulation studies on unaged cables with cables aged in operation [3].

# Chapter 2

# In Search of Non-Destructive Diagnostic Quantities

Currently, the nuclear industry depends mostly on manufacturers' qualification data to ensure adequate cable performance, and very little testing is performed to verify that cables remain reliable for long term service, except for cable troubleshooting[1]. With plant life extension efforts currently under way, cable condition monitoring techniques are taking center stage both at utilities and regulatory agencies [10, 31].

The assessment of cable conditions has long been researched in an attempt to identify an effective technique that can be used to determine the existing cable condition, as well as to predict their future performance. Effective in-situ condition monitoring techniques are considered an important aspect of managing cable aging. They also play an important role in the validation of the physical and chemical degradation models providing useful experimental data from the field.

Related to the development of new CM techniques, is the establishment of acceptance criteria [9] that can be used to make decisions regarding the acceptability of the condition of cables currently installed in nuclear plants (see section 1.3). While a CM parameter may provide an indication of cable aging degradation, specific acceptance criteria are needed to determine if the current condition, which may include degradation from "hot spots" and localized anomalies, is acceptable for continued service. In many cases, CM parameters provide a measure of cable physical condition, such as material hardness, through destructive testing. The correlation of these measurements with insulation electrical parameters is very important, since it could provide useful information for the development of non-destructive condition

[1] Insulation Resistance (IR) testing is a typical troubleshooting technique used by plant operators to confirm or localize suspected or known problems; however, IR tests do not detect insulation damage or other circuit degradation prior to very severe deterioration. In the case of low-voltage cables, the insulation usually can provide sufficient dielectric strength to prevent the detection of degradation by these tests [1, 12]

monitoring techniques.

## 2.1 State of the art in nuclear power plant cable condition monitoring

So far, it is generally accepted that a single condition monitoring technique is not sufficient to assess insulation degradation or predict remaining life, but there are a number of new promising CM methods. A combination of tests is usually required to provide an indication of cable degradation. The desirable attributes of a CM technique can be listed as follows [5]:

- non-destructive and non-intrusive;
- simple to use under field conditions;
- capable of being used during normal operation;
- does not require disconnection of equipment;
- the measured property can be correlated with an identifiable failure criterion, such as elongation at break applicable to commonly used cable materials and configurations;
- capable of identifying "hot-spot" degradation;
- reproducible and capable of compensation for environmental conditions such as temperature and humidity;
- less expensive than cable replacement.

Currently available techniques can be classified as either non-destructive or destructive. Early destructive tests required large sections of cables. Replacement of the cable to establish its condition is generally unacceptable unless the cable is representative of a large population of cables subjected to similar conditions. Hence, methods using very small specimens (e.g. milligrams) have been developed. These lab tests require very small samples to be removed from in-service cables.

The following sections illustrate the CM methods which have been investigated widely in the past, particularly focusing on measurements of mechanical properties (i.e. tensile testing), thermal analysis (OIT, OITp, TGA), FTIR and density whose results will be used in the discussion. For a complete description of the currently available CM techniques see references [3, 9, 10, 12, 32].

### 2.1.1 Tensile Testing

Tensile testing is used to obtain information about the mechanical properties of a material, such as elongation at break, stiffness (Young's modulus, $\sigma/\epsilon$) and strength at break, by stretching the sample until it breaks (Fig.2.1) while recording load and extension. Since embrittlement and structural integrity changes are very important consequence of polymer degradation due to aging, the elongation at break has been considered a suitable degradation-sensitive property, which is generally accepted to assess cable functionality.

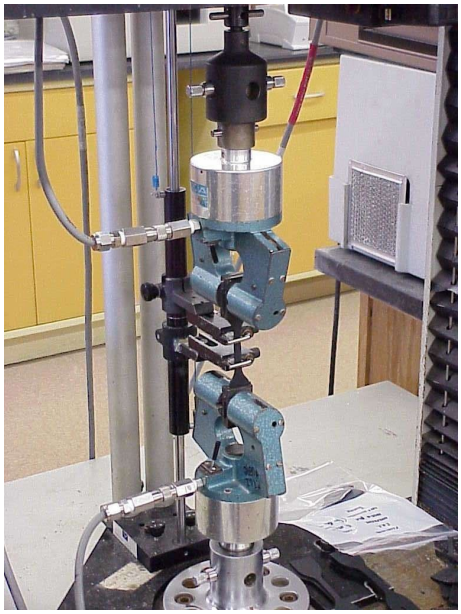

Figure 2.1. Tensile testing machine for rubbers.

Elongation at Break has a comprehensible life-end-point criterion and its values usually markedly change with cable aging (see sections 1.3 and 1.5). This feature make EaB the benchmark technique to which other CM techniques are usually compared [2, 10, 33]. Historically, a value of elongation at break equal to 50% (absolute or relative, as specified by standards [34, 35]) has been defined as the end of life criterion for polymer cables. In particular, the value of 50% EaB shall be proved for LOCA cables by type testing.

The main advantages of EaB measurements are [5]:

- the presence of international standards for tensile testing [34, 36];
- the general reliability of the EaB as condition indicator. It decreases gradually with the amount of induced degradation for most polymeric materials, this

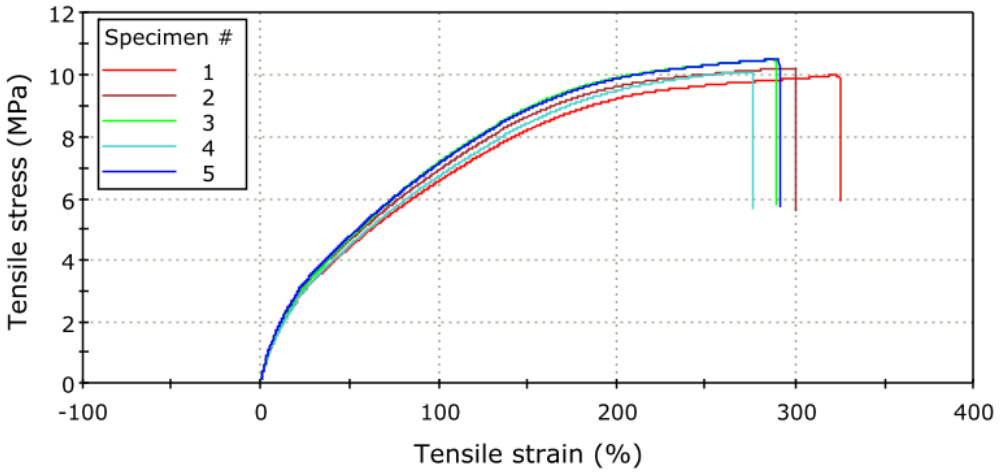


Figure 2.2. Example of tensile testing measurement result of an EPDM-based cable insulation.

degradation being either thermally or radiation induced. This is the reason why most CM techniques have been correlated to EaB measurements.

The behavior of other mechanical properties, such as Young's modulus and strength at break, can vary during type testing depending on materials and stress level applied. They are often used to understand the prevailing degradation phenomena rather than as CM indicators [37].

The main limitations to elongation measurements can be listed as follows [5]:

- requirement of large samples. Sampling is destructive from the viewpoint of the cable. Sampling may not be destructive from the viewpoint of the NPP if a cable deposit is available or cable replacement has been planned;
- for cross-linked polyolefins, EaB is not often a very good condition indicator because it remains quite constant over a long period of time and then rapidly decreases to the end-of-life value;
- EaB measurements may not be possible, or not be representative, if the material consists of a composite based on fibre reinforced polymers or two bonded inseparable layers.

Sample size, tensile test speed and temperature are important test parameters, which can lead to misleading or inconsistent test results. Therefore, it is important to define the test methodology and keep record of these parameters, to allow test reproducibility [10, 38, 39]. In many cases, appropriate "dumb-bell" samples can be cut out of cable jackets but the smaller cable insulation samples are usually tested

as (hollow) tubes. Sample preparation it is another important procedure which can alter tensile testing outcomes; for example, the extraction of the conductor from a cable sample can damage the insulation, especially the most severely degraded.

Although tensile testing provides useful data for cable condition assessment, the use of this technique as a routine CM method is not desirable, since it is destructive and intrusive. Furthermore, long outages are associated with cable removal and replacement. However, the method is particularly useful where cable samples have been placed in a sample deposit, specifically for CM (see section 1.3), and the interpretation of the results is made easier by the information reported in literature [5, 7, 11, 12, 19, 27].

As mentioned previously, significant reductions in elongation are only seen for some cable materials in the last quarter of total life. For this reason, although elongation is used as the main indicator of degradation, other parameters which could show changes in the earlier stages of degradation are particularly useful in assessing the state of cables. Examples of these degradation parameters are, for example, oxidation induction time and temperature.

### 2.1.2 Oxidation Induction Time and Temperature

Oxidation Induction Time (OIT) test is carried out on small polymer samples weighing $1 - 10$ mg. The samples are usually cut up into small pieces and placed in the sample pan of a DSC. The sample is heated quickly to a predetermined temperature, in an inert atmosphere (usually nitrogen) and once the heat flow has stabilized, the inert gas is replaced by oxygen. After an induction period, the sample begins to oxidize and the time at which this occurs can be measured because it is associated with an exothermic heat flow, recorded by the instrument. A typical OIT thermogram is shown in Fig.2.3. As aging continues, the OIT usually becomes shorter.

OIT can be measured for almost all standard polymer materials used for cables in NPPs, and it has been demonstrated to be appropriate particularly for XLPE and EPR. Also this technique presents the advantage of being standardized [40, 41, 42]. Great care has to be taken while testing halogenated materials (PVC, CSPE, PCP) as the degradation products from these materials can damage expensive calorimeter cells.

The sample preparation and instrumentation for Oxidation Induction Temperature measurements (Fig.2.4) is identical to that for OIT but in this case the sample is heated at a slow ramp rate (usually 10°C/min) in oxygen [29, 43]. Oxidation in the sample is characterized by an increase in exothermic heat flow which accelerates as the temperature increases. As the level of degradation increases, the OITp usually decreases.

Unlike the OIT test, physical transitions such as glass transition and melting points may appear on the DSC thermogram, as an endothermic process. In this case,

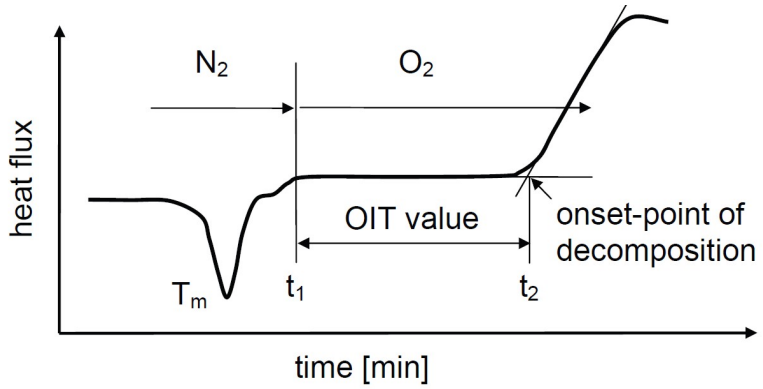


Figure 2.3. Schematic example of OIT thermogram. OIT is defined as the time between $t_1$ and $t_2$, whereby $t_2$ is given by the intersection (onset of decomposition) of the extension of the baseline with the steepest tangent of the reaction peak. This evaluation method is called the tangent method.

the melting point $T_m$ and the melting enthalpy $\Delta H_c$ are recorded. Real polymeric samples usually show complicated DSC thermogram and the evaluation of the peak evaluation is not as easy as pointed in Fig.2.5.

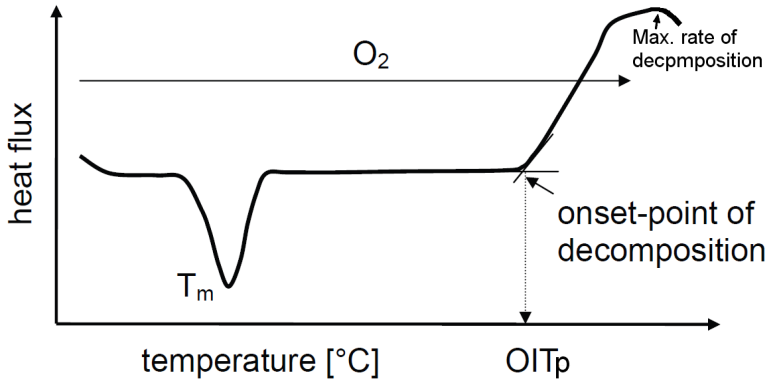


Figure 2.4. Schematic example of OITp evaluation. The evaluation should be done using the tangent method.

Since the OIT and the OITp are related to the content of antioxidants, they can be suitable parameters for monitoring cable insulation degradation [2, 43, 44]. The OIT measurement does not give an absolute indication of the cable condition. This means that the end-of-life criterion is undefined. Therefore, for cable insulation and jackets which have been subjected to aging monitoring and to assessment of residual service lifetime, the OIT values have been correlated to elongation at break, through the use of correlation curves (property cross-plots). It is assumed, that each cable needs its own correlation curve [44, 45].

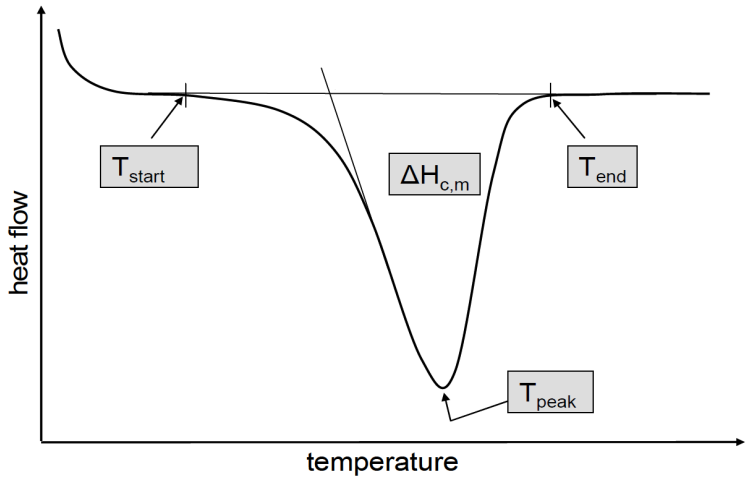


Figure 2.5. Illustration of DSC parameters. $\Delta H_c$ is the integral of the DSC curve between $T_{start}$ and $T_{end}$.

### 2.1.3 Density

If a polymer is aged in air, oxidation normally is the dominating cause of degradation, leading to both crosslinking and chain scission, and also resulting in the formation of oxidation products together with the release of gases. The density of the polymer is increased by most of these processes. The oxidation products increase the density through the substitution of hydrogen atoms with oxygen atoms, which are significantly heavier. As many polymers have fillers of high densities, the release of degradation products from the comparatively low-density polymer chain leads to a higher density through a decrease in the polymer to filler ratio. Shrinkage from a tightening of the polymer chain is often a result from crosslinking, and this is also a cause of an increase in density [25].

This method is considered essentially non-destructive because of the small size of the samples required ($< 1$ mg). The density can be measured in a couple of ways. The older way consists of placing the sample in a column with a density gradient. The sample then falls to a position where the density of the sample corresponds to the density of the surrounding liquid. This method is time consuming, as the time required to reach density equilibrium is comprised between a few minutes for large samples to hours for small ones [24].

A more recent way for measuring the density is using the Archimedes' principle, and weighing the samples, both in air and in a liquid with a density lower than that of the polymer, on a precision balance. The density of the polymer is then determined as:

$$\rho_{polymer} = \left[\frac{m_{air}}{m_{air} - m_{liq}}\right] \rho_{liq} \tag{2.1}$$

where $m_{air}$ and $m_{liq}$ are the measured weights in air and liquid, respectively, and $\rho_{liq}$ is the density of the liquid. This method is fast and produces results of good accuracy [25, 46].

This method can give satisfactory information about the aging for a number of different materials, for example XLPE, CSPE, EVA, EPR and PVC. However, in many cases, the density increase is slow at the beginning of the aging, with an increase at later stages, showing the so-called induction time-effect. Materials that have a near-linear increase in density with aging, and show no such induction time, include PVC and LDPE [25]. As for OIT, the results from this kind of measurements need to be correlated to a property such as elongation at break.

### 2.1.4 Thermogravimetric Analysis

Termogravimetric Analysis (TGA) is a technique where the mass of polymer is measured as a function of temperature or time while the sample is subjected to a controlled temperature ramp in a controlled atmosphere [47, 48, 49]. Upper limit for polymer applications is usually 1000°C. A purge gas flow creates the atmosphere that can be inert, reducing or oxidizing. Volatile components such as absorbed moisture, residual solvents or low molecular additives evaporate usually between ambient temperature and 300°C. TGA can give information about the chemical structure of the polymeric macromolecules and additives thermal stability, especially for flame retardants (see section 1.1). Sample preparation for TGA tests is the same as that used for OIT tests. TGA can be coupled to and Gas Chromatography or Mass Spectroscopy to enable comprehensive quantitative and qualitative determination of the released products. This test is usually carried out on samples that evolve corrosive degradation products (e.g. CSPE, whose thermal properties depend on the number of hydrogen atoms replacement in polyethylene main chain with -Cl and -$SO_2$-Cl functional groups) as the sample chambers in TGA equipment are chemically far more robust than those used in DSC. The technique provides an alternative thermal test method for these materials, although the data for CSPE are limited and suggest a lack of sensitivity for thermally degraded CSPE.

Applying TGA to NPP cable materials, samples demonstrate usually bimodal thermal decay. Four regions of the material decomposition can be identified (Fig.2.6):

- release of low molecular weight products and water ($200 - 300$°C);
- decomposition of pendant groups, emission of water and low molecular weight additives ($300 - 420$°C);
- degradation of hydrocarbon backbone (420°C-plateau);
- residuals.

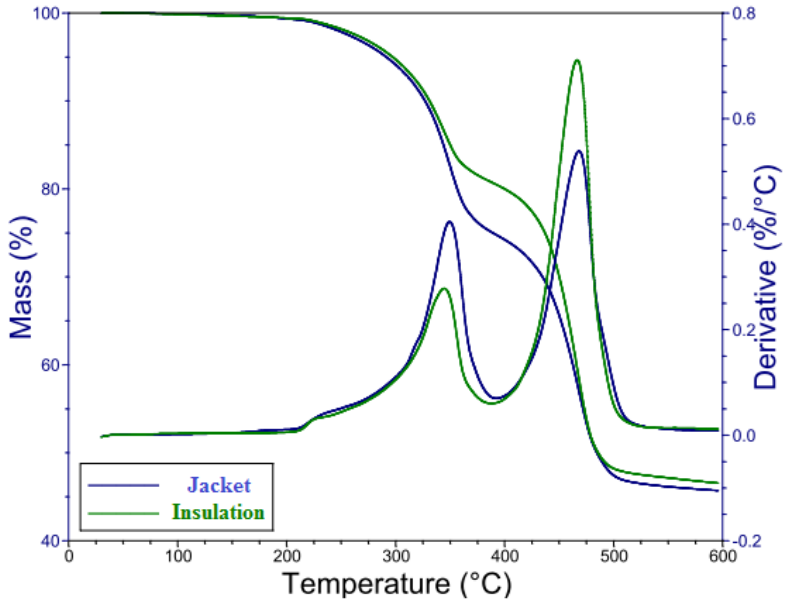


Figure 2.6. An example of TGA thermogram. The polymer (EVA-based insulation and jacket) loss of mass and its rate are shown as a function of temperature.

Flame retardants in the form of metal hydroxides are the agents that at elevated temperatures decompose emitting water according to the following reactions:

$$2Al(OH)_3 + 1075\ kJ/kg \rightarrow Al_2O_3 + 3H_2O \tag{2.2}$$

$$2AlOOH + 700\ kJ/kg \rightarrow Al_2O_3 + H_2O \tag{2.3}$$

$$Mg(OH)_2 + 1220\ kJ/kg \rightarrow MgO + H_2O \tag{2.4}$$

Thermal decomposition of commonly used aluminum hydroxide takes place in the range $(200 - 320°C)$. Mass reduction below 400°C is attributed predominantly to the release of water molecules, assuming that aluminum hydroxide is used as a flame retardant.

TGA can be applied to EVA insulation and jacket materials. Ethylene-vinyl acetate is a copolymer of ethylene and vinyl acetate of various vinyl acetate weight percentage (usually from 10 to 40%). For the pure copolymer (without additives), a ratio between both components determining macroscopic properties of the material might be estimated on a basis of TGA measurements, since the decomposition of acetic acid occurs at lower temperatures than the thermal decay associated with the presence of other polymeric domains (hydrocarbon chains).

The activation energy of the thermal degradation and/or the service life of the polymers might be obtained by analysis of the relationship between the temperature and the weight of polymers using various procedures. The temperature at which the

sample weight has decreased to 95% of its original value is usually taken as the reference point. The value of this temperature depends on the level of aging in some polymers and will tend to decrease with increased aging levels [10, 20]. Initial thermo-oxidative degradation parameters, such as temperature of initial decomposition, activation energy of initial decomposition and time-to-failure, characterize the first moment of deterioration of polymer material. Therefore, the lifetime of a polymer material could be reasonably predicted from the semi-log plots of time-to-failure as a function of $1/T$. This technique is effective for cross-correlating radiation degradation in PVC materials [3, 50, 51, 52].

### 2.1.5 Fourier Transform Infrared Spectroscopy

Fourier Transform Infrared (FTIR) Spectroscopy is a well-known laboratory technique for studying the molecular structure of materials. It is performed using a spectroscope, in which a small material sample is exposed to infrared radiation. The absorbance or transmittance of this radiation by the material at various wavelengths is then measured. The principle behind this test is that, as radiation passes through a polymer, atoms absorb radiation and begin to vibrate. For a particular chemical bond, maximum vibration occurs for a specific wavelength of radiation. By irradiating a specimen with a continuous spectrum of infrared radiation and identifying the wavelengths at which maximum absorbance or transmittance occurs, the chemical bonds that are vibrating can be identified by comparison with known characteristics for chemical bonds available from literature. A high level of skill, experience and knowledge in the operation of the FTIR spectrometer, FTIR spectroscopy and polymer chemistry is required to properly use this technique [32].

Monitoring the carbonyl region typically requires less than 10 mg of sample. The carbonyl (C=O) peak appears around $1720cm^{-1}$ and belongs to ketones, carboxylic acid and aldehydes. This peak is a direct indicator of polymer oxidation. Another important wavelenght is $2900cm^{-1}$, and represents the C-H stretching of $-CH_2$ bond that is part of the polymer's backbone structure. The magnitudes of the peaks in the spectra reflects the changes in the polymer molecular structure, since oxidation is characterized by an increasing presence of carbonyl bonds and decreasing number of $-CH_2$ bonds. An oxidation index can be defined as the ratio of the area of the carbonyl absorption to the area of $-CH_2$ stretch absorption peak. The oxidation index is useful for quantifying the extent of oxidation, however the technique does not take into consideration different types of oxidative products, e.g. *C-O-C*, *C-O-O-H*, *C-O-O-C*, *C-O-H*. Additionally, it should be taken into account that these bonds may also be present in the other constituents, like additives of the polymer material formulation [22, 53].

The FTIR spectroscopy technique has been used successfully to characterize aging degradation for XLPE and EPR cable insulation and CSPE jacket material

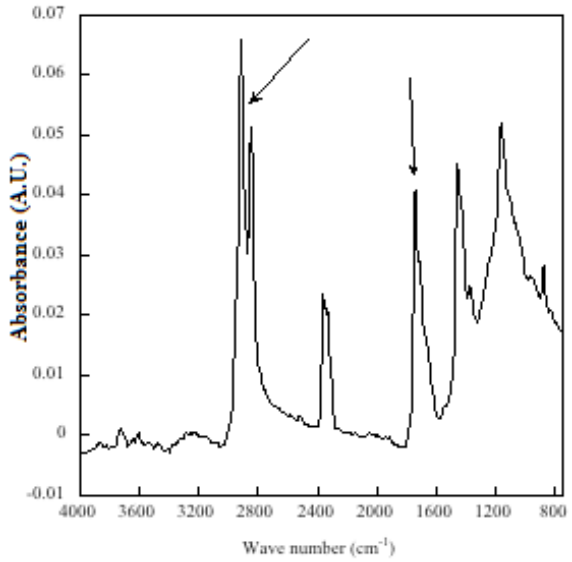


Figure 2.7. Example of FTIR results: the carbonyl peak ($\approx 1720 cm^{-1}$) and the $-CH_2$ stretch peak ($\approx 2900 cm^{-1}$) are indicated by arrows.

[54, 55, 56]. For materials that demonstrate ($C = O$) absorption band before aging, e.g. EVA, the sensitivity of the assay is limited. It is not conclusively known how well the method will work with other types of materials used for cable insulation and jacket materials. Because of the variations in the polymer formulations for each manufacturer, the effects of additives and dyes, and the non-homogeneous distribution of antioxidants throughout the material, an absolute acceptance criterion does not exist. Variations in the testing technique, the type of refracting crystal used, and difficulties in maintain good optical contact with the specimens as they age and become more rigid also complicate the establishment of absolute acceptance criteria.

An advantage of this technique is that samples can be obtained from very small areas of cable; therefore, it can be considered a non-destructive technique. In addition, quantitative results are provided that can be trended over time for use in tracking the condition of the cable. A disadvantage of the FTIR spectroscopy technique is that it is a surface examination procedure. Under harsh environmental condition (i.e. elevated dose rates) an oxidation gradient could develop at the specimen surface, resulting in the spectroscope detecting a higher amount of oxidation than the average bulk value (see section 1.4).

Correlation of FTIR results for such cables with results from other techniques that accurately reflect average bulk properties, such as EaB, could be problematic. This deviation from average bulk conditions would be exacerbated as aging temperatures increase. More accurate estimates of bulk aging would be expected for cable specimens naturally-aged at service temperatures, low enough to mitigate the

establishment of an oxidation gradient within the cable material [57].

Unfortunately, FTIR is difficult to run on black (e.g. carbon-black filled) materials or materials with peaks already present in the carbonyl region before aging, e.g. EVA. In addition, for the aging of many materials, the growth in the carbonyl region is often extremely slow until just before failure where the growth rate of the carbonyl peaks greatly accelerates; in such instances, condition monitoring will give no warning of imminent failure. In addition, the growth in the carbonyl region is often extremely slow until just before the practical end-of-life when the growth rate of the carbonyl peaks greatly accelerates; in such instances, condition monitoring by FTIR gives little warning of imminent end-of-life [31, 54].

## 2.2 The European Project ADVANCE

Among the non-metallic components of nuclear power plants, electric cables and their assessment constitute one of the top research priorities. This Ph.D. thesis has been carried out in the framework of the European Project ADVANCE (Aging Diagnostic and Prognostics of Low-Voltage I&C Cables). This project aims at [58]:

- adapting, optimising and assessing promising electrical condition monitoring techniques for nuclear cables that are non-destructive and can be used in the field to determine the current condition of installed cables over the entire length;
- using of condition monitoring techniques to predict remaining useful life, including the establishment of acceptance criteria and correlation of physical cables properties to electrical properties;
- correlating condition indicators of cables near the end of life with accident survivability;
- investigating new cables design and formulation adapted to full-length electrical CM techniques to provide fundamental knowledge for the next generation of cables for future NPPs with improved diagnostic capability.

To simulate global and local aging, accelerated cable aging (thermal and irradiation) has been performed on a representative selection of cables already installed in European NPPs as well as on new cables for future plants. The values of condition indicators given by promising electrical CM techniques are then correlated to those obtained with more conventional CM methods like those described in sections. End-of-life values of cable condition indicators will be determined by appropriate correlations and/or by tests under accident conditions.


Figure 2.8. ADVANCE logo.

## 2.3 Aim of this work

This Ph.D. thesis aims at studying the impact of cable aging on the electrical parameters. The main objectives are:

- to understand the evolution of the electrical properties associated with cable degradation to identify suitable aging markers;
- to correlate the evolution of electrical properties with the physical/chemical degradation mechanisms of polymers for different kinds of cable materials and composition;
- to evaluate the feasibility of non-destructive electrical CM techniques as potential substitutes for destructive methods.

The electrical properties of cable insulators will be monitored and characterized mainly by dielectric spectroscopy, polarization/depolarization current analysis and space charge distribution; these techniques have been developed mainly for HV and MV cables to study their performance and aging. Quantities such as the total stored charge density in the insulation and/or trap-controlled charge mobility could be significantly sensitive to aging and could be interesting diagnostic indicators to follow. Furthermore, processes like oxidation, cross-linking and polymer chain scission resulting from irradiation at high temperature, affect material proprieties such as density and degree of cristallinity. The electrical properties of insulation

materials, like insulation capacitance and loss factor, are known to be sensitive to these variations.

Since the aforesaid techniques have been shown their effectiveness mainly on HV and MV cables, the assumption is that the effect of radiation and thermal stresses could be revealed independently of the voltage level applied to the insulation. A connection between these electrical measurements and polymer structural changes will be established through chemical-physical analysis and mechanical analysis, in order to understand how diagnostic markers are influenced by the amount of internal polymer degradation. This will help to define critical values of the electrical indicators for the residual lifetime estimation.

### 2.3.1 State of the art in electrical CM techniques

Currently, the low-voltage cable electrical parameters most often tested by NPPs are voltage withstand and insulation resistance (IR).

Voltage withstand tests can be performed by applying a given voltage (above the normal operating voltage) to the insulation, for a given time (typically 1 or 5 minutes but it may be more). The principle behind the test is that if defects (local or global) are present in the cable, the high voltage will force them to fail. If the breakdown does not occurs, the insulation has successfully passed the test. This test is potentially destructive and intrusive, because it requires the disconnection of cable terminations.

For IR measurements, a DC voltage (typically 500 V) is applied to the cable for a short period of time and the DC current is measured. Also this method requires cable disconnection. The insulation resistance is given by the ratio between the applied voltage and the measured current, and it is usually expressed in $M\Omega$. The Polarisation Index (PI) is defined as the ratio of IR measurements at two different times:

$$PI = \frac{IR(t_2)}{IR(t_1)} \tag{2.5}$$

where in general $t_1 = 60$s and $t_2 = 600$s. For some insulations, the dielectric absorption current decreases rapidly (see section 2.3.4) and the PI can be measured at $t_1 = 30$s and $t_2 = 60$s. In that case, the ratio is called Dielectric Absorption Ratio (DAR).

Nevertheless, other properties, such as capacitance, attenuation, and/or signal propagation can be measured as well on coaxial and triaxial cables. In this case, the test is passed if the cable parameters do not change during its service period. Indeed, it is believed that by the time a significant change in the electrical characteristics of the cable is found, the cable might already be well beyond the point where it needs replacing [10].

Most of these tests are certainly effective as pass/fail indicators of functionality, but studies over many years in the nuclear industry suggest that there are no reliable data yet available that allow an appropriate correlation between these measurements and cable aging. Some of these tests require high voltages (dielectric breakdown is a destructive test), and thus may be considered inappropriate for use on I&C cables in-situ for fear of insulation damage.

Most of the techniques are not very sensitive to insulation degradation but can be sensitive to conductor integrity (e.g. loose connections, corrosion of connectors). The advantage of electrical techniques is in their in-situ and remote testing capability. Many of the electrical measurements can be performed on installed cables in an operating plant and can often reveal problems along the whole length of a cable, in contrast with methods that are limited to providing data at the localized point where the sample is withdrawn (e.g. tensile testing and thermal analysis).

At present, there are no CM methods based on electrical measurements that are applicable to CBQ programs. They are most useful in identifying and locating problems in NPP cable systems and confirming functional performance. Literature regarding the effect of aging on electrical properties of low-voltage insulation is still lacking. The long-term relation between physical/chemical degradation mechanisms and the electrical property variations have not been studied in detail for LV cable materials. Some techniques have shown potential for measuring aging degradation, but more research is needed to validate their use [10].

One technique for cable CM that has been studied with some success is the measurement of the dielectric loss tangent (or dissipation factor Tan Delta) of cable insulation. Tan Delta is a dimensionless property of a dielectric, that is determined by the insulator's structure. Therefore, changes in structure due to aging should affect Tan Delta. The measurement can be carried out over a range of frequencies at low voltages, using standard impedance bridge instruments. Normally the Tan Delta of cable insulation is measured between conductors in adjacent cores or between single conductors and shielding, at power frequency ($50 - 60$ Hz). In some cases, measurements can be carried out on jackets between shielding and an external ground plane (e.g. metal conduit). While this technique does not require sample removal, it does require disconnection of equipment and is susceptible to interference from electrical noise. This technique has also been shown to be very sensitive to the detection of water ingress in cables, especially when the test is performed at low-frequency, typically 0.1 Hz [10, 32].

Impedance measurements, including inductance (L), capacitance (C) and resistance (R) are made using an LCR instrument at specific frequencies to verify the characteristics of the cable conductor, insulating material and the end device. Results are evaluated to determine if they are as expected for the type of circuit being tested. Imbalances, mismatches or unexpectedly high or low impedances between the cable leads would indicate problems due to cable degradation and aging, faulty

connections and splices, or physical damage. For example, abnormal capacitance measurements are indicative of a change in the dielectric or insulation of the cable when compared to a calculated value or baseline measurement [10].

### 2.3.2 Space Charge Measurement

Space charge, i.e. free charge accumulated in the insulation bulk due to traps present in the insulation matrix, is usually associated with insulation systems subjected to high DC voltage (HVDC). Under HVDC, in fact, a significant amount of electric charges (positive/negative) can be injected from the electrodes into insulation bulk where chemical and physical traps are present. Therefore, electric charges can be trapped for a time that is correlated to trap depth (the deeper the trap depth, the longer the time needed for charges to escape). This may lead to space charge accumulation in the insulation bulk with an extent that depends on the density/depth of the traps present in the insulating material. Since trap distribution is correlated to material morphology/structure, aging can be detected by means of measurements of space charge accumulation [59, 60, 61].

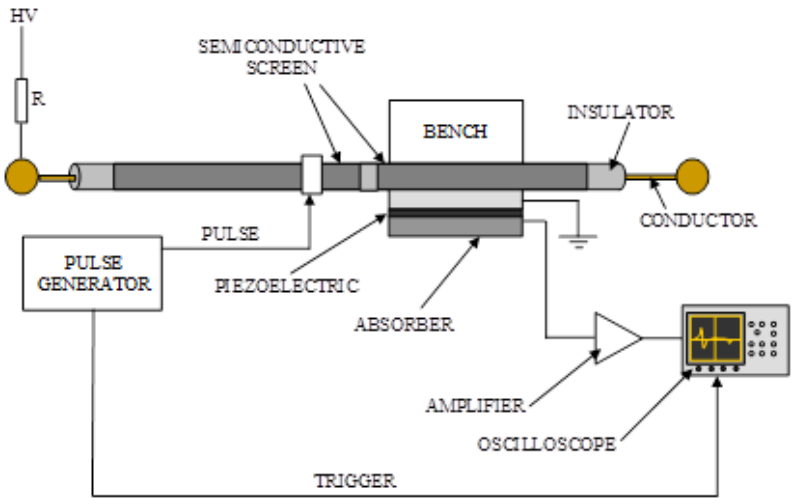


Figure 2.9. Schematic representation of PEA measurement experimental setup.

Space charge measurements can be carried out through several techniques. The pulsed electro-acoustic (PEA) technique [62], is a non-destructive technique for profiling space charge accumulation in polymeric materials providing a good spatial resolution of the space charge profile in the material bulk. The specimen could consist of a small plaque of insulating material or a length of a cable. A sequence of high-voltage pulses of very short time length ($5 - 40$ ns) at repetition frequencies in the range $0.050 - 10$ kHz is applied to the insulation specimen subjected to a DC

field (Fig.2.9). Each generated pulse produces an electric force displacing internal charges and generating pulsed acoustic pressure waves in correspondence of each charge layer in excess with respect to neutrality. The resultant pressure pulse is detected by a piezoelectric transducer, so that the charge distribution in the specimen under test is proportional to the output voltage profile provided by the transducer. The output signal is amplified and visualized by a digital oscilloscope. The analysis of space-charge profiles (Fig.2.10) is restricted to one dimension: this assumption imposes to consider that space charge density, electric field distribution and acoustic wave propagation can vary only along the specimen thickness.

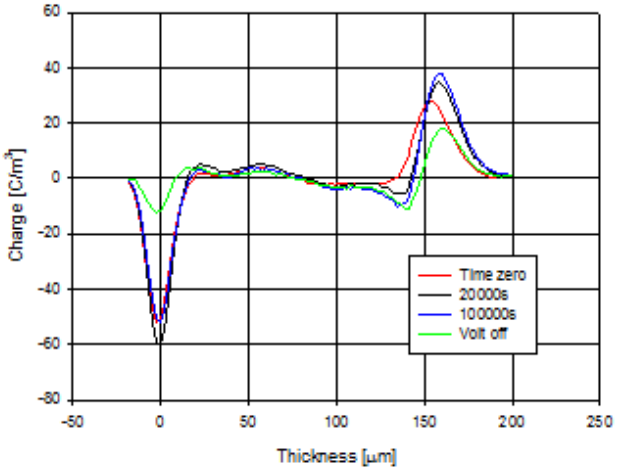


Figure 2.10. Examples of space charge profiles recorded during the measurement.

The first step is the estimation of the mean (absolute) space charge density from the charge density profile of Fig. 1.2. This quantity, $q(t,EP)$, has the following expression [61]:

$$q(t,E_p) = \frac{1}{(x_l - x_0)} \int_{x_0}^{x_l} |q(x,t;E_p)|\, dx \tag{2.6}$$

where $x_0$ and $x_l$ are the electrode positions, t is the time at which the measurement is done, $E_p$ is the field, $q(x,t;E_p)$ is the charge profile. In order to calculate the value of $q(t;E_p)$, reference can be made properly with charge profiles observed during depolarization (i.e., the volt-off). In the following, $q(t;E_p)$ and $q(x,t;E_p)$ will be referred as $q(t)$ and $q(x,t)$ respectively, for the sake of brevity, but keeping in mind that they are actually relevant to a given poling field $E_p$.

Plotting the values of q(t) thus obtained in relative value with respect to $q_0 = q(t_0)$, where $t_0$, is a reference time (generally 1 to 10 s after the volt-off), as a function of the depolarization time, the so-called depolarization characteristic can be obtained (Fig.2.11). An estimate of the average trap-controlled mobility could be

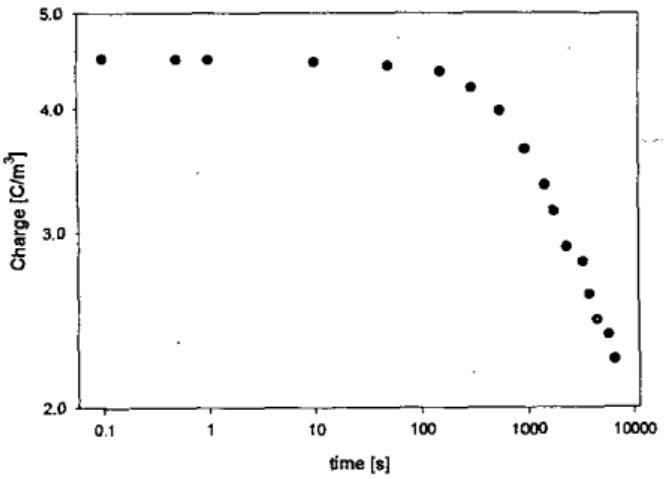


Figure 2.11. Example of depolarization characteristic.

derived, in principle, through appropriate processing of charge vs time depolarization characteristic. Apparent trap-controlled mobility is only a very rough approximation of the mobility as usually defined, but, even if affected by significant approximation, can be useful for material characterization and aging diagnosis. The expression of apparent trap-controlled mobility is the following [63, 64]

$$\mu = \frac{2\epsilon}{q^2(t)} \frac{dq(t)}{dt} \tag{2.7}$$

where $q(t)$ is the charge density that can be calculated at any depolarization time, $dq(t)/dt$ is the slope of the depolarization curve at time t, $\epsilon$ is an average estimate coming from specific measurements of permittivity carried out on the specimens tested. Once known apparent trap-controlled mobility the trap depth could be estimated. This is a difficult problem, which has not been solved yet in a totally convincing way. An approximate method to obtain the trap depth distribution, $\Delta U$, is described in [63] and provides the following equation:

$$\Delta U = kTln\left(\mu \frac{h}{eR^2}\right) \tag{2.8}$$

where $R$ is the mean distance between localized states, $e$ is the electron charge and $h$ is the Planck's constant. Therefore, the values of the trap depth can be determined from the values previously calculated for $\mu$.

Space charge measurements can be performed on every kind of solid insulating material used in cables and accessories. This technique is typically used for HV and MV cable insulation which are usually subjected to high field, where space charge

accumulation is an important factor and can create electric field distortion in the insulation bulk. On the contrary, space charge accumulation does not constitute a problem for the insulation of low voltage cables. Anyway, this technique can be used as a tool to detect morphology modification of the material due to aging (radiation and temperature).

Bulk degradation due to thermal and radiation stresses can be detected with this method since it is associated with modification of distribution of both chemical and physical traps. Chemical traps are characterized by chemical species present in the matrix different from the polymer, e.g. anti-oxidant, contaminants, cross-linking by-products. Physical traps can be associated with morphological non-homogeneities of the polymer chains, particularly at the interface between the crystalline and amorphous phase. As the polymer ages, physical and chemical changing in the matrix occur. Oxidation, bond breaking, free radicals and new chemical species formation are claimed to be the main effects of both thermal/electrical aging of polymers. Such aging effects can alter trap density and depth, usually increasing the number or the depth of charge traps . Therefore, quantities such as those defined in equations 2.7 and 2.8 could be significantly sensitive to the bulk aging caused by radiation/temperature [65, 66].

### 2.3.3 Dielectric Spectroscopy

Dielectric spectroscopy (sometimes called impedance spectroscopy) measures the dielectric properties of a medium as a function of frequency. It is based on the interaction of an external field with the electric dipole moment of the specimen, i.e. electrical polarization. The main parameter which accounts for polarization is the complex permittivity [67]:

$$\epsilon^* = \epsilon' - i\epsilon'' \tag{2.9}$$

This technique measures the impedance of a system over a range of frequencies, and therefore the frequency response of the system. There are several tools for analyzing the dielectric response of an insulation system in the frequency domain, between $10^{-5}$ and $10^{9}$ Hz, like dielectric analyzers and network analyzers.

The dielectric analyzer can evaluate the real and imaginary part of permittivity, $\epsilon'$ and $\epsilon''$, in the frequency range $10^{-2} - 10^{6}$ Hz, by accurately measuring the impedance of the specimen as a function of frequency. This instrument consists of two major components:

- a frequency response analyzer with a sine wave and DC-bias generator and two AC voltage input channels. Each input channel measures the AC voltage amplitude of an applied sine wave. In addition, the phase shift between the sine waves applied to the both inputs is detected. In particular, each channel

measures the amplitude and phase angle of the harmonic base wave component of a signal applied to the input. The harmonic base wave component is measured at the frequency of the AC sine wave generator. Most other signal components are suppressed. In addition, higher harmonics may be measured.

- a dielectric (or impedance) converter with a wide dynamic range current to voltage converter and a set of precision reference capacitors.

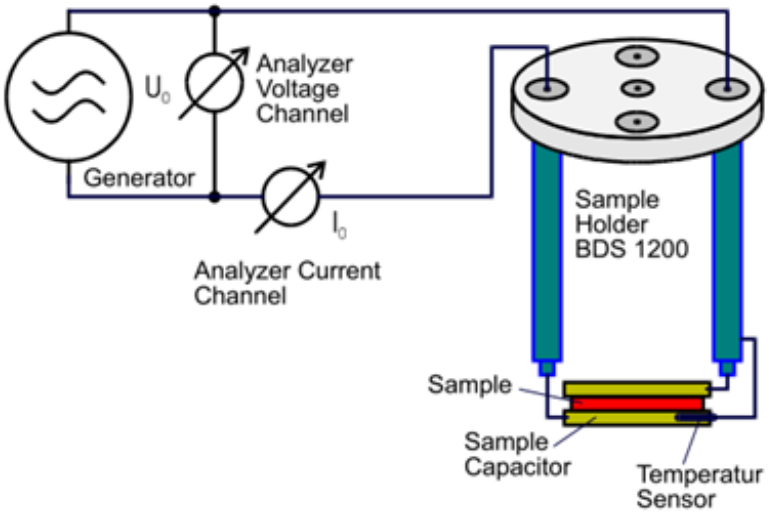


Figure 2.12. Schematic representation of the experimental setup for dielectric spectroscopy.

Fig.2.12 schematizes the experimental setup used for flat specimens. The specimen is usually mounted in a sample cell between two electrodes forming a flat capacitor. For cable specimens, the input voltage electrode is connected to the inner conductor and the low voltage electrode to a metal sheath wrapped around the cable.

A voltage with amplitude $V_0$ at fixed frequency $\omega/2\pi$ is applied to the sample capacitor. The result is a current of amplitude $I_0$ at the same frequency. In addition, there will generally be a phase shift between current and voltage described by the phase angle $\varphi$. The ratio between $V_0$ and $I_0$ and the phase angle $\varphi$ are determined by the sample properties (permittivity and conductivity) and by the sample geometry. Using the complex notation, the expression for voltage and current becomes:

$$V(t) = V_0 sin(\omega t) = \Re(V^* e^{i\omega t}) \tag{2.10}$$

$$I(t) = I_0 sin(\omega t + \varphi) = \Re(I^* e^{i\omega t}) \tag{2.11}$$

$$V^* = V_0; \qquad I^* = I' + iI''; \qquad I_0 = \sqrt{I'^2 + I''^2}; \qquad tan(\varphi) = \frac{I''}{I'} \tag{2.12}$$

For a sample with linear electromagnetic response, the measured impedance of the sample capacitor

$$Z^* = Z' + iZ'' = \frac{V^*}{I^*} \tag{2.13}$$

is connected with the complex permittivity of the material by

$$\epsilon^*(\omega) = \epsilon' - i\epsilon'' = \frac{-i}{\omega Z^*(\omega)} \frac{1}{C_0} \tag{2.14}$$

where $C_0$ is the capacity of the empty sample capacitor, also called the reference capacitance.

Like space charge measurements, dielectric spectroscopy can reveal bulk degradation due to thermal and radiation stresses. Morphological changes of insulating materials due to oxidation, bond breaking, free radicals and new chemical species formation caused by both thermal/electrical aging of polymers, can give rise to variation of polarization properties of the material,in particular the imaginary part of permittivity which is correlated to dielectric losses.

Note that dielectric permittivity is a complex function of at least two variables, frequency and temperature. The investigation of the dielectric response leads to information about different molecular motions and relaxation processes. Polymer relaxations are associated with thermally activated processes involving polymer morphology, degree of cristallinity, functional groups and dipoles resulting from oxidation. Most polymers exhibit more than one region of dielectric relaxations, called $\alpha$, $\beta$, $\gamma$ and $\delta$ motional processes in descending order of temperature, which result in characteristic relaxation peaks (Fig.2.13).

In an amorphous polymer, the $\alpha$-transition or $\alpha$-relaxation corresponds to the glass transition and depends upon the chemical structure of the polymer. In general, it is found that the transition temperature ($T_g$) is increased as the main chain becomes stiffer. Side-groups raise the ($T_g$) if they are polar or large and bulky, and reduce it if they are long and flexible. The assignment of particular mechanisms to the secondary transitions can sometimes be difficult since their position and occurrence depends upon which polymer is being studied.

The interpretation of the relaxation behaviour of semi-crystalline polymers can be extremely difficult, because of their complex two-phase structure. It is sometimes possible to consider the crystalline and amorphous regions as separate entities with the amorphous areas having a glass transition. It is clear, however, that as particular molecules can traverse both the amorphous and crystalline regions, this picture may be too simplistic.

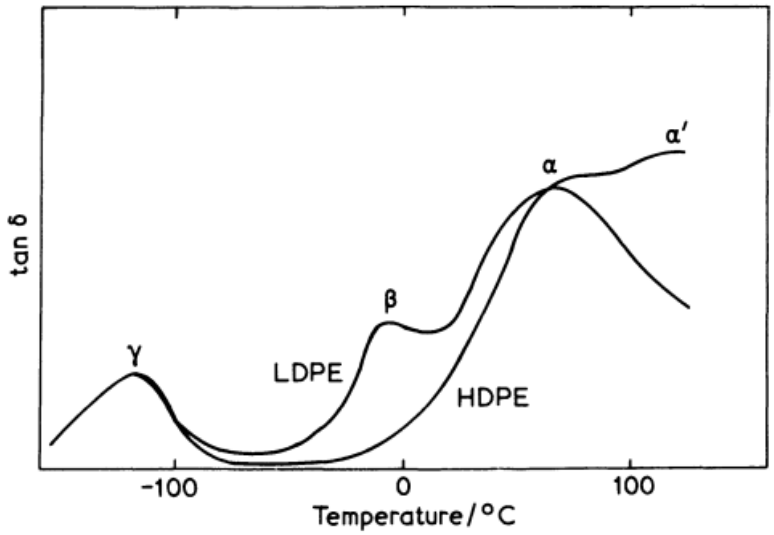


Figure 2.13. Variation of Tan Delta with temperature for high and low-density polyethylene [68].

The relaxation behavior of polyethylene has probably been more widely studied than that of any other semi-crystalline polymer and so this will be taken as an example, even though it is not completely understood. Fig.2.13 shows the variation of Tan Delta with temperature for two samples of polyethylene, one high density (linear) and the other low density (branched). In polyethylene there are four transition regions designated $\alpha'$, $\alpha$, $\beta$ and $\gamma$. The $\gamma$ transition is very similar in both the high and low-density samples whereas the $\beta$-relaxation is virtually absent in the high density polymer. The $\alpha$ and $\alpha'$ peaks are also somewhat different in the pre-melting region.

The presence of branches upon the polyethylene molecules produces a difference in polymer morphology as well as in the molecules themselves. The degree of crystallinity and crystal size and perfection are all reduced by the branching and this can lead to complications in interpretation of the relaxation behaviour. The intensities of the $\alpha'$ and $\alpha$-relaxation decrease as the degree of crystallinity is reduced, implying that they are associated with motion within the crystalline regions. On the other hand, the intensity of the $\gamma$-relaxation increases with a reduction in crystallinity, indicating that it is associated with the amorphous material and it has been tentatively assigned to a glass transition in the non-crystalline regions. The disappearance of the $\beta$-transition with the absence of branching has been taken as a strong indication that it is associated with relaxations at the branch-points. In general, the assignment of the peaks in crystalline polymers to particular types of molecular motion is rather difficult and often a matter for some debate [68].

A relaxation is dielectrically active only when there is a reorientation of a dipole

moment vector and also a release of space charges. Any presence of $C = O$ dipole and polar additives will introduce dipole moments in polyethylene, which may couple the molecular motions of a polymer to the external field. An effective dipole moment was obtained in oxidized polyethylene due to the presence of a $C = O$ group, and it has been suggested that the $\alpha$ relaxation arose from carbonyl groups in the crystalline region of polyethylene. Dielectrically active $\beta$ and $\gamma$ relaxations occur in the disordered regions of polyethylene, and also in this case the dipoles are carbonyl groups. Thus, it may be stated that the dielectric relaxations of polyethylene owe their origin to the extraneous carbonyl group and/or other impurity dipoles [69]. Polyethylene has been deeply studied for HV and MV cable applications. Dielectric spectroscopy is sensitive to aging and can reveal the effects of a wide range of degradation mechanisms, related to electrical, thermal or radiation stresses [70, 71, 72].

As previously mentioned, EVA is widely used as cable insulation and sheath material. Vinyl acetate content has two fundamental effects that influence the properties of EVA copolymers. The first effect is to disrupt the crystalline regions formed by the ethylene segments of the copolymer: increasing the VA content, at some point between 40 and 50 wt% VA, the material becomes completely amorphous. Some of the most important properties of EVA are in part controlled by the degree of crystallinity. The second overriding effect of vinyl acetate content results from the polar nature of the acetoxy side chain. Thus, the polarity of the copolymer increases with the vinyl acetate content. This increase in polarity also gives rise to a number of interesting and important properties that are again, in part, responsible for the wide diversity of applications for EVA copolymers [73]. Since the vinyl acetate plays an important role in EVA radio-oxidation, it is reasonably possible to detect polymer degradation using dielectric spectroscopy [74].

Dielectric spectroscopy measurements can be performed on every kind of insulation system (solid and liquid). In particular this tool can be easily adapted for different insulation systems, e.g. thick power cables, thin I&C cables, shielded/unshielded cables, flat specimens, etc. Dielectric spectroscopy measurements can be performed on-field on coaxial cables of any length and size. In case of multipolar non-shielded cables the measurement can be performed considering each couple of conductors as electrodes: the tested insulation in this case is the series of the insulation surrounding the conductors.

### 2.3.4 Polarization-Depolarization Current Measurement

Polarization-depolarization current measurement is a useful technique to investigate the conductivity and the dielectric response in the time domain of polymeric dielectric materials. The measurement is constituted by two phases; the first consists of applying a DC voltage to the insulating material and acquire the value of the current as a function of time; once the current has reached a steady value, the polarization

phase is completed. The second phase starts switching off the voltage generator; the specimen is instantly short-circuited and the value of the depolarization current is recorded until it reaches negligible values [75, 76, 77].

During the first phase, the transient current circulating through an insulation may be considered as the sum of three currents:

- the capacitive current, corresponding to the current that charges the insulation like a pure capacitor. It's a current with a high value at the beginning which decreases to zero quiet rapidly. After a few seconds or tens of seconds or more depending on the capacitance of the tested cable, it becomes negligible compared to the current to be measured.

- the absorption or polarization current, including different polarization effects but representing at the time scale of our concern the current generated by the alignment of polar molecules in the applied DC electric field and by the presence of heterogeneities in the dielectric. This current decreases slower than the capacitive current. It may require several minutes or more depending on the insulation quality to reach a value close to zero.

- the conduction current (resistive or leakage current), corresponding to the current that continuously flows through the insulation and giving the relevant information concerning the quality of the insulation. It is small and stable in time for good insulations. It is large and may increase with time for poor insulations.

Polarization-depolarization currents evaluate bulk properties of the insulation. Changes in these characteristics, which are caused by structural changes in the material due to various modes of deterioration such as water treeing, oxidation, presence of contaminants, and so on, could be related to insulation aging [75, 78].

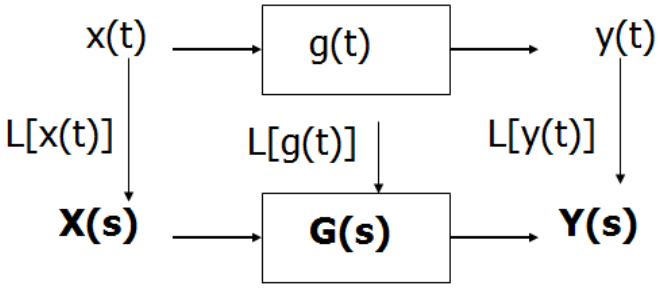


Figure 2.14. Scheme of the Laplace transform approach for the evaluation of the dielectric response.

The time domain analysis of the dielectric response, $g(t)$, requires the solution of linear differential equations with time-dependent coefficients. For the solution of

these equations, the Laplace's transform can be used. A schematic representation of this method is presented in Fig.2.14, where $G(s) = L[g(t)]$ represent the dielectric system, $X(s) = \epsilon_0 E(s)$ is the perturbation, $Y(s) = P(s)$ is the polarization caused by the electric field. Making three assumptions:

- $g(t) = 0$ for $t < 0$, i.e. system initially at rest;
- $g(t) = 0$ for $t \to \infty$, no permanent polarization;
- linear system (superposition of the effects is allowed),

the relation between $X(s)$ and $Y(s)$ become:

$$P(s) = \epsilon_0 E(s) G(s), \tag{2.15}$$

whose inverse transform gives the expression of $P(t)$:

$$P(t) = \epsilon_0 E(t) * g(t) = \epsilon_0 \int_0^t E(t-\tau) g(\tau) d\tau \tag{2.16}$$

The contribution to the response of the system at time $t$, caused by the impulse of area $\epsilon_0 E(t-\tau_i)$, $\Delta\tau$, applied at time $(t-\tau_i)$ is expressed by:

$$P_i(t) = \epsilon_0 E(t-\tau_i) g(\tau_i) \Delta\tau \tag{2.17}$$

Because of the third hypothesis, the overall response at time $t$ is given by the sum of individual contributions:

$$P(t) \cong \sum_{i=1}^{n} \epsilon_0 E(t-\tau_i) g(\tau_i) \Delta\tau \tag{2.18}$$

where $g(\tau_i)$ is a weighting function that allow us to know at the time $t$, the effect of the applied electric field on the polarization $\tau_i$ seconds before; $g(\tau_i)$ is therefore an indicator of the memory of the system. Applying a step input $E(t) = Eu(t)$, the polarization $P(t)$ become:

$$P(t) = \epsilon_0 E \int_0^t g(\tau) u(t-\tau) d\tau \tag{2.19}$$

knowing that:

$$D(t) = \epsilon_0 E(t) + P(t) = \epsilon_0 E \left[ u(t) + \int_0^t g(\tau) u(t-\tau) d\tau \right] \tag{2.20}$$

As known, the polarization current density can be expressed as

$$J_c = J_s + \frac{\partial D(t)}{\partial t} = \gamma E + \frac{\partial \left[\epsilon_0 E(t) + P(t)\right]}{\partial t} \tag{2.21}$$

where the first term $J_s$ is the conduction current, and the second term is the displacement current. The expression of the displacement current becomes: where $\delta(t)$ is the Dirac delta. The displacement current becomes zero at the end of the charging phase, so the value of the conductivity is given simply by the relation:

$$\gamma = \frac{J_c}{E} \tag{2.22}$$

Once the steady current condition is reached, the voltage is removed and the specimen is short-circuited ($E = 0$). This corresponds to the application of a new perturbation to the system, with expression

$$x(t) = -Eu(t) \tag{2.23}$$

which gives raise to a depolarization current. Applying the Laplace's transform, it is possible to obtain:

$$J_d(t) = -\epsilon_0 E \left[\delta(t) + g(t)\right] \tag{2.24}$$

For $t > 0$, the expression of the dielectric response in the time domain becomes:

$$g(t) = -\frac{J_d(t)}{\epsilon_0 E} \tag{2.25}$$

Frequency domain analysis can be performed using Fourier's transform. Applied to the dielectric response, $g(t)$, it holds:

$$F\left[g(t)\right] = G(j\omega) = \int_0^{+\infty} g(t) exp(-j\omega t) dt \tag{2.26}$$

providing the frequency spectrum $G(j\omega)$. Starting from the expression of the inverse transform $P(t) = L^{-1}[P(s)]$,

$$F\left[g(t)\right] = G(j\omega) = \int_0^{+\infty} g(t) exp(-j\omega t) dt \tag{2.27}$$

and applying Fourier's transform, the following expression is obtained:

$$P(\omega) = \epsilon_0 E(\omega) \chi(\omega) \tag{2.28}$$

where $\chi(\omega) = F[g(t)]$ is a complex quantity. The real part represent the polarization in phase with the field, the imaginary part is quadrature component.

$$\begin{aligned}\chi(\omega) =&\chi'(\omega) - j\chi''(\omega) = \int_0^{+\infty} g(t)exp(-j\omega t)dt \\ &= \int_0^{+\infty} g(t)cos(\omega t)dt - j\int_0^{+\infty} g(t)sin(\omega t)dt\end{aligned} \tag{2.29}$$

When $\omega = 0$ the imaginary part of the complex susceptibility $\chi(\omega)$ is equal to zero and the real part must be finite:

$$\chi'(0) = \int_0^{\infty} g(t)dt \tag{2.30}$$

$$\chi''(0) = 0 \tag{2.31}$$

Actually, the real part of susceptibility obtained using the FFT is associated only with interfacial polarization, and is indicated with $\Delta\chi'$. Indeed, it is impossible to evaluate the contribution of electronic and dipolar polarization, since the relaxation times associated with these phenomena are generally below 1 ms. Low frequency property variations are usually associated with the degree of crystallinity, especially for semicrystalline polymer. The polarization process is in this case predominantly influenced by the interfaces between crystalline and amorphous phases. In carbon black filled materials, with relatively high conductivity, low-frequency polarization is often hidden by the quasi-DC conduction process [67], with dielectric losses proportional to $1/\omega$.

This technique is currently used for MV and HV cables. Because on-site tests can only be performed on de-energized cables, the tests had to be coordinated with the regular maintenance work schedule of the utility. A large change in depolarization current could indicate advancing deterioration of the insulation and increasing probability of failure. Long-term aging of miniature cables resulted in a significant increase in the area under the polarization current curve [79]. Also the short-term depolarization currents vary with cable aging; the advantage of this technique is the very short time required to perform such measurements. These measurements take seconds, whereas the commonly used techniques of the long-term depolarization current measurements require minutes or even hours [79, 80].

Concerning the possible application to low-voltage NPP cables, polarization-depolarization currents can complete the information obtained from IR meaurements, applied in standards of LV accessories [81]. The measurement presents similar pros and cons to those previously mentioned for dielectric spectroscopy, especially when the properties of unshielded cables have to be evaluated.

# Chapter 3

# Experimental Setup and Results

The following sections, 3.1 and 3.2, describe the cable selection and the accelerated aging carried out to obtain a significant degradation of the cable materials in reasonable times. The experimental setup for electrical testing is described in sections 3.3.1, 3.3.2 and 3.3.3, for space charge, dielectric spectroscopy and polarisation-depolarisation current, respectively. The experimental setup for tensile tesing is described in section 3.3.4. Finally, experimental results are presented in sections 3.4.1-3.4.4.

## 3.1 Specimens

The selection of cables to test in the ADVANCE project was an important task, because the results of the project are based on the initial cable choice. On the one hand, the selection should present a wide range of different cable types, which are representative of different NPP designs (see section 1.1). On the other hand, cable selection must take into account the limited access to cable samples, especially those aged in operation. Samples of operation aged cables which can be used for testing are extremely limited. Usually, cables taken out from the containment cannot be used because of strict waste handling requirements. In some plants, there are small amounts of samples placed near the cables in operation which can be easily taken out, but the length is often too short for electrical measurement and LOCA-test.

Within the EU project, each partner had the right to propose at least one cable. Therefore, 7 different cables were aged and studied. When performing accelerated aging under radiation, very high values of dose rate compared to those found in NPP have to be used, in order to accelerate aging reactions. In these conditions, diffusion-limited oxidation could in some cases produce non-homogeneous degradation along the sample thickness (see section 1.4.1). Furthermore, insulations and fillers are usually made of different materials; this fact would complicate the interpretation

of the results. Lastly, space charge density measurements do not allow multipolar cables to be tested. Taking into account these considerations, the cable outer sheath and the electromagnetic shield (when present) were removed, leaving only the inner wires subjected to thermal and radiation stresses. When possible, the jacket was peeled with a lathe, in order to produce flat specimens (side $30 - 60$ mm, thickness $0.1 - 0.5$ mm) which were also aged. However, due to the irregularity of the sample surface, the results of electrical testing are not repeatable and won't be presented in this work.

For the aim of this Ph.D. thesis, the analysis will be focused on three cable insulating materials, i.e. XLPE, EPR-based and EVA-based insulation. The description of the cable samples is presented below. Further information about material formulations are confidential and cannot be disclosed in this work.

### 3.1.1 Cross-Linked Polyethylene

The XLPE insulation is taken from the LOCA coaxial cable shown in Fig.3.1. The cable is composed of the following parts:

- conductor: copper; solid wire, diameter: 0.6 mm;
- electrical insulation: XLPE (almost pure); thickness: 1.6 mm;
- three screening layers of copper/polyester tape, copper wire braid, copper/polyester tape;
- outer sheath: EVA-PE blend (39.5% polymer); thickness: 4.3 mm.

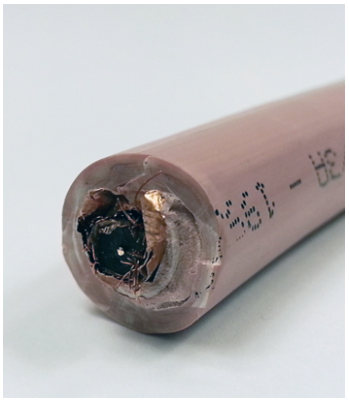

Figure 3.1. LOCA coaxial cable. XLPE insulation.

### 3.1.2 Ethylene-Propylene Rubber

The EPR-based insulation investigated is taken from the LOCA power cable shown in Fig.3.2, composed of the following parts:

- conductors: copper; stranded wire, total diameter: 7 mm;
- electrical insulation: EPR-based (63.5% polymer); thickness: 1.2 mm;
- inner sheath (filler): CSPE-based (Hypalon);
- screen: 2 layers of steel; total thickness: 0.4 mm;
- other protectors: glass silk tapes (over and under the screen);
- outer sheath: CSPE-based (Hypalon); thickness: 2 mm.

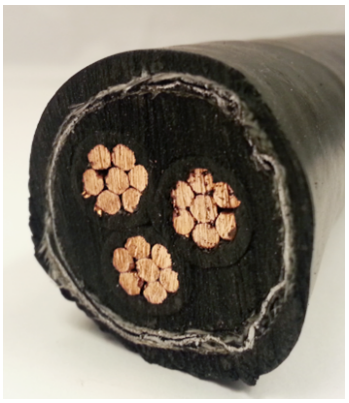

Figure 3.2. LOCA power cable. EPR-based insulation.

### 3.1.3 Ethylene-Vinyl Acetate

The EVA-based insulation investigated is taken from the LOCA measurement/instrumentation cable shown in Fig.3.3, composed of the following parts:

- conductors: copper; stranded wire, total diameter: 1.3 mm;
- electrical insulation: EVA-based, crosslinked (42% Polymer); thickness: 0.6 mm;
- inner sheath (filler): EVA-PE blend, crosslinked (36.5% Polymer) ;
- screen: copper wire braid;
- outer sheath: EVA-PE blend, crosslinked (36.5% Polymer). Thickness: 1.3 mm.

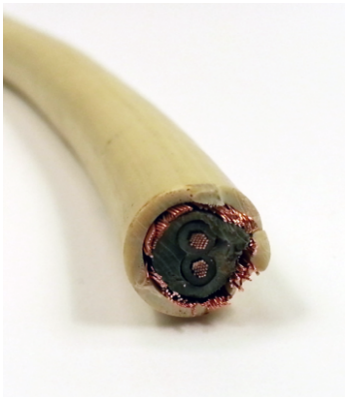

Figure 3.3. LOCA measurement/instrumentation cable. EVA-based insulation.

## 3.2 Accelerated Aging Experiment

For the multi-stress ageing of cable samples, a factorial experiment, consisting in the application of gamma-radiation at different dose rates and temperatures, was carried out. Thermal and radiation stresses were applied simultaneously in order to take into account synergistic effects.

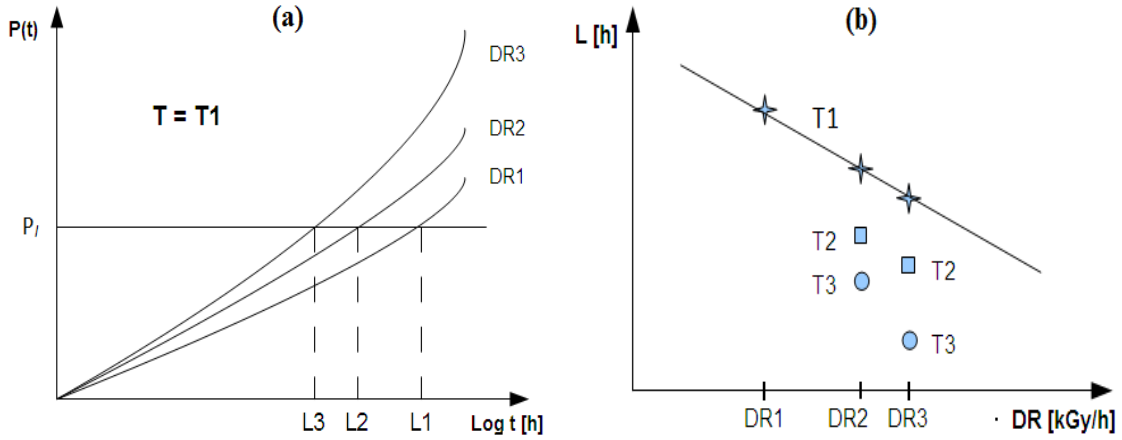


Figure 3.4. (a) $P(t)$ is a generic aging indicator, related to the cable electrical properties. $P_l$ is the value corresponding to 50% absolute EaB. (b) The cable life, based on the electrical property, can be plotted as a function of dose rate and temperature.

The goal is to obtain the relation between an aging indicator (based on electrical properties) and the aging time or the total absorbed dose, at fixed temperature. Fig.3.4a shows a schematic example, where $P(t)$ is a generic aging indicator. The

end-of-life value $P_l$ should be correlated with mechanical properties, e.g. elongation at break. Once this property falls below the 50% absolute, the corresponding electrical property value is taken as the end-of-life. In this way, the life ($L$) can be plotted as a function of the dose rate and temperature (Fig.3.4b).

The accelerated aging experiment was performed by ÚJV Řež a.s. (http://www.ujv.cz/en/). The irradiation facility is a well-type $^{60}Co$ gamma-ray source, with the cobalt placed in the center of a cylindrical irradiation chamber (Fig.3.5a). The dose rate depends generally on the distance from the cobalt source. The dose rate gradient within the sample depends on the sample thickness and composition (see section 1.4.1). The vertical non-homogeneity depends on the distance from the cobalt source and its size. To perform irradiation at elevated temperature, a thermobox was assembled before starting the experiments. The thermobox presented two circular heating elements in the bottom, while a fan distributed homogeneously the air inside the thermobox. During the experiment, the thermobox is closed by a top cover.

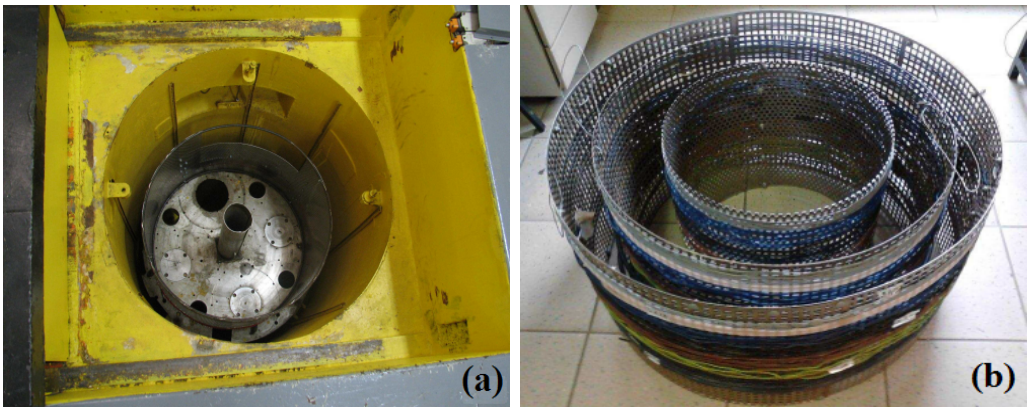


Figure 3.5. (a) ÚJV Řež a.s. irradiation facility ROZA. (b) Samples fastened on perforated stainless steel cylinders in order to obtain three different dose rates.

The chosen dose rates aimed at obtaining a total absorbed dose between $10^5$ and $10^6$ Gy within 1000 hours. Samples were carefully fastened on three perforated stainless steel cylinders with diameter 0.4 m, 0.6 m and 0.8 m, in order to obtain three different dose rates at the same time (Fig.3.5b). Cylinders were placed inside the thermobox, symmetrically around the guide tube for the cobalt source. Continual fanning of the irradiation shaft ensured periodical change of fresh air inside the thermobox (see section 1.4.1). The temperature was recorded using a thermometer with two sensors, while dosimetry was based on the system alanine/electron spin resonance (ESR) spectrometry [82]. A 10 meter-long cable specimen was carefully fastened on each cylinder. The scheduled total duration of tests is 1000 hours, for each combination of dose rate and temperature. The cable properties are measured

every 200 hours.

Test specifications involved initially three radiation dose rates and three temperatures, i.e. 9 combinations dose rate-temperature in all (factorial experiment). After the first aging experiment (Exp. 1-2-3, Table 3.1), ÚJV Řež a.s. decided to replace the $^{60}Co$ source, because of its low activity. After the replacement, dosimetry was performed to evaluate the dose rate increase on each support cylinder. It was thus decided to perform a new experiment at the same temperature of the first one, with higher radiation dose rates. This means that test specifications are still composed of 9 different stress combinations (Table 3.1) but involve now six radiation dose rates and two temperatures, renouncing the intermediate aging temperature. Hence, test temperatures were only $T_3 = 85°C$ and $T_1 = 55°C$. Due to the huge number of measurements required to perform a complete factorial experiment, only one cable was aged with all possible stress combinations.

Table 3.1. Accelerated aging experiment identification numbers.

| **Exp. No.** | **Temperature** [°C] | **Dose Rate** [kGy/h] |
|---|---|---|
| 1 | 85 | 0.86 |
| 2 | 85 | 0.39-0.42 |
| 3 | 85 | 0.28-0.30 |
| 4 | 85 | 2.72-2.74 |
| 5 | 85 | 1.06-1.58 |
| 6 | 85 | 0.76-0.94 |
| 7 | 55 | 2.72-2.74 |
| 8 | 55 | 1.06-1.58 |
| 9 | 55 | 0.76-0.94 |

## 3.3 Experimental Setup

The following sections present the experimental setup for space charge measurement (3.3.1), dielectric spectroscopy (3.3.2) and polarization-depolarization current measurements (3.3.3). Tensile testing (3.3.4) was perfomed at the Department of Fibre and Polymer Technology (KTH, http://www.kth.se/en/che/divisions/polymeric-materials) in the framework of the Training and Mobility Program of ADVANCE.

### 3.3.1 Space Charge

A schematic representation of the space charge measurement (PEA method) experimental setup has been previously shown in Fig.2.9. The experimental setup consists of:

- high voltage DC generator;
- pulse generator (peak amplitude: 4 kV; pulse width: 40 ns; repetition frequency: 110 Hz); the pulse generator needs, like input, a high voltage DC ranging between 0 and 5 kV.
- Pulsed Electro-Acoustic (PEA) cell;
- digital oscilloscope;
- PC equipped with software LabView for signal acquisition;
- a GPIB card to interface computer and oscilloscope.

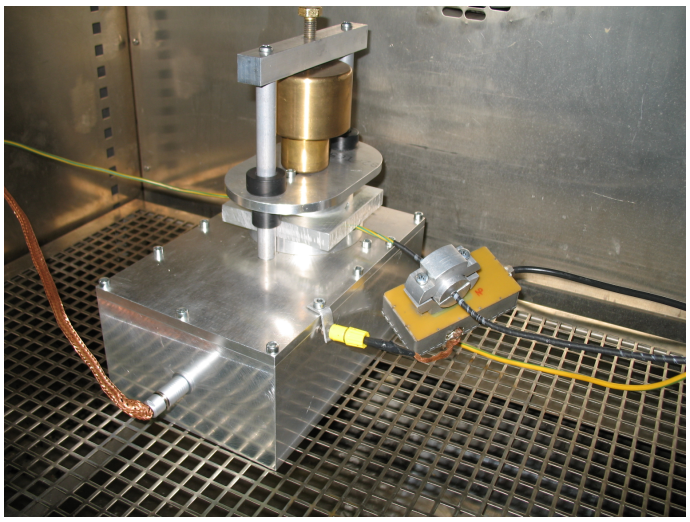

Figure 3.6. The PEA cell for cable testing. Note the semi-conductive tape and the pulse output connector.

The PEA cell presents the low-voltage electrode, a piezoelectric transducer and an amplifier with wide bandwidth. Each specimen was placed on the PEA cell with the addition of a silicon oil drop to improve sample and electrode coupling. Since low-voltage cables do not present a semi-conductive screen, a portion of the cable is wrapped in a semi-conductive tape (Fig.3.6). At this position, the pulse is injected through an opportune connector. The average poling field $E_p$ was set to 20 kV/mm. Experiments were performed at room temperature.

### 3.3.2 Dielectric Spectroscopy

A schematic representation of dielectric spectroscopy experimental setup has been previously shown in Fig.2.12. Dielectric spectroscopy is performed using a dielectric analyzer:

- frequency range: $10^{-2} - 10^{6}$ Hz;
- input voltage: 3 $V_{rms}$;
- test temperature: 50°C.

For cable testing, a cylindrical geometry like that of coaxial cables, is required. The input voltage is supplied to the cable conductor, while an outer wire mesh constitutes the second electrode (Fig.3.7). In order to obtain the actual values of $\epsilon'$ and $\epsilon''$, the reference capacitance $C_0$ has to be calculated. The control software considers only a planar geometry, therefore the values of equivalent sample thickness $s$ and electrode area $A$, has to be found using the relation:

$$\frac{C_0}{\epsilon_0} = \frac{A}{s} = \frac{2\pi l}{ln\frac{R_2}{R_1}} \tag{3.1}$$

where $l$ is the length of the wire mesh, $R_1$ the conductor radius and $R_2$ the cable radius.

The choice of the test temperature is another important issue (see section 2.3.3). After many tests carried out at different temperatures, it was observed that a higher temperature improved test repeatability. In order to stay below the lowest aging temperature (55°C), the test temperature of 50°C was chosen for dielectric spectroscopy.

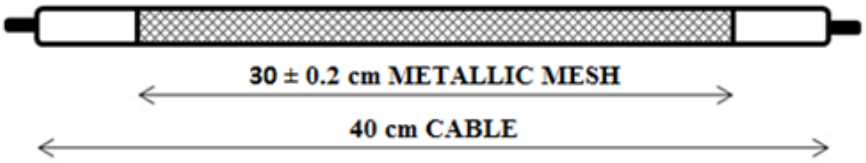


Figure 3.7. Dielectric spectroscopy. Cables are tested using a wire mesh as low-voltage electrode [83].

### 3.3.3 Polarization-Depolarization Current Measurement

The experimental setup of polarization-depolarization current measurement is composed by (Fig.3.8):

- high voltage DC generator;
- programmable electrometer;
- test cell;
- PC equipped with software LabView for signal acquisition;
- a GPIB card to interface computer and oscilloscope;
- a switch;

During the polarization phase, the DC generator supplies the voltage to the specimen (switch (1) in position A). Once the current reaches a steady value, the specimen is short-circuited (switch 1 in position B) and the depolarization phase begins. The current is measured by a programmable electrometer connected to the PC with a GPIB. The resistor protects the electrometer: its value reduces the current in case of breakdown and does not influence the results.

One of the main drawbacks of polarization-depolarization current measurement is the long test duration. The orientation of electric dipoles within the dielectric, and therefore the achievement of the conduction current at steady state, can take several hours. For this reason, a system able to test three samples at the same time was developed. The test cell is shown in Fig.3.9.

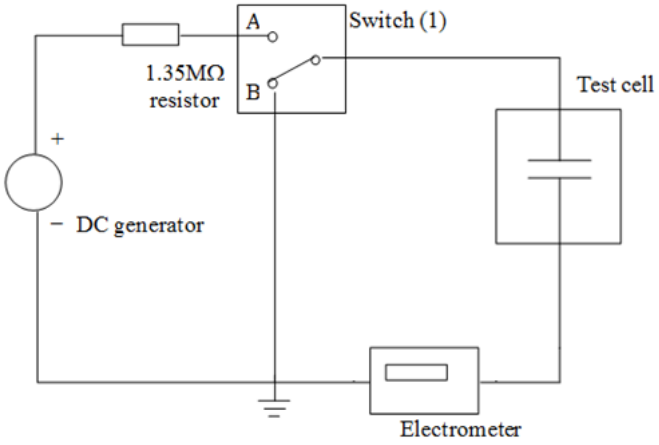


Figure 3.8. Polarization-depolarization current measurement. Experimental setup scheme.

Fig.3.9 shows three samples under test. Labels A, B and C indicate the main parts of the system:

- (A) high voltage distributor, connected to the high voltage DC generator;

- (B) guard ring, in order to ground any current flowing on the cable outer surface, without affecting the measured values;
- (C) measurement zone; as for dielectric spectroscopy, a wire mesh was used to realize a cylindrical capacitor. For these measurements, the length of the mesh was 10 cm.

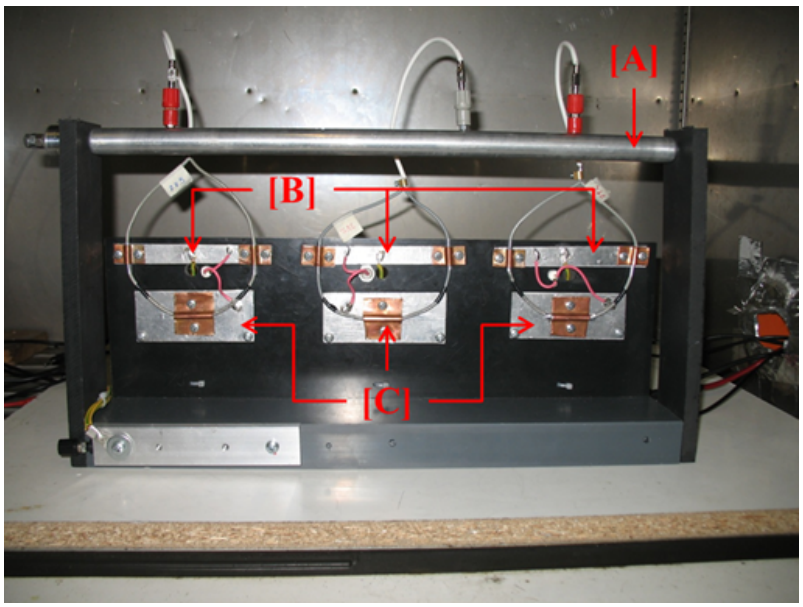


Figure 3.9. Polarization-depolarization current measurements. The cell used for low-voltage cable samples [83].

All the guard rings are connected to the ground of the HVDC generator. Measured currents are in the range of $10^{-9} - 10^{-13}$ A, therefore, this kind of measurement is very sensitive to electromagnetic background noise. For this reason, the system was placed in a metallic box, to screen electromagnetic interferences.

The electrometers send data to a PC, by means of a GPIB card. The acquisition software was developed in LabVIEW environment. The current values were recorded at fixed time intervals and the depolarization current files can be subsequently processed by FFT. The user interface allows to set the acquisition intervals.

The test temperature was set to 50°C for XLPE and EPR-based insulation, while EVA-based insulations were tested at room temperature. Test voltage was optimized to obtain conduction current values above the electrometer sensitivity, approximately $10^{-12}$ A. After many attempts, the test voltage for the evaluation of the electrical properties was fixed to:

- $V_{test} = 8$ kV for XLPE cable insulation;

- $V_{test} = 0.6$ kV for EPR-based insulation;
- $V_{test} = 4.8$ kV for EVA-based insulation.

### 3.3.4 Tensile testing

The tensile properties were measured using a load frame testing machine 3.10:

- extension rate of 50 mm/min;
- initial gauge length of 40 mm;

Samples were conditioned at 25°C and 50% relative humidity for 24 hours prior to testing.

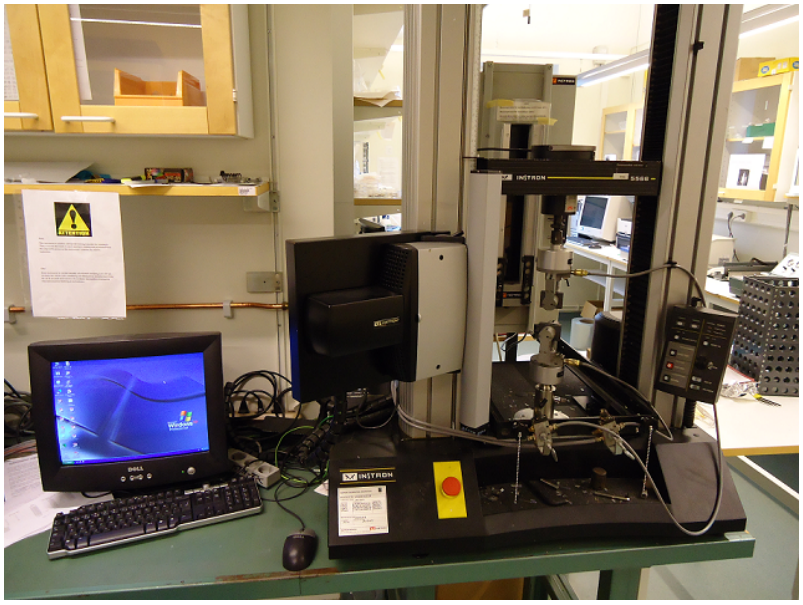

Figure 3.10. Tensile testing experimental setup.

In the case of XLPE insulated cable, sample preparation resulted difficult because of the cable design (Fig.3.1). The thin conductor often breaks during the extraction and it is very difficult to produce $70 - 80$ mm long samples required for a gauge length of 40 mm. Therefore, the tensile properties were measured using a load frame testing machine with extension rate of 25 mm/min and initial gauge length of 20 mm. Samples were conditioned at 25°C and 50% relative humidity for 24 hours prior to testing.

## 3.4 Experimental Results

The following section briefly presents the experimental results of space charge measurements (3.4.1). Then, dielectric spectroscopy and polarization-depolarization current measurement results are instead discussed more deeply in sections 3.4.2-3.4.4 for each cable insulation tested, i.e. XLPE, EPR-based and EVA-based.

### 3.4.1 Space charge measurement results

The application of the PEA method on XLPE insulations always resulted in very low and noisy signal amplitude. This fact was explained considering the thin conductor which characterizes the XLPE-insulated wire, which affects the pulse propagation.

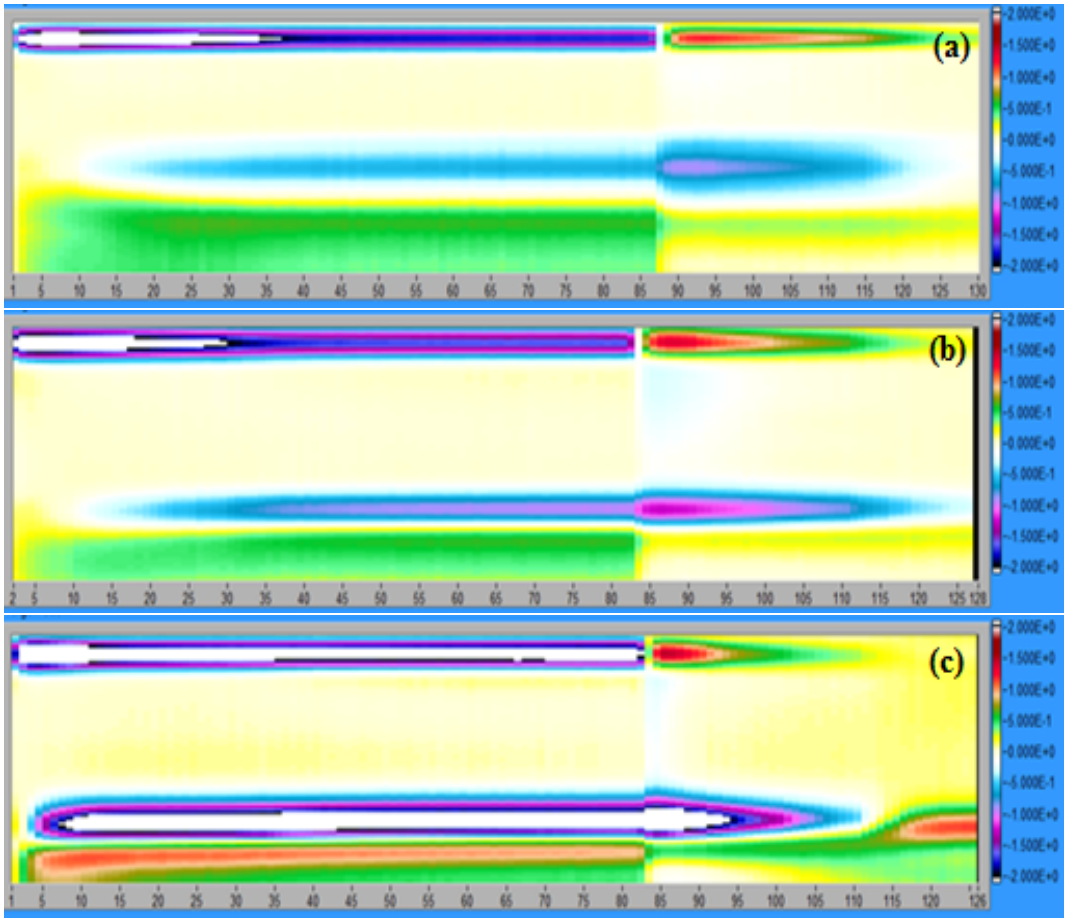


Figure 3.11. Space charge measurement patterns of EPR-based insulation after (a) 200, (b) 600, (c) 1000 aging hours at 55°C with irradiation dose rate of 1.58 kGy/h. Pattern scale: $\pm$ 2 $C/m^3$.

The main characteristic of each pattern is heterocharge formation at the anode (Fig.3.11). Almost certainly, this charge accumulates at the interface between the insulation and the PET film placed between conductor and insulation. This film is used by cable manufacturers to improve the extrusion process. This layer, however, can create a barrier to charge transport in the insulation. The accumulated charge clearly increases with aging. Heterocharges may be formed when one of the electrodes (in this case the anode, where the PET film is located) partially blocks the extraction of charges injected by the other one. Heterocharge formation results in enhancement of both electrode fields and reduced field stress in the bulk as it was appreciable for cables aged at the higher dose rates. Specimens aged at lower dose rate however, display a very small space charge accumulation. In addition to the heterocharge accumulating at the interface between insulation and PET foil, some positive charge appears in the bulk of the insulation as aging proceeds.

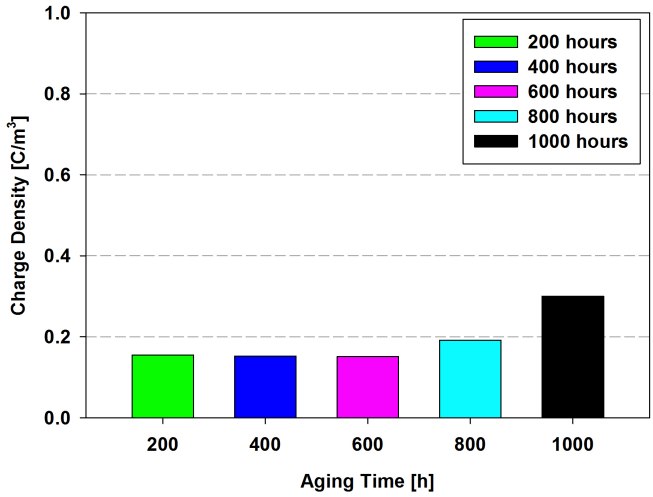


Figure 3.12. Variation of the maximum stored charge density with aging time for EPR-based insulations aged at 85°C with a radiation dose rate of 0.39 kGy/h.

The maximum stored charge density (Fig.3.12) slightly increases with the aging time. Anyway, these variations are close to the sensitivity of the instrument, which is (0.1 $C/m^3$). Depolarization curves, obtained 10 s after the volt-off, are shown in Fig.3.13 for samples aged at 85°C with irradiation dose rates of 0.39 kGy/h and 1.58 kGy/h. The depolarization curves obtained from specimens aged at 0.39 kGy/h show almost negligible variations with the aging time. The charge slowly leaves the insulation: after 100 seconds, the amount of charge is still the 90% of the initial value.

A higher dose rate leads to more evident aging effects, and the charge decay becomes faster increasing the aging time. Higher dose rates give rise to a completely

different behavior: the amount of charge after 100 s is around the 50% of the initial value. The variation of the apparent trap-controlled mobility with aging is not monotone, but depends on the applied stress level. As a result, it is not possible to derive suitable aging indicators from this property [84].

Qualitatively, the EVA-based insulation behaves similarly to the EPR-based one. Also in this case, the main characteristic of every pattern is heterocharge formation at the anode, i.e. at the interface between the insulation and the PET film. The depolarization curves obtained testing EVA-based cable insulation were almost overlapped. This in turn means that quantities like apparent trap-controlled mobility and trap depth distribution are not sensitive to aging.

Concluding, the application of space charge measurements to low-voltage NPP cables can give only a qualitative evaluation of material degradation. The interpretation of the results is not easy. The amount of accumulated charge is low for samples aged at low dose rate. Although differences depending on the aging stress level can be seen, the trend with aging time is not always clearly identified. Similar considerations can be made for trap-controlled mobility and trap depth distribution. The maximum charge after the volt-off usually does not present a monotone trend correlated with aging. The main issue consists in the cable design: loose contacts, small thickness, dispersive materials (additives) blurs the results of HV tests like space charge measurements [85, 84].

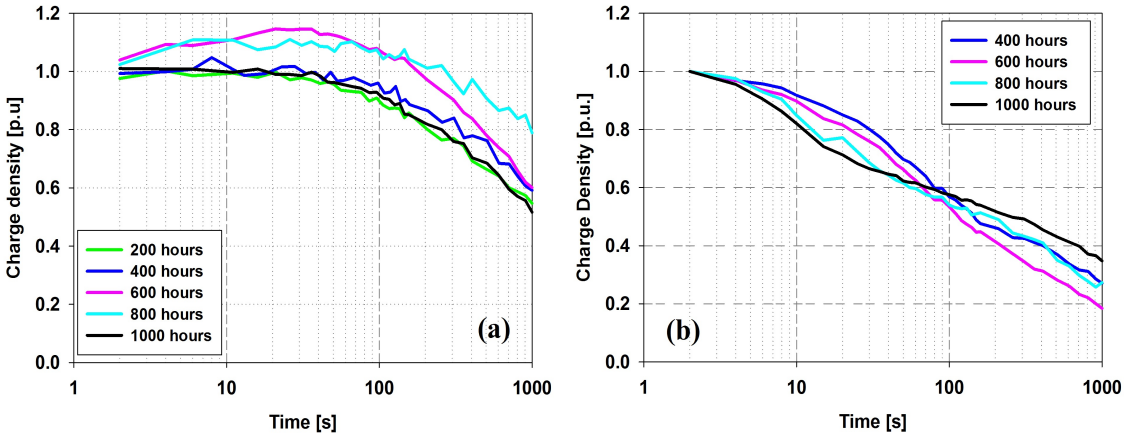


Figure 3.13. Depolarization current of EPR-based specimens aged at 85° with irradiation dose rates of (a) 0.39 kGy/h and (b) 1.58 kGy/h.

### 3.4.2 Cross-Linked Polyethylene

Figures 3.14, 3.15 and 3.16 depict the behavior of the real and imaginary part of permittivity vs. frequency, at different aging times.

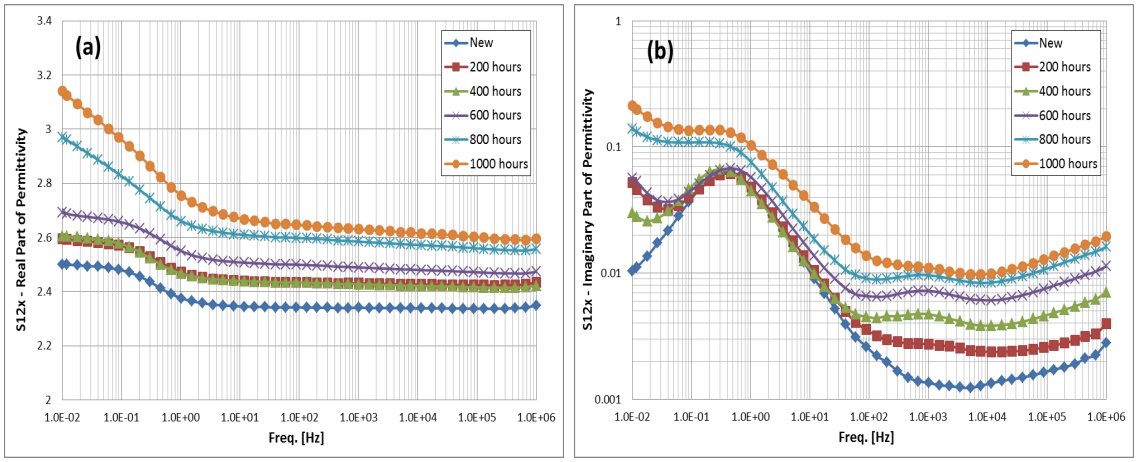


Figure 3.14. (a) Real and (b) Imaginary Part of Permittivity vs. frequency for XLPE specimens aged at 85° with irradiation dose rate of 0.42 kGy/h

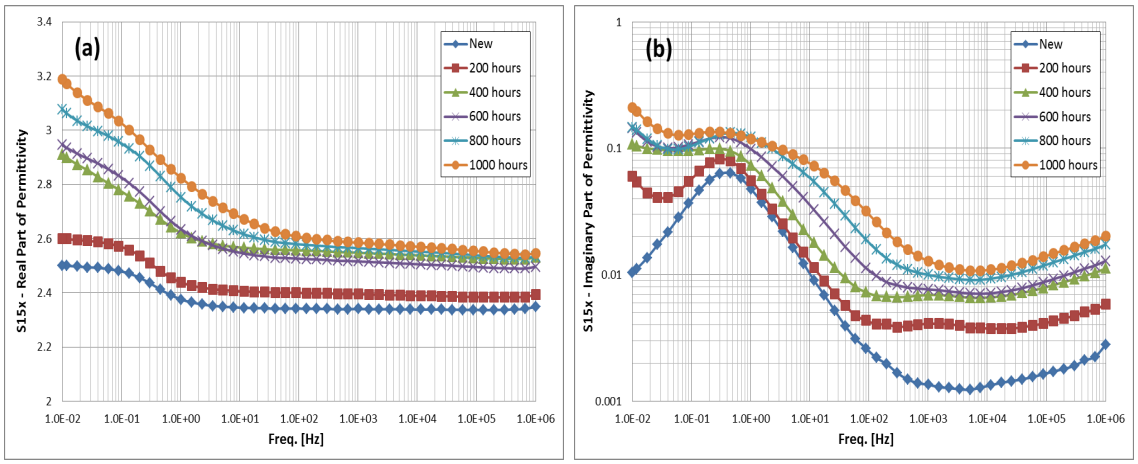


Figure 3.15. (a) Real and (b) Imaginary Part of Permittivity vs. frequency for XLPE specimens aged at 85° with irradiation dose rate of 1.06 kGy/h.

In Fig.3.14, samples are aged at 85°C with a dose rate of 0.42 kGy/h. Both properties increase gradually over the whole frequency range, and the increment of $\epsilon'$ becomes particularly evident at low frequency. Increasing the dose rate up to 1.06 kGy/h (Fig.3.15), the polarization peak of $\epsilon''$, located between 0.1 and 1 Hz,

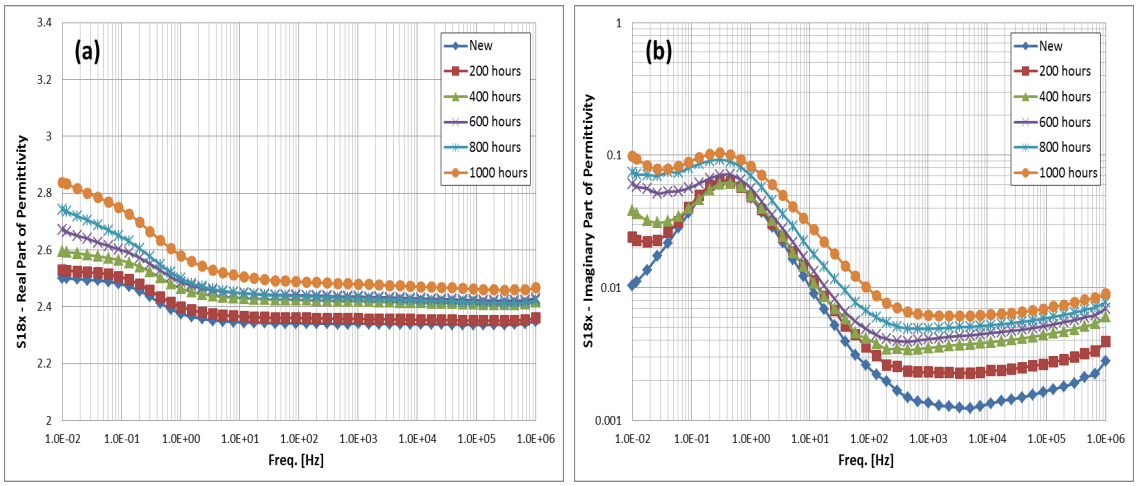


Figure 3.16. (a) Real and (b) Imaginary Part of Permittivity vs. frequency for XLPE specimens aged at 55° with irradiation dose rate of 1.06 kGy/h.

broadens. This is the main effect of the dose rate increase. Indeed, considering the absolute values of the properties, some differences are noticeable only at 200 h and 400 h of aging. The effect of aging temperature becomes clear comparing Fig.3.15 with Fig.3.16. At 55°C the increment of $\epsilon'$ and $\epsilon''$ with aging time over the whole frequency range is smaller, and the width of the polarization peak is comparable to that of samples aged at 85°C and 0.42 kGy/h.

The evolution of $\epsilon'$ and $\epsilon''$ with aging time and total absorbed dose can be compared choosing appropriate reference frequencies. In this case:

- 0.1 Hz will be representative of the low-frequency part of the spectra;
- 50 Hz will be representative of the middle-frequency region;
- 100 kHz will represent the high-frequency region.

Fig. 3.17, 3.18 and 3.19 show the real and imaginary part of permittivity as a function of the aging time at the chosen reference frequencies, 0.1 Hz, 50 Hz and 100 kHz, respectively. All properties except $\epsilon''$ at 50 Hz show similar trends: both properties increase linearly with the aging time and two behaviors related to the aging temperature are clearly identifiable. The effect of the dose rate can be noticed observing specimens aged at 85°C: the increment of $\epsilon'$, especially in the low-frequency range, appears smaller for samples aged at 0.42 kGy/h during the first half of the aging experiment. At 50 Hz (Fig.3.18b) the evolution of $\epsilon''$ follows an exponential law, related to the width of the polarization peak located between 0.1 and 1 Hz which broadens with aging time and increasing dose rate.

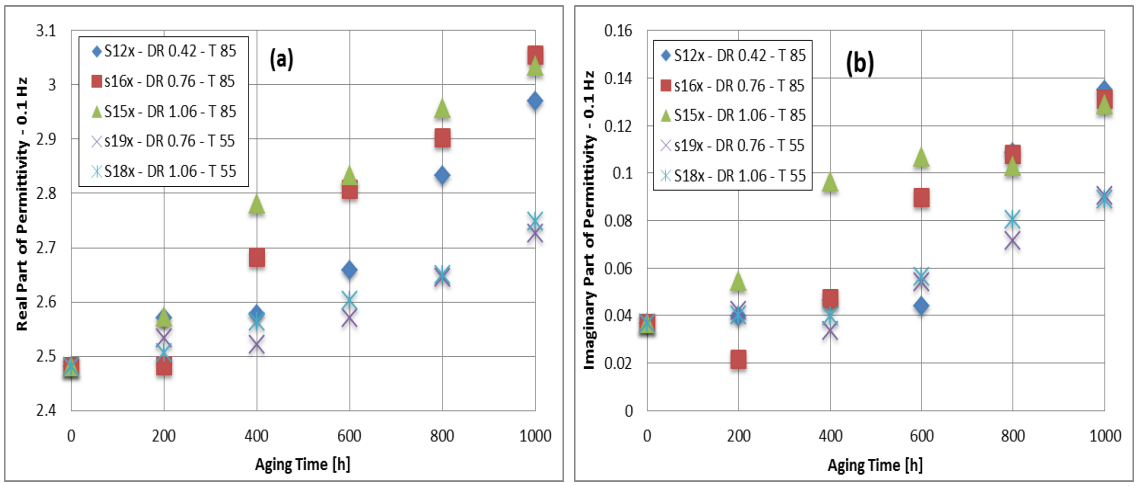


Figure 3.17. (a) Real and (b) Imaginary Part of Permittivity at 0.1 Hz vs. aging time for XLPE specimens.

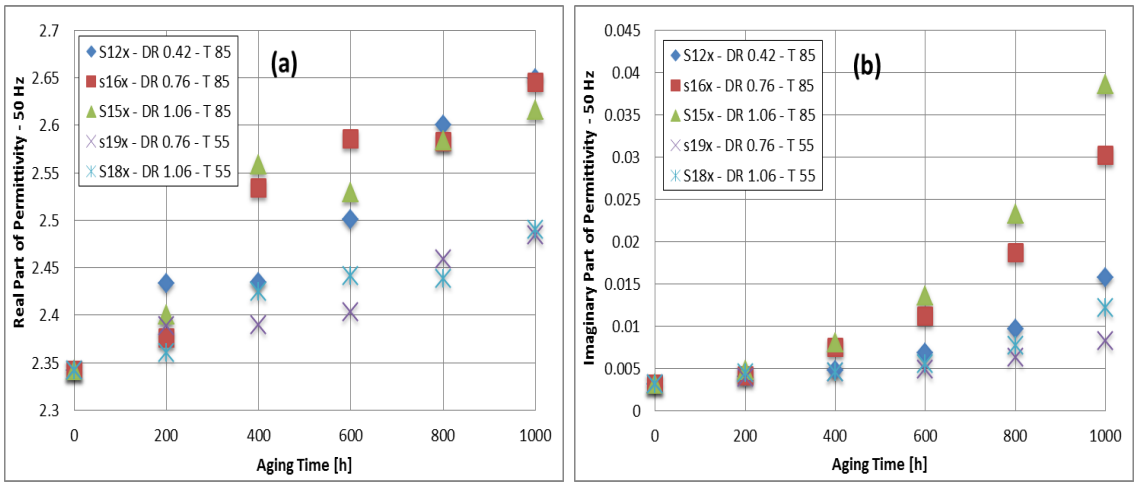


Figure 3.18. (a) Real and (b) Imaginary Part of Permittivity at 50 Hz vs. aging time for XLPE specimens.

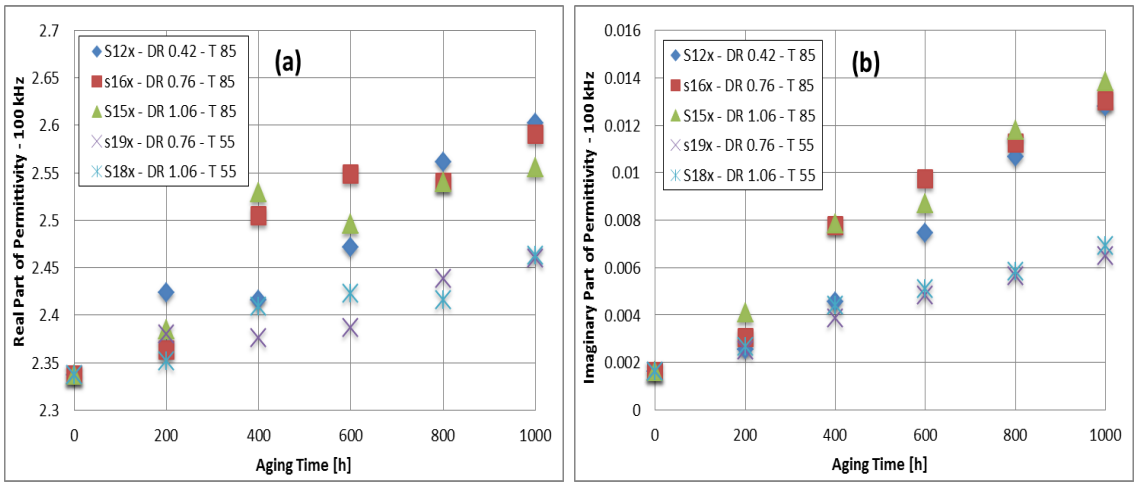


Figure 3.19. (a) Real and (b) Imaginary Part of Permittivity at $10^5$ Hz vs. aging time for XLPE specimens.

Fig.3.20, 3.21 and 3.22 show the real and imaginary part of permittivity as a function of the the total absorbed dose, at the chosen reference frequencies, 0.1 Hz, 50 Hz and 100 kHz, respectively. When the data are reported as a function of the total absorbed dose, the effect of the dose rate is highlighted, as a greater dose is required to reach the same value of $\epsilon'$ and $\epsilon''$. The imaginary part of permittivity at 50 Hz is presented in a semi-log plot in fig.3.21, therefore, its trend appears linear.

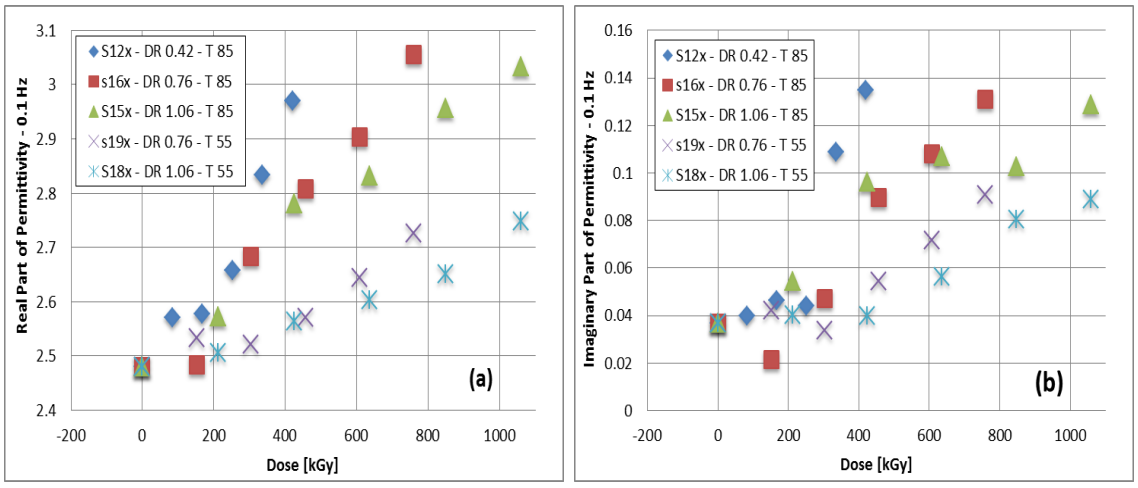


Figure 3.20. (a) Real and (b) Imaginary Part of Permittivity at 0.1 Hz vs. absorbed dose for XLPE specimens.

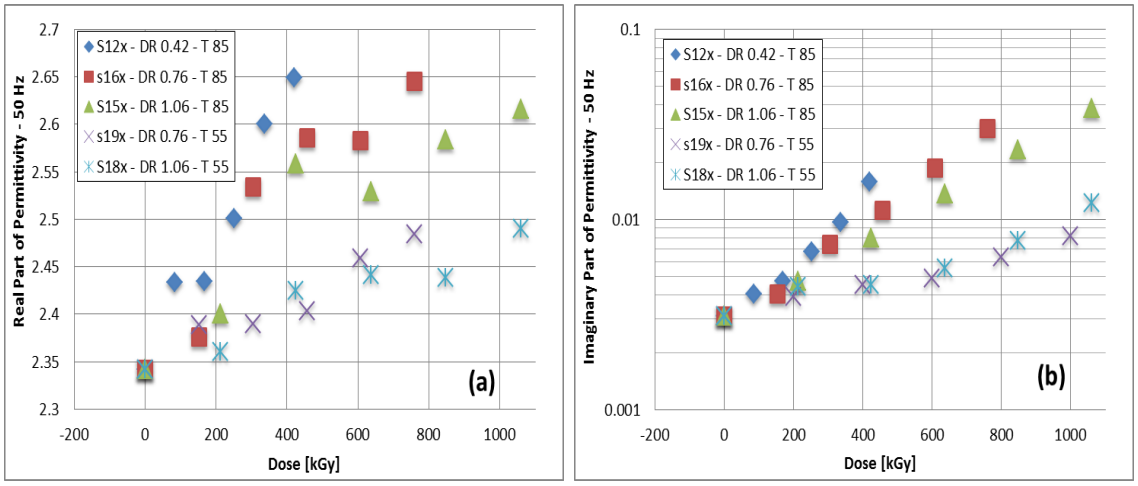


Figure 3.21. (a) Real and (b) Imaginary Part of Permittivity at 50 Hz vs. absorbed dose for XLPE specimens.

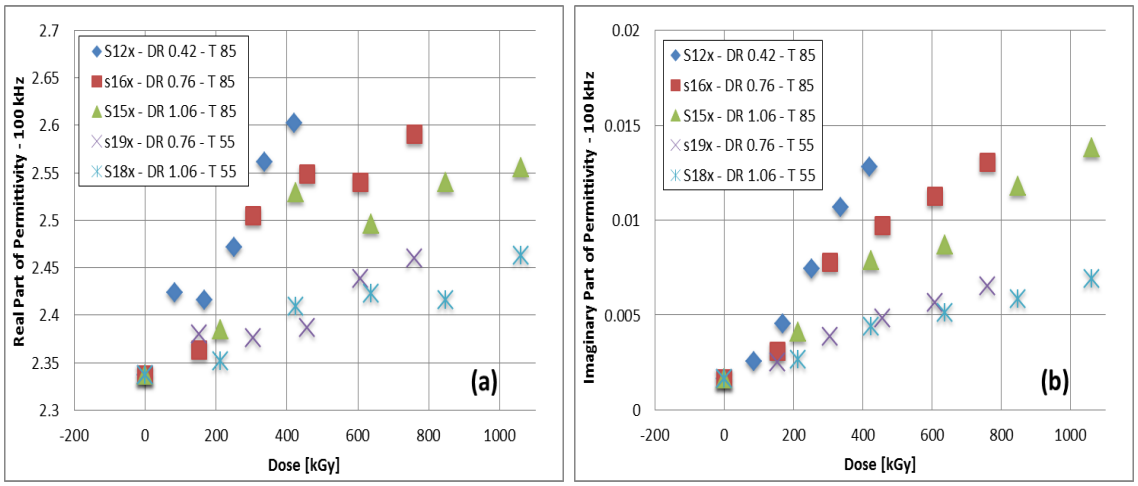


Figure 3.22. (a) Real and (b) Imaginary Part of Permittivity at $10^5$ Hz vs. absorbed dose for XLPE specimens.

Figures 3.23-3.26 summarize the results of polarization-depolarization current measurements carried out on XLPE insulation.

For samples aged at 85°C, the conduction current decreases with aging, but its behavior is non-monotone (Fig. 3.23a). Furthermore, for specimens aged at 55°C (Fig.3.23b), the conduction current falls below the measurement sensitivity already after 200 aging hours. This occurrs even increasing test voltage and temperature; above the chosen test voltage, i.e. 8 kV, the measurement became noisy because of the inception of partial discharges.

The behavior of the investigated electrical properties at very low frequency (VLF) is summarized by Fig.3.24. $\Delta\chi'$ increases with aging; below $10^{-2}$ Hz, its variation with frequency is almost negligible. $\chi''$ presents a polarization peak between 0.1 Hz and 0.01 Hz, which corresponds to the one evidenced by dielectric spectroscopy. Dielectric losses do not show significant variations below 0.01 Hz.

From the analysis at VLF, two quantities were extracted, i.e. $\Delta\chi'$ at $10^{-3}$ and the maximum value of $\chi''$, in order to compare their evolution with aging time and total absorbed dose at different stress levels (Figs.3.25 and 3.26). Both properties increase with aging, but considering the measurement uncertainty, it is not possible to draw robust conclusions about the effect of the different aging stress levels applied.

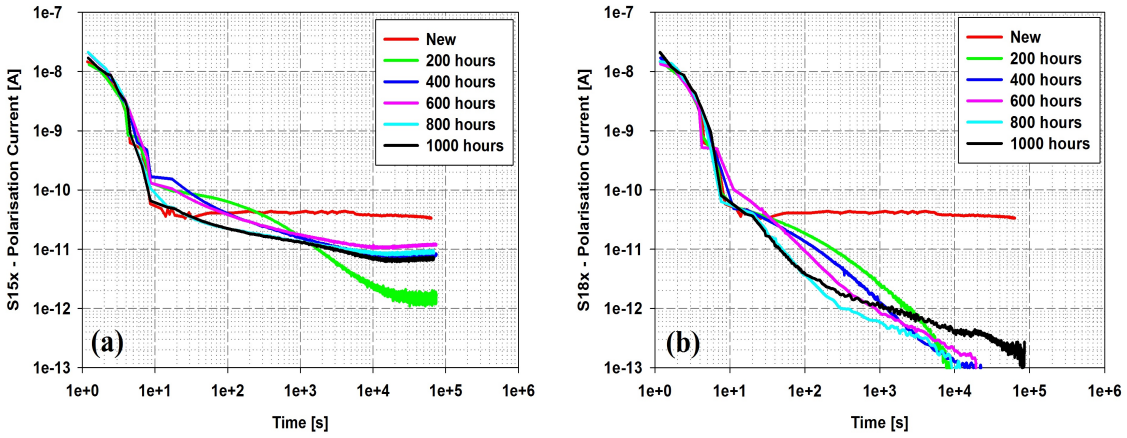


Figure 3.23. Polarisation current of XLPE samples aged at (a) 85°C and (b) 55°C with a dose rate of 1.06 kGy/h.

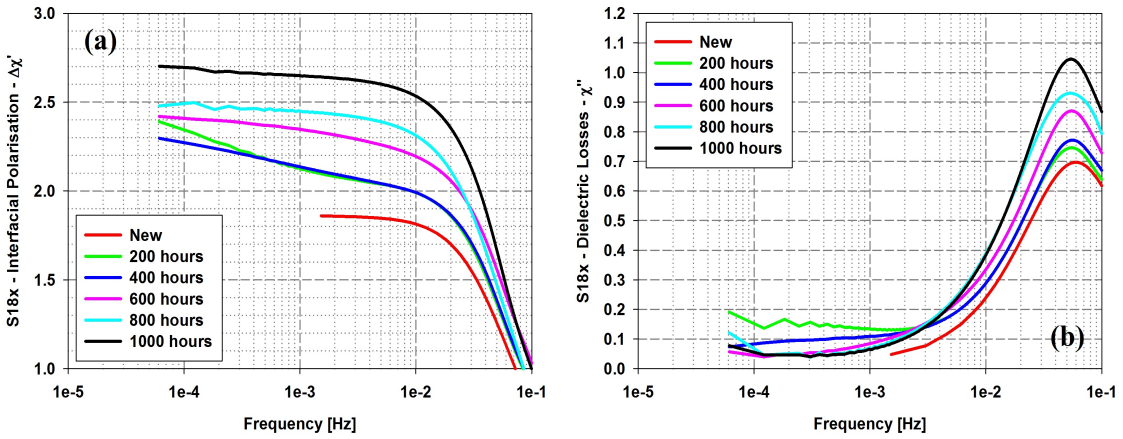


Figure 3.24. (a) Interfacial contribution to the Real Part of Susceptibility and (b) Dielectric Losses vs. frequency for XLPE specimens aged at 55°C and 1.06 kGy/h.

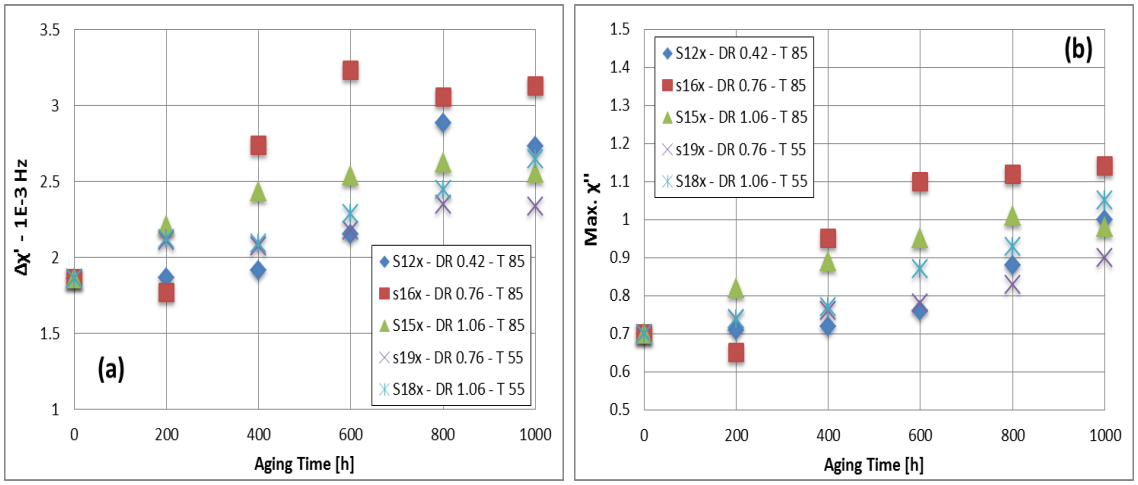


Figure 3.25. (a) Interfacial contribution to the Real Part of Susceptibility at $10^{-3}$ Hz and (b) maximum value of low-frequency dielectric losses vs. aging time for XLPE specimens.

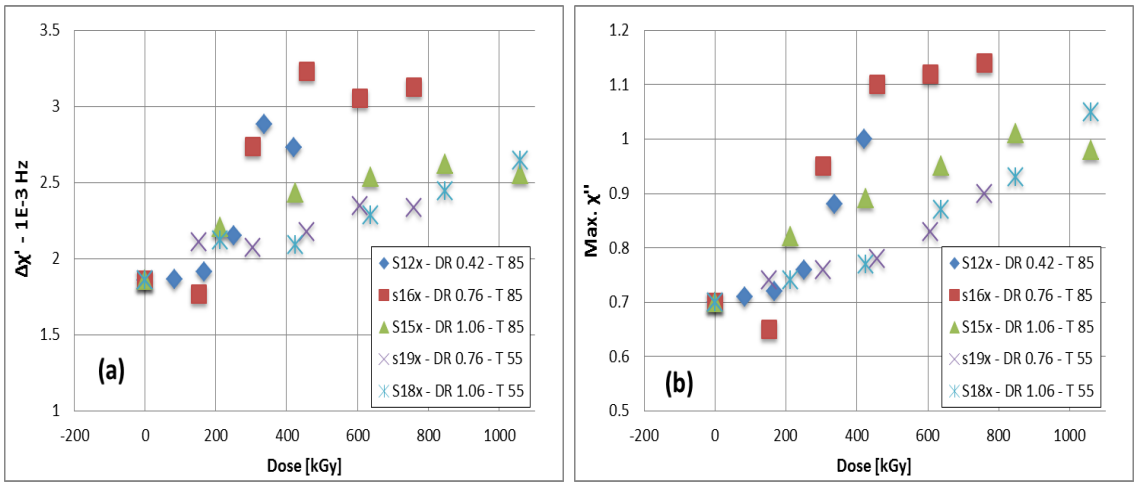


Figure 3.26. (a) Interfacial contribution to the Real Part of Susceptibility at $10^{-3}$ Hz and (b) maximum value of low-frequency dielectric losses vs. absorbed dose for XLPE specimens.

The results of mechanical testing are reported in figs. 3.27-3.30. Among the investigated properties, only the EaB has shown a monotone decrease which depends both on the aging time and the aging stress level. Indeed, the Young's modulus does not exhibit a regular trend with aging because its value is affected by a greater uncertainty (Figs. 3.29 and 3.30). Due to measurement errors caused by the reduction of the sample length (see section 3.3.4) for testing, the EaB values are higher than what would be expected for XLPE, but the relative changes between the samples are correct. Possible relationships between mechanical and electrical data would also be maintained, and since this is the main objective of this Ph.D. thesis, EaB data are acceptable for the use.

In fig.3.27, EaB values are reported in log-log plot to highlight a linear decrease, therefore following an inverse power law. It is noteworthy that the elongation at break decreases faster for higher dose rates, comparing specimens aged at 85°C. Moreover the effect of the temperature is clearly visible, in particular comparing specimens aged at 1.06 kGy/h and 0.76 kGy/h: the increment of the aging temperature causes a reduction of the cable life, as expected.

Plotting the EaB vs. the total absorbed dose (Fig.3.28) the effect of the dose rate is highlighted. The so-called physical dose rate effect can be observed comparing specimens aged at 0.42 kGy/h with those aged at 0.76 kGy/h: when the dose rate increases, a larger dose is required to reach the same level of degradation. This effect is clear at the beginning of the aging experiment, but becomes negligible above 200 kGy. Furthermore, the physical dose rate effect is blurred by the harsh aging conditions, which cause the EaB value to drop very fast when the dose rate is increased.

Visual inspection revealed that tensile testing results are affected by the formation of cracks on the insulation surface, i.e. local degradation. The physical dose rate effect becomes less evident for specimens aged at 55°C (Fig.3.28b). The effect of the aging temperature is also noticeable: as expected, decreasing the temperature, an higher dose is required to reach the same level of degradation.

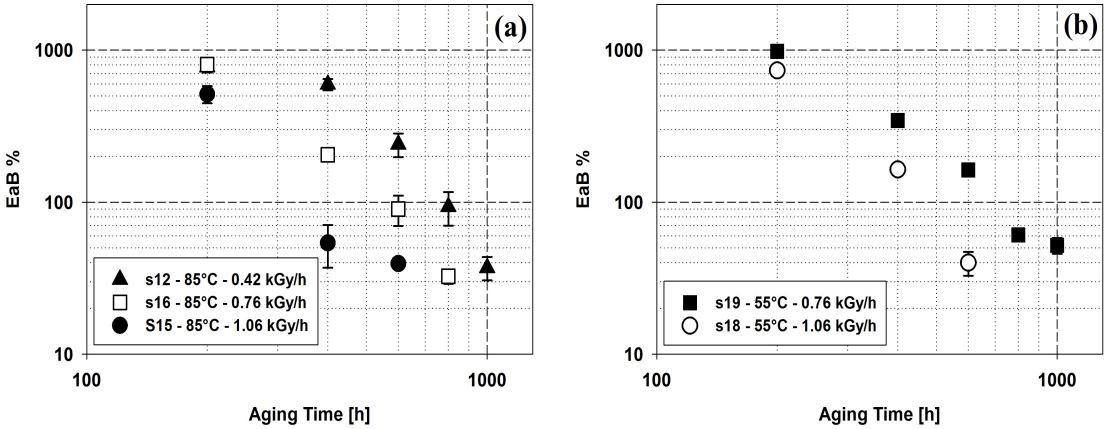


Figure 3.27. Elongation at break vs. aging time for XLPE samples aged at (a) 85°C and (b) 55°C.

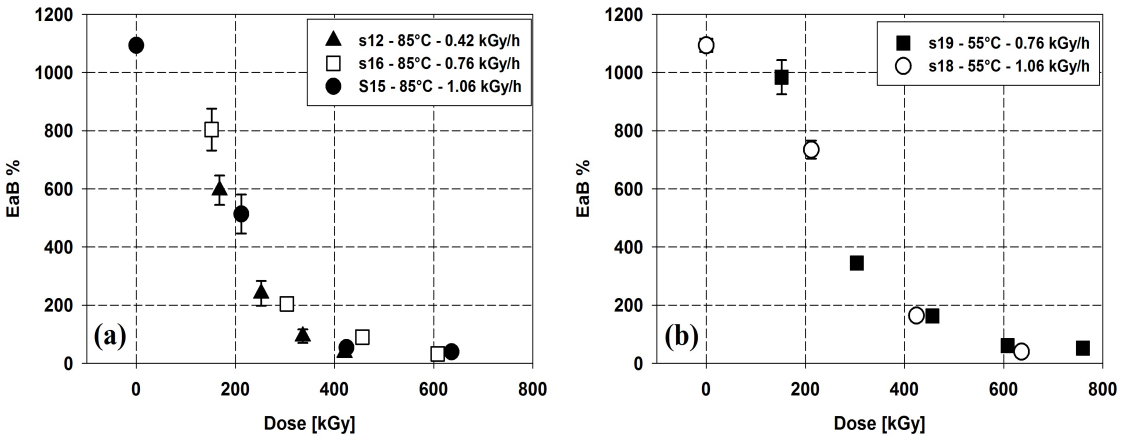


Figure 3.28. Elongation at break vs. absorbed dose for XLPE samples aged at (a) 85°C and (b) 55°C.

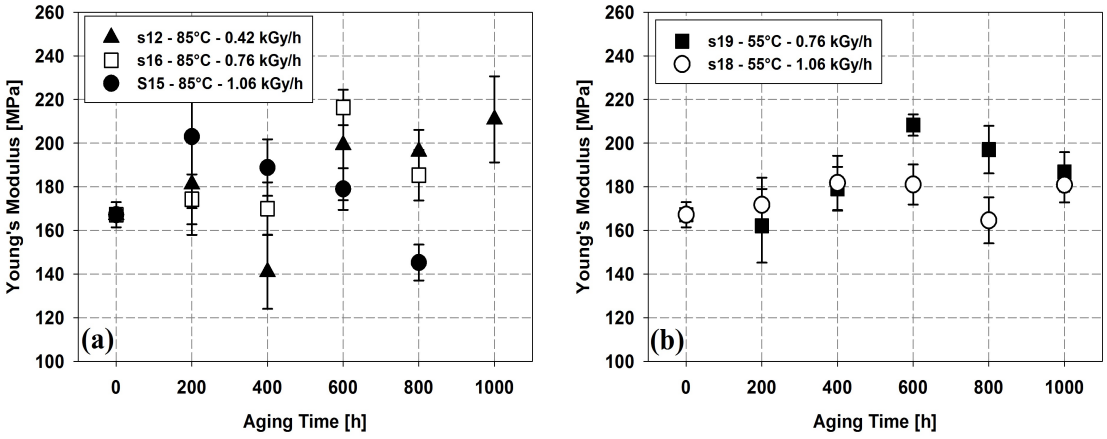


Figure 3.29. Young's Modulus vs. aging time for XLPE samples aged at (a) 85°C and (b) 55°C.

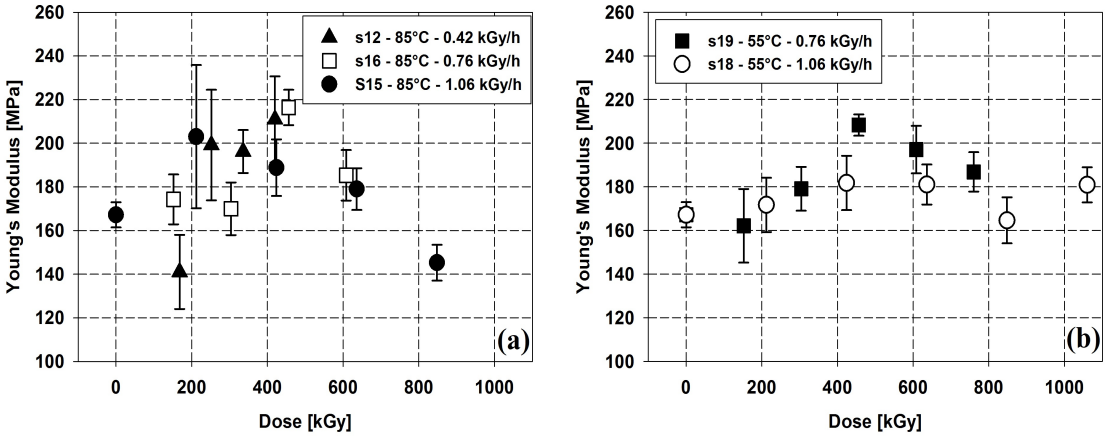


Figure 3.30. Young's Modulus vs. absorbed dose for XLPE samples aged at (a) 85°C and (b) 55°C.

### 3.4.3 Ethylene-Propylene Rubber

Figures 3.31, 3.32 and 3.33 depict the behavior of the real and imaginary part of permittivity vs. frequency, at different aging times. In Fig.3.31, samples are aged at 85°C with a dose rate of 0.39 kGy/h. The real part of permittivity increases over the whole frequency range, while for the imaginary part, the effect of radio-oxidation appears only below 0.1 Hz and above 10 Hz.

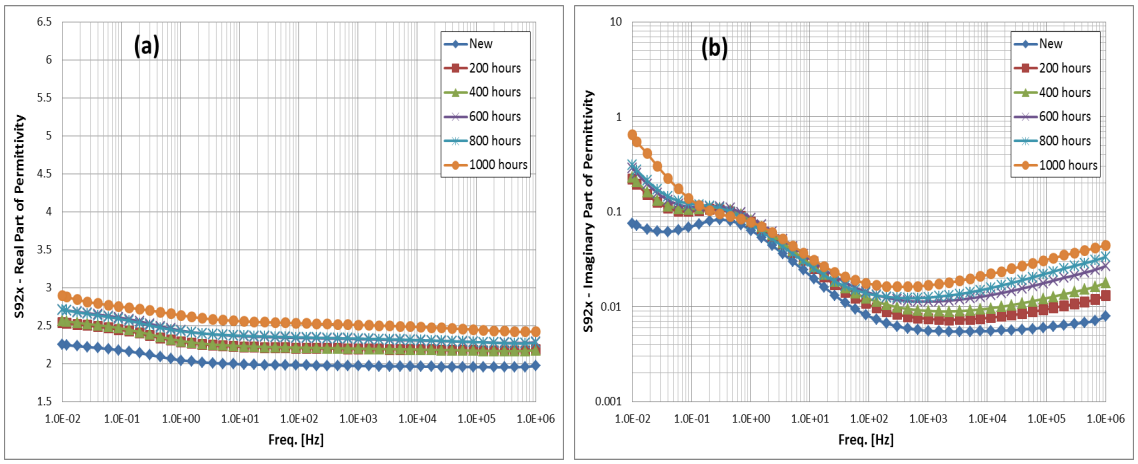


Figure 3.31. (a) Real and (b) Imaginary Part of Permittivity vs. frequency for EPR specimens aged at 85° with irradiation dose rate of 0.39 kGy/h

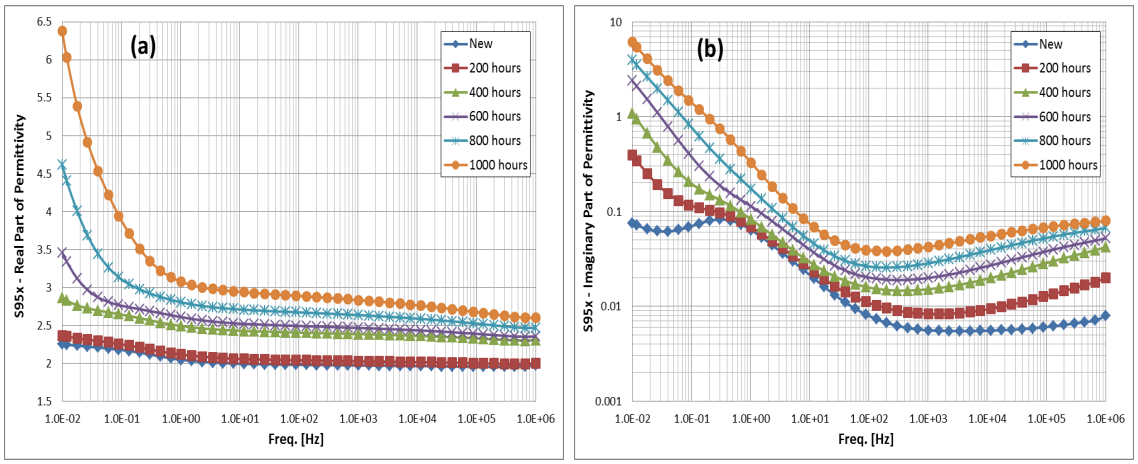


Figure 3.32. (a) Real and (b) Imaginary Part of Permittivity vs. frequency for EPR specimens aged at 85° with irradiation dose rate of 1.58 kGy/h

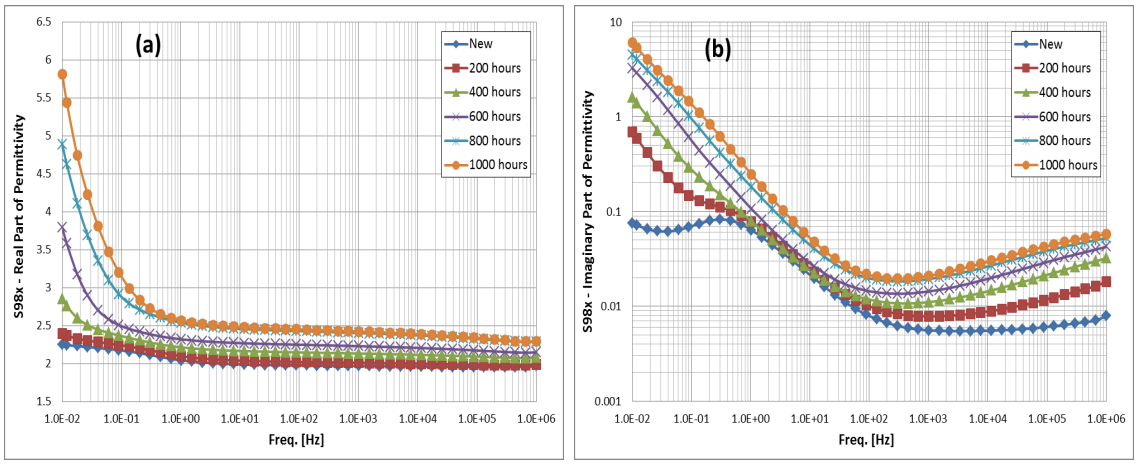


Figure 3.33. (a) Real and (b) Imaginary Part of Permittivity vs. frequency for EPR specimens aged at 55° with irradiation dose rate of 1.58 kGy/h

Increasing the dose rate up to 1.58 kGy/h, the variation of the real part of permittivity becomes particularly evident at low-frequency. The polarization peak of $\epsilon''$ at about 0.3 Hz disappears after 400 hours, being hidden by conduction processes. This is the main effect of the higher dose rate.

The effect of the aging temperature becomes clear comparing Fig.3.32 with Fig.3.33. At 55°C the increment of $\epsilon'$ and $\epsilon''$ over the whole frequency range is slightly smaller, but the polarization peak again disappears after 400 hours.

Also in this case, the evolution of $\epsilon'$ and $\epsilon''$ with the aging time can be compared choosing appropriate reference frequencies. Again:

- 0.1 Hz will be representative of the low-frequency part of the spectra;
- 50 Hz will be representative of the middle-frequency region;
- 100 kHz will represent the high-frequency region.

Figs. 3.34, 3.35, 3.36 show the real part of permittivity as a function of the aging time at the chosen reference frequencies, 0.1 Hz, 50 Hz and 100 kHz, respectively. The property increases linearly with the aging time independently of the frequency chosen. The effect of the temperature becomes noticeable comparing samples aged at 85°C and 55°C respectively; a higher aging temperature causes a further increase of $\epsilon'$ with the aging time, especially after 200 aging hours. The effect of the dose rate comes out comparing samples aged at 85°C, with dose rates of 0.39 kGy/h and 1.58 kGy/h. It can be observed that the slope of both $\epsilon'$ and $\epsilon''$ vs. aging time decreases reducing the dose rate. Only at the beginning of the accelerated aging procedure, the lower dose rate causes a larger increase of the property, noticeable

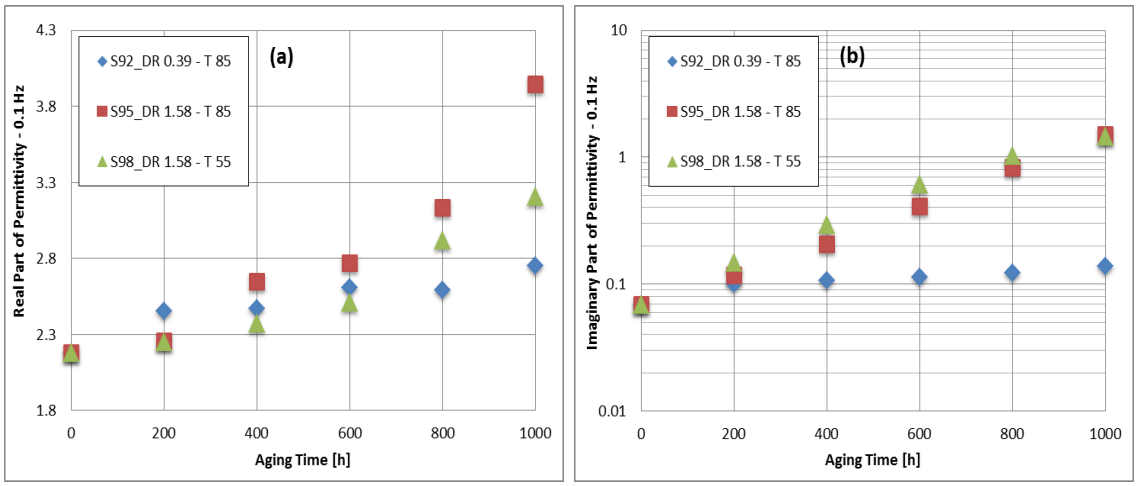


Figure 3.34. (a) Real and (b) Imaginary Part of Permittivity at 0.1 Hz vs. aging time for EPR specimens.

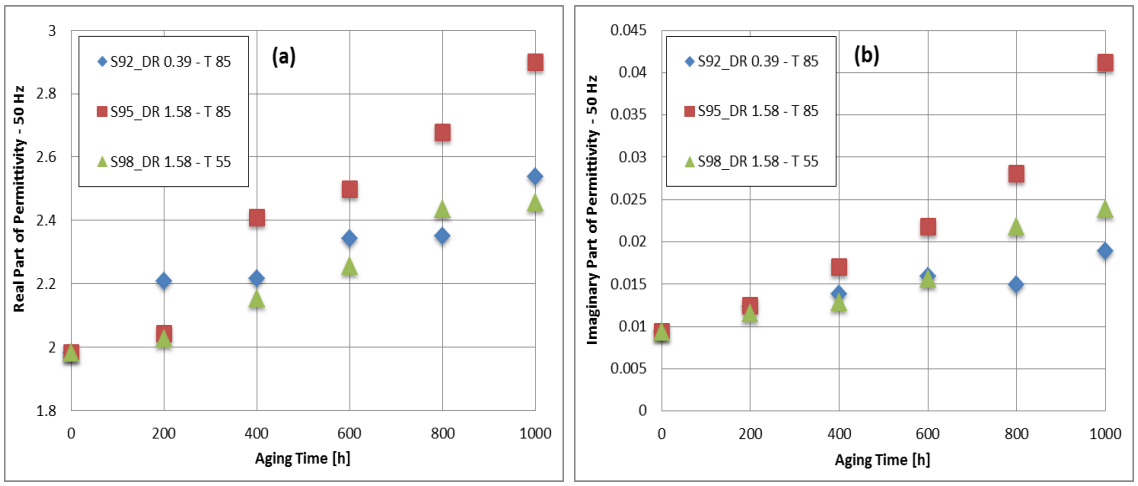


Figure 3.35. (a) Real and (b) Imaginary Part of Permittivity at 50 Hz vs. aging time for EPR specimens.

after 200 aging hours. Concerning $\epsilon''$, its increment is larger at 0.1 Hz and the data are presented in lin-log scale. At 0.1 Hz, the effect of the aging temperature becomes almost negligible.

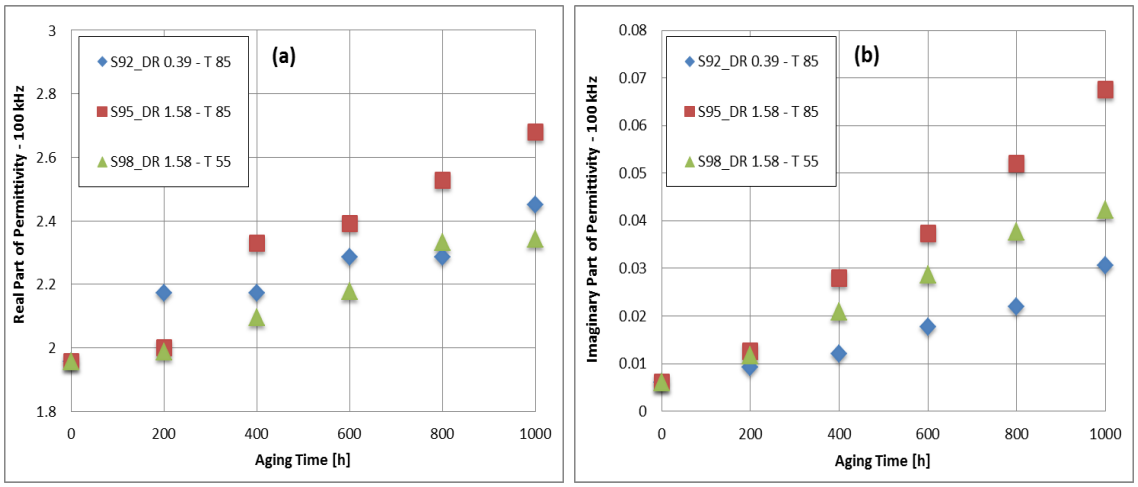


Figure 3.36. (a) Real and (b) Imaginary Part of Permittivity at 100 kHz vs. aging time for EPR specimens.

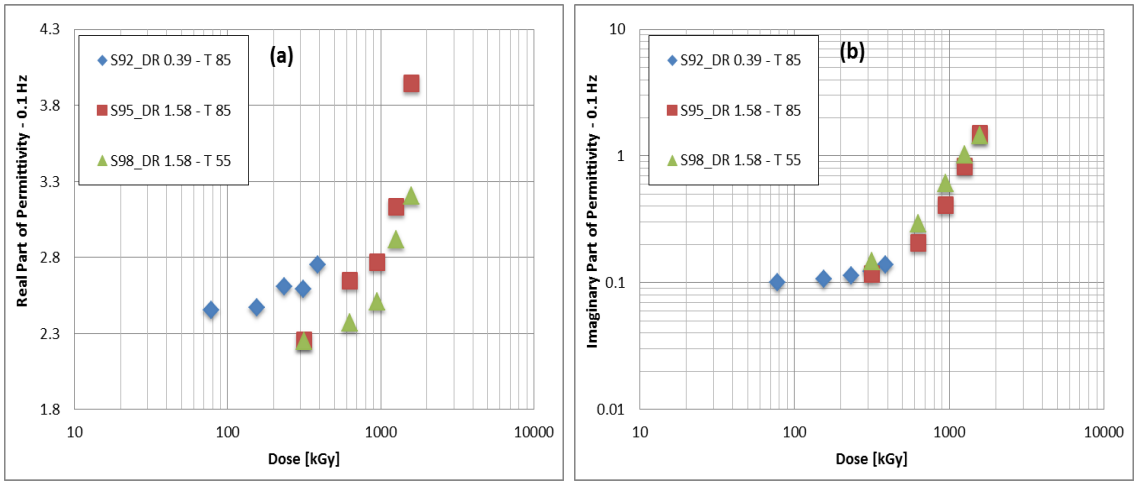


Figure 3.37. (a) Real and (b) Imaginary Part of Permittivity at 0.1 Hz vs. dose for EPR specimens.

Figs. 3.37, 3.38 and 3.39 show the real and imaginary part of permittivity as a function of the the total absorbed dose, at the chosen reference frequencies, 0.1 Hz, 50 Hz, 100 kHz, respectively. It is interesting to note that the real part of

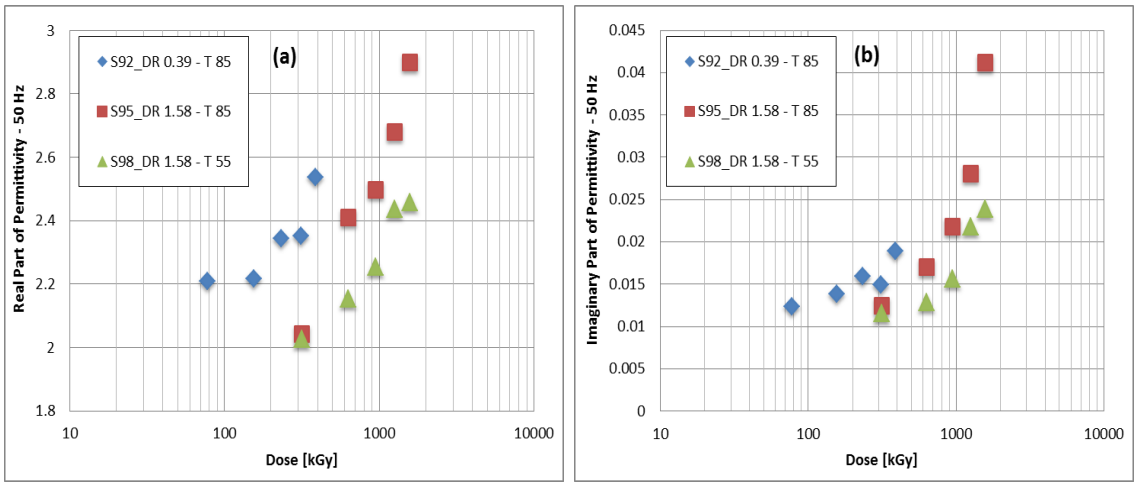


Figure 3.38. (a) Real and (b) Imaginary Part of Permittivity at 50 Hz vs. dose for EPR specimens.

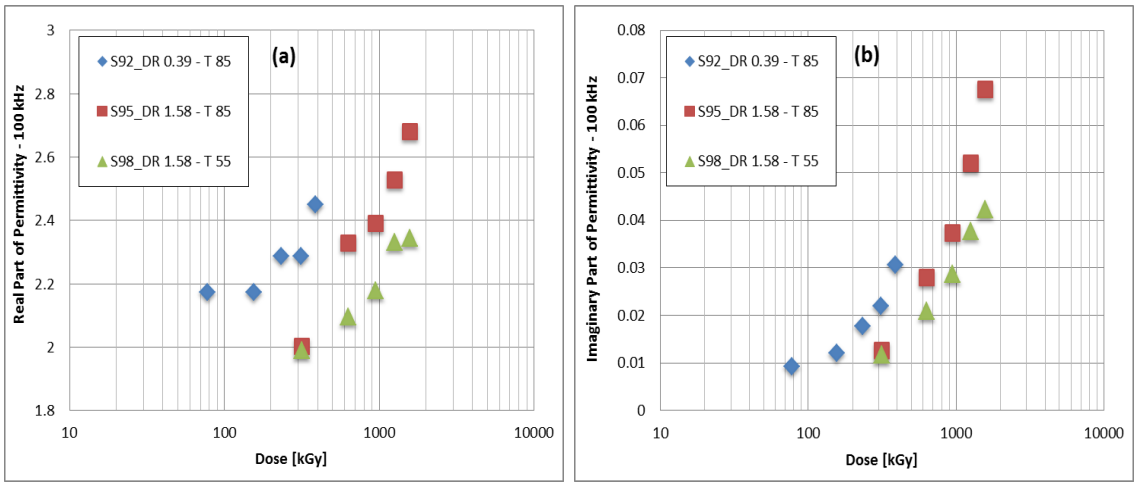


Figure 3.39. (a) Real and (b) Imaginary Part of Permittivity at 100 kHz vs. dose for EPR specimens.

permittivity shows always a clear dose rate effect. This is true also for $\epsilon''$ at 50 Hz and 100 kHz. At 0.1 Hz the effect of the dose rate on $\epsilon''$ disappears, even comparing specimens aged at different temperature.

The results of polarization-depolarization measurement are shown in Figs.3.40-3.46. The charging current shows (Fig.3.40a) a clear increase of both capacitive and absorption currents, while the conduction current (Fig.3.40b) increases after the first 200 h, but it does not present a regular trend as aging proceeds.

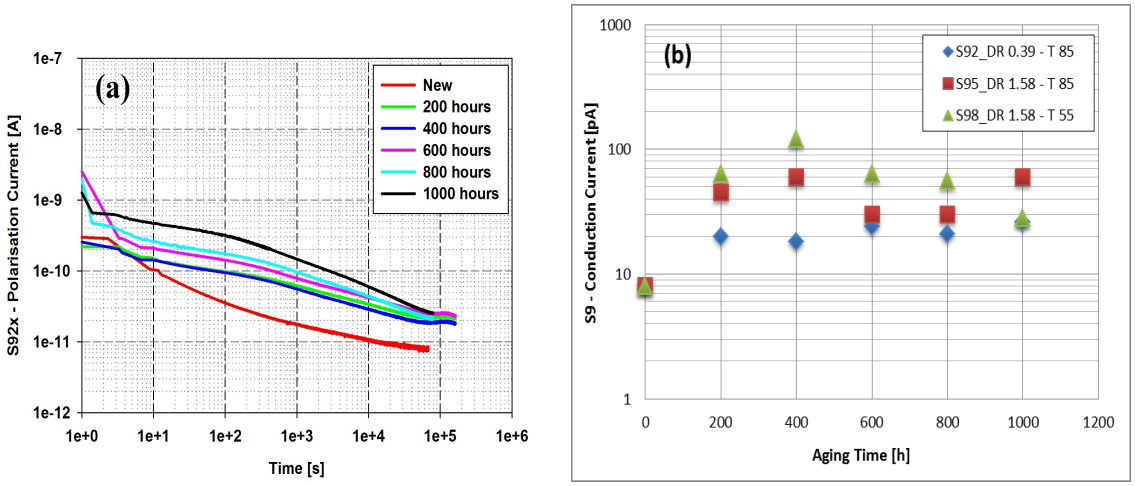


Figure 3.40. (a) Polarisation current of EPR samples aged at 85°C with irradiation dose rate of 0.42 kGy/h. (b) Conduction current vs. aging time for EPR samples.

From the elaboration of the depolarization characteristics, the interfacial contribution to $\chi'$, i.e. $\Delta\chi'$, and the dielectric losses, $\chi''$, are obtained as a function of the frequency. Fig.3.41 shows the behavior of these properties for specimens aged at 85°C with a dose rate of 0.39 kGy/h. $\Delta\chi'$ remarkably increases with the aging time below $10^{-3}$ Hz, already after 200 hours. Similarly, $\chi''$ increases with the aging time, but the increment is noticeable already below $10^{-2}$ Hz.

Fig.3.42 shows the results of VLF analysis for specimens aged at 55°C with a dose rate of 1.58 kGy/h. In this case, $\Delta\chi'$ shows a sharper increase, which becomes visible already between 0.1 Hz and 0.01 Hz. After 600 hours, the property reaches a sort of saturation value below $10^{-4}$ Hz. Also in this case, the increment of $\chi''$ caused by radio-oxidation is already noticeable at higher frequency, i.e. 0.1 Hz. A broad polarization peak becomes clearly visible after 400 hours; this peak shifts to higher frequency as the aging time increases. Specimens aged at 85°C and 1.58 kGy/h show a similar behavior, as confirmed by figs. 3.43-3.46 where $\Delta\chi'$ and $\chi''$, at the reference frequencies of $10^{-3}$ Hz and $10^{-4}$ Hz, are reported as a function of the aging time (Figs. 3.43 and 3.45) and total absorbed dose (Figs.3.44 and 3.46). The behavior

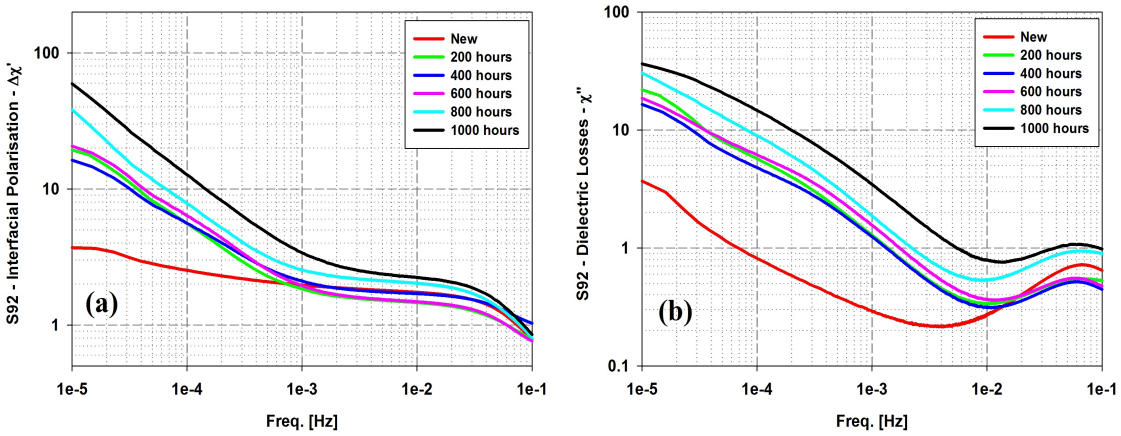


Figure 3.41. (a) Interfacial contribution to the Real Part of Susceptibility and (b) Dielectric Losses vs. frequency for EPR specimens aged at 85°C and 0.39 kGy/h.

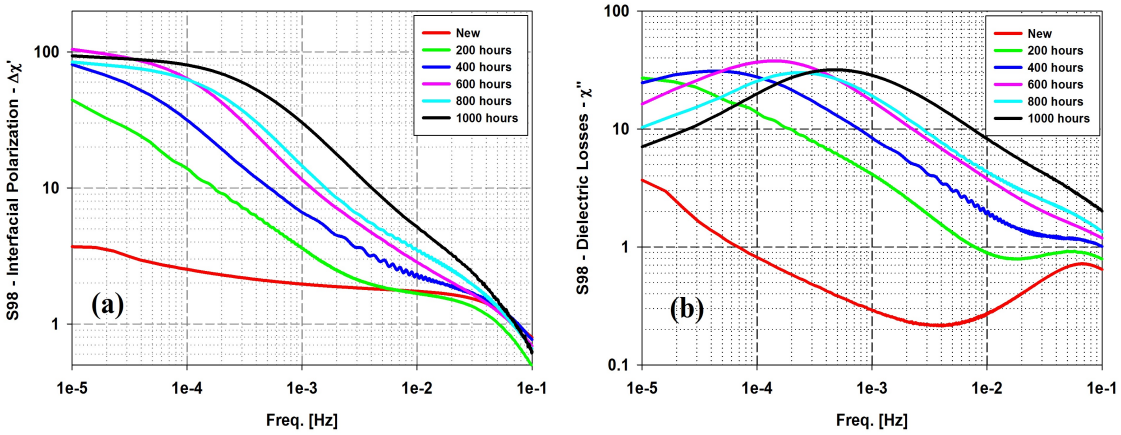


Figure 3.42. (a) Interfacial contribution to the Real Part of Susceptibility and (b) Dielectric Losses vs. frequency for EPR specimens aged at 55°C and 1.58 kGy/h.

of the investigated electrical properties confirms what was observed with dielectric spectroscopy (cfr. figs. 3.34 and 3.37) at 0.1 Hz. In this case however, the dose rate effect is negligible for both $\Delta\chi'$ and $\chi''$ (see figs. 3.44-3.46). For samples aged at 1.58 kGy/h, the value of $\chi''$ at $10^{-4}$ Hz stabilizes after 400 hours; this happens because the polarization peak shifts to higher frequency.

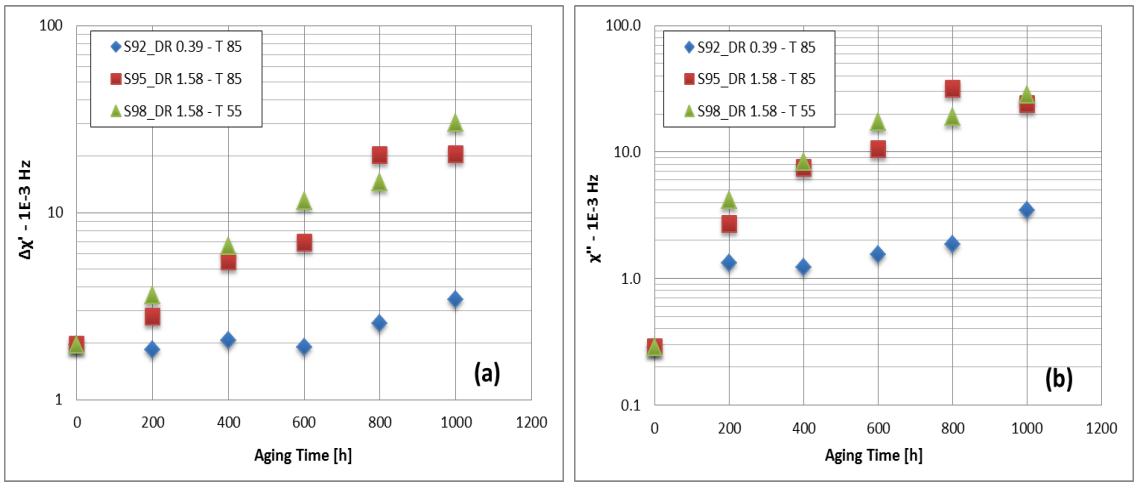


Figure 3.43. (a) Interfacial contribution to the Real Part of Susceptibility and (b) Dielectric Losses at $10^{-3}$ Hz vs aging time for EPR specimens.

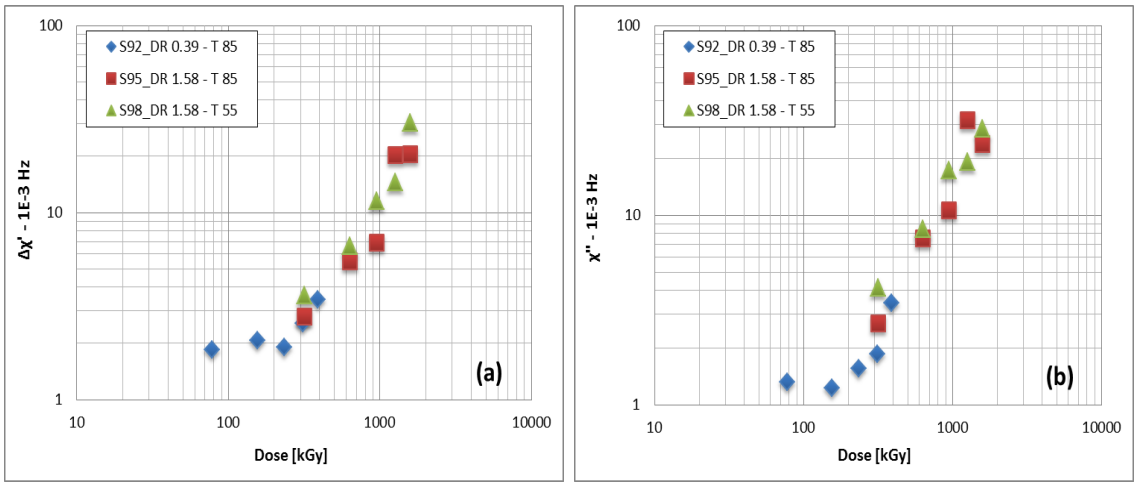


Figure 3.44. (a) Interfacial contribution to the Real Part of Susceptibility and (b) Dielectric Losses at $10^{-3}$ Hz vs absorbed dose for EPR specimens.

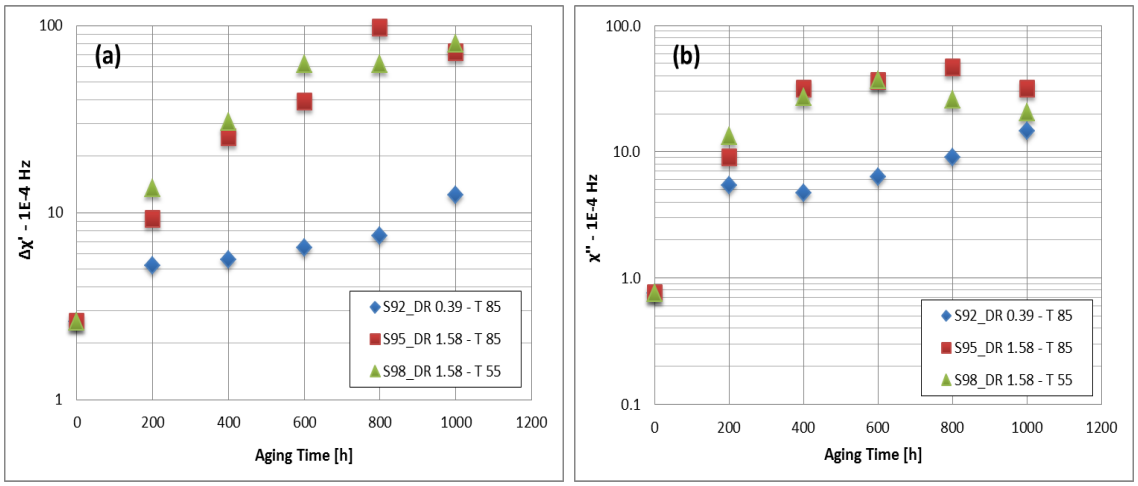


Figure 3.45. (a) Interfacial contribution to the Real Part of Susceptibility and (b) Dielectric Losses at $10^{-4}$ Hz vs aging time for EPR specimens.

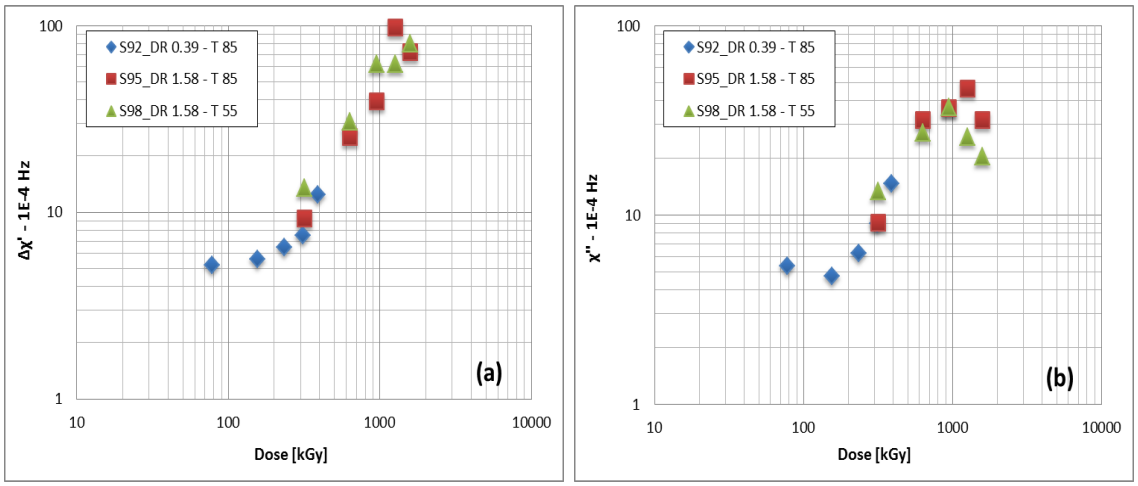


Figure 3.46. (a) Interfacial contribution to the Real Part of Susceptibility and (b) Dielectric Losses at $10^{-4}$ Hz vs absorbed dose for EPR specimens.

The results of tensile testing are reported in figs. 3.47 and 3.48, where EaB and Young's modulus are expressed as a function of (a) aging time and (b) dose.

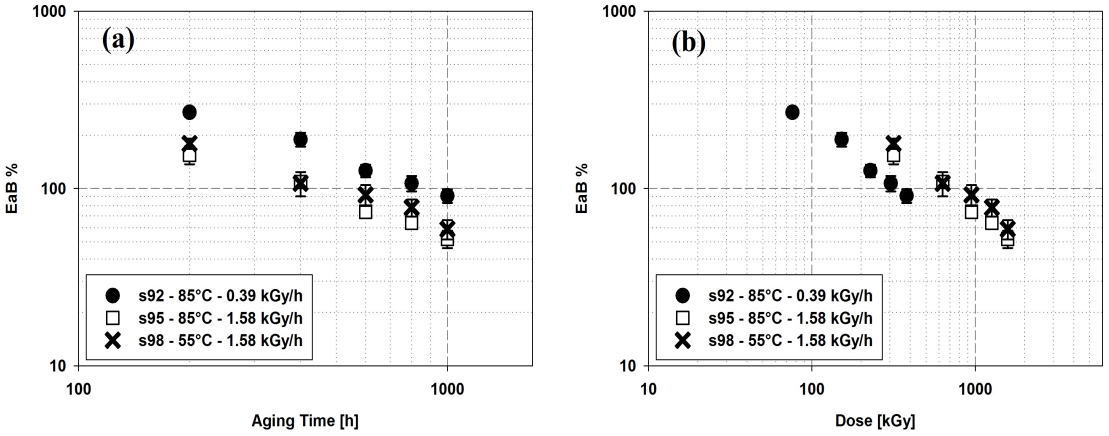


Figure 3.47. Elongation at break vs. (a) aging time and (b) absorbed dose for EPR specimens.

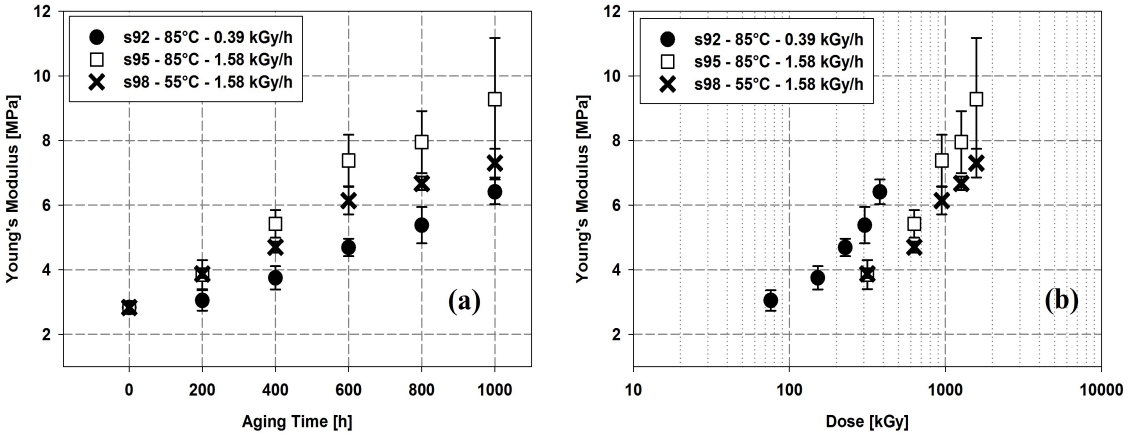


Figure 3.48. Young's Modulus vs. (a) aging time and (b) absorbed dose for EPR specimens.

Both properties exhibit a monotone trend which depends both on aging time and applied stress level. The Young's modulus remarkably increases, indicating that the material becomes stiffer with radio-oxidation.

### 3.4.4 Ethylene-Vinyl Acetate

Figures 3.49 and 3.50 depict the behavior of the (a) real and (b) imaginary part of permittivity vs. frequency, at different aging times, for EVA-based insulations aged at 85°C and 55°C with a dose rate of 1.5 kGy/h.

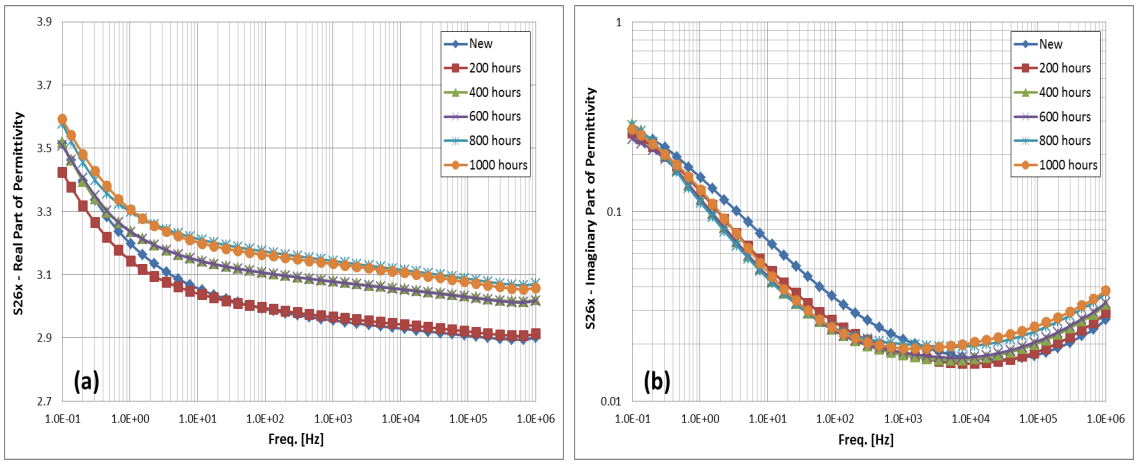


Figure 3.49. (a) Real and (b) Imaginary Part of Permittivity vs. frequency for EVA specimens aged at 85°C with irradiation dose rate of 0.94 kGy/h.

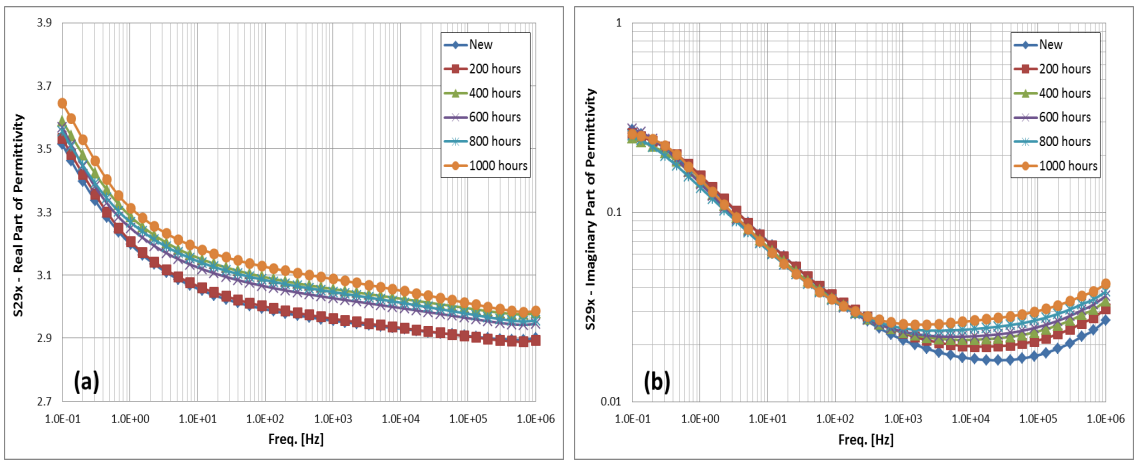


Figure 3.50. (a) Real and (b) Imaginary Part of Permittivity vs. frequency for EVA specimens aged at 55°C with irradiation dose rate of 0.94 kGy/h.

The real part of permittivity generally increases over the whole frequency range, but the relative variation remains always below 10%. The imaginary part of permittivity is almost constant below 100 Hz, in particular observing the behavior of

samples aged at 55°C. Increasing the aging temperature, $\epsilon''$ slightly decreases below 10 kHz after 200 hours, then stabilizes. Above this frequency, $\epsilon''$ increases gradually with the aging time.

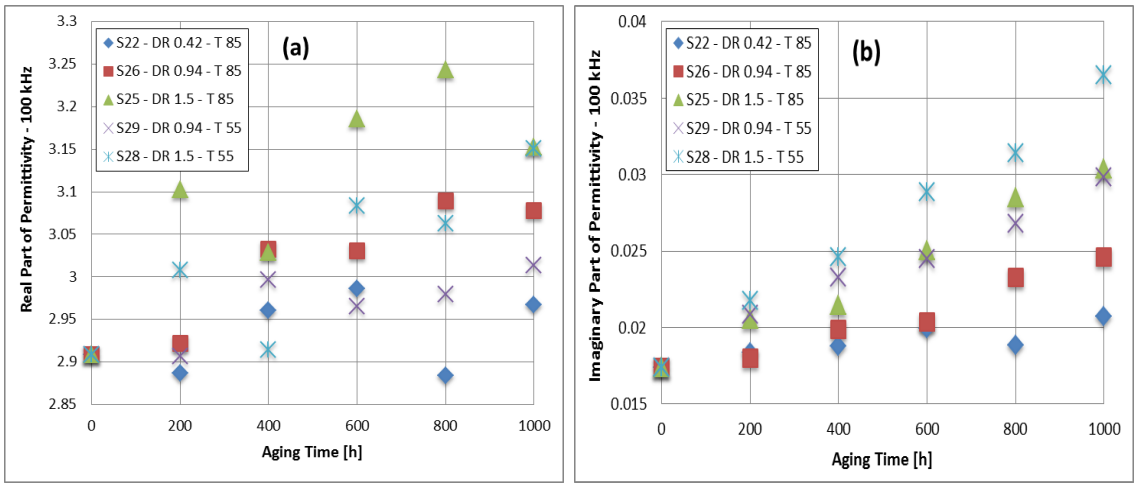


Figure 3.51. (a) Real and (b) Imaginary Part of Permittivity at 100 kHz vs. aging time for EVA specimens.

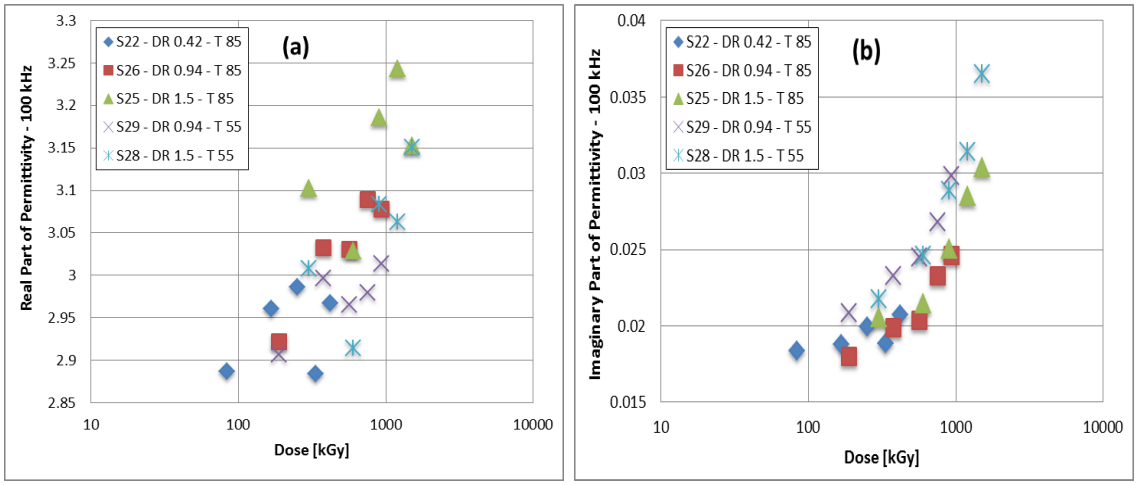


Figure 3.52. (a) Real and (b) Imaginary Part of Permittivity at 100 kHz vs. absorbed dose for EVA specimens.

It is possible to compare the evolution of $\epsilon'$ and $\epsilon''$ with the aging time choosing an appropriate reference frequency. In this case, the reference frequency of 100 kHz has been chosen to represent the high-frequency region, where the larger variations

of $\epsilon''$ are observed. Figs.3.51 and 3.52 show the behavior of the investigated properties as a function of aging time and absorbed dose. On the one hand, the real part of permittivity increases with aging; however, considering the measurement uncertainty, this property can't be considered as a good aging marker. On the other hand, $\epsilon''$ increases linearly with the aging time and its increment depends on both aging temperature and dose rate. It is noteworthy that samples irradiated at 55°C surprisingly exhibit a larger variation of $\epsilon''$.

Fig.3.53 summarizes the results of polarization-depolarization current measurements. The conduction current (Fig.3.53a) initially decreases, then fluctuates without a clear correlation with aging. Concerning the depolarization characteristics, an example is shown in Fig.3.53b for samples irradiated at 55°C with a dose rate of 0.94 kGy/h. After an initial variation, they almost overlap. Therefore, polarization-depolarization current measurements are not able to evaluate the degradation state of this EVA-based insulation.

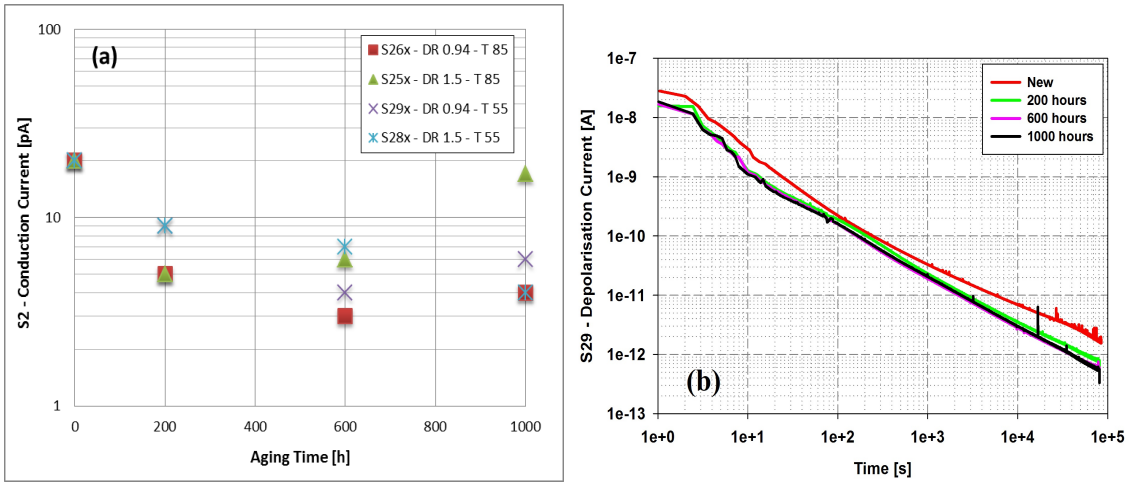


Figure 3.53. (a) Conduction current vs. aging time for EVA samples and (b) Depolarisation current vs. time for specimens aged at 55°C with irradiation dose rate of 0.94 kGy/h

The results of mechanical testing are reported in figs.3.54-3.57. Among the investigated mechanical properties only the EaB have shown a monotone decrease which depends both on aging time and applied stress level (Fig.3.54). Young's Modulus, after an initial increase, fluctuates around a constant value. Its behavior is shown in figs. 3.56 and 3.57 as a function of aging time and absorbed dose, respectively.

It is noteworthy that the values of elongation at break vs. time are always lower as the dose rate increases. Anyway, their variation becomes faster as the dose rate is reduced: the slope of samples irradiated at 0.42 kGy/h is definitely steeper than the

slope of samples irradiated at 1.5 kGy/h (Fig.3.54). The temperature has a similar effect: the relative decrease of samples irradiated at 55°C is larger compared with samples irradiated at 85°C.

Finally, plotting the EaB vs. the total absorbed dose (Fig.3.55), it is possible to highlight the effect of the dose rate, which appears almost negligible in the range of doses investigated.

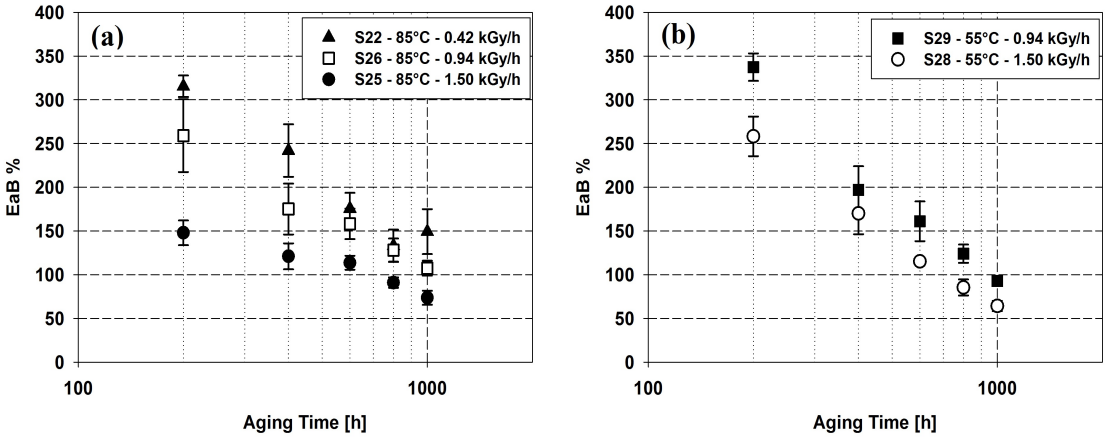


Figure 3.54. Elongation at break vs. aging time for EVA-based samples aged at (a) 85°C and (b) 55°C.

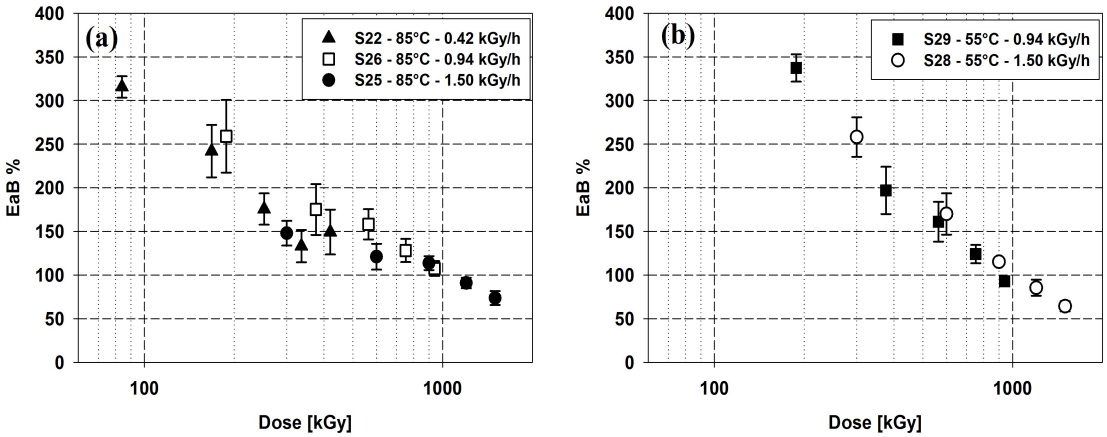


Figure 3.55. Elongation at break vs. absorbed dose for EVA-based samples aged at (a) 85°C and (b) 55°C.

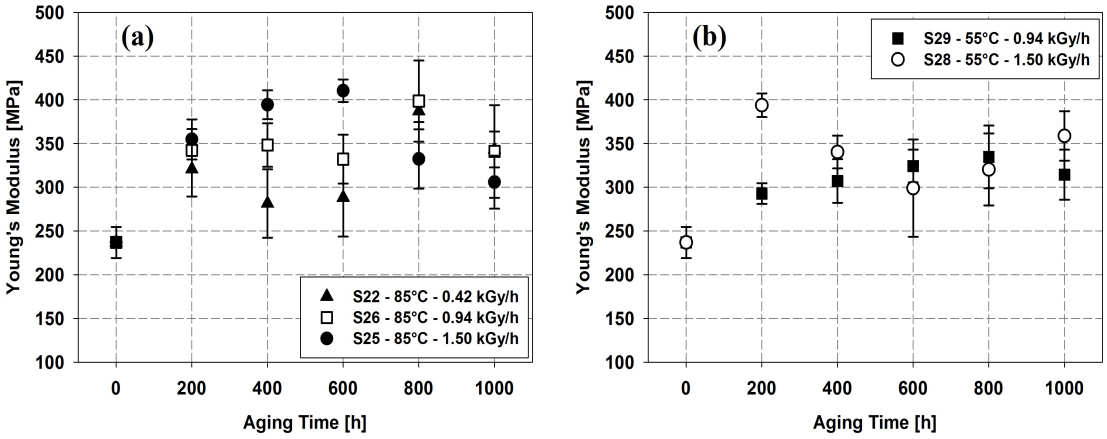


Figure 3.56. Young's Modulus vs. aging time for EVA-based samples aged at (a) 85°C and (b) 55°C.

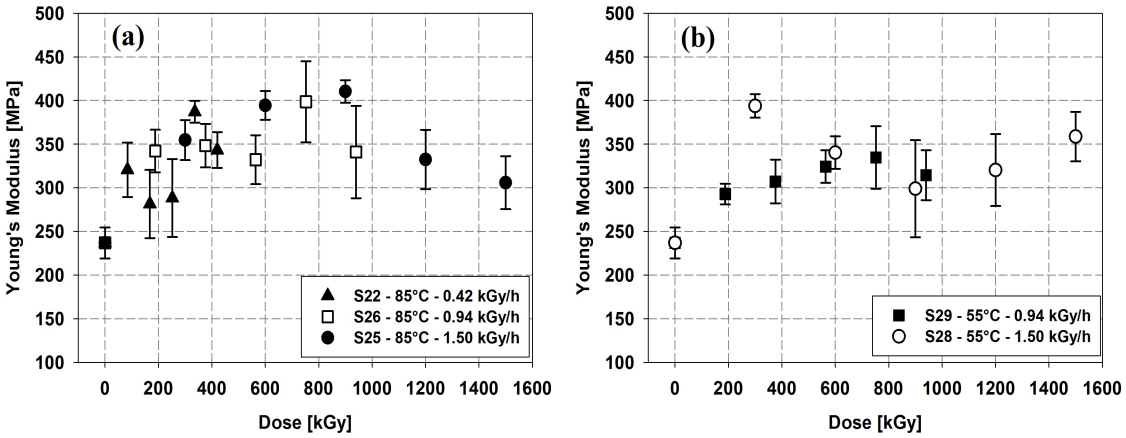


Figure 3.57. Young's Modulus vs. absorbed dose for EVA-based samples aged at (a) 85°C and (b) 55°C.

# Chapter 4

# Discussion

The integrity and function of NPP low voltage cables are frequently monitored through insulation resistance, voltage withstand tests and mechanical properties. Among the mechanical properties, EaB is generally considered one of the best aging indicators. The advantage in using EaB lies in its effective correlation with aging, which allows also the comparison of the results obtained with different stress levels. In order to study the evolution of the material properties in a reasonable time, accelerated aging is usually required; empirical and mathematical models able to correlate accelerated test results with aging in operation have been already widely investigated, especially for EaB. Nevertheless, the disadvantage presented by the use of destructive techniques, which often require an appropriate laboratory, is driving to search for electrical properties which can be possibly measured on-line by non-destructive tests. Literature regarding the effect of aging on electrical properties of low voltage insulation is still lacking. Furthermore, experimental results shown in the previous chapter revealed the importance of choosing an appropriate reference frequency. As can be immediately noticed, the dielectric response exhibits only small variations with aging at power frequency $(50 - 60)$ Hz, which is frequently used for capacitance and Tan Delta measurements. Tan Delta measurements are also carried out at 0.1 Hz; at this frequency however, the dielectric response of EVA-based insulation appears insensitive to degradation.

Insulation aging is defined as the irreversible process resulting in the variation of insulation structure (physical and/or chemical) and properties, compromising its function. An important characteristic of a useful condition indicator is that it demonstrates a trend that changes monotonically with degradation and can be correlated with the safety related performance. For example, the parameters used as condition indicators could monitor the change in the chemistry of the material, monitor the physical properties, or monitor electrical properties of the material. The aging marker should be sensitive to the effects of aging for the particular material at different stress levels, and its variation must be irreversible.

It should be borne in mind that insulating polymers produced by cable manufacturers involve many inorganic compounds playing the role of flame retardants, anti-oxidants, stabilizers, lubricants, plasticizers and dyes. Additives can improve the mechanical or chemical properties of the insulation and may exceed the 60% of the material composition. Their presence obviously alters the effects of aging: the application of different aging stress levels, e.g. performing accelerated aging tests, can change the balance between the reactions (such as chain scissions, cross-linking and oxidation), with different consequences on the macroscopic properties of the investigated materials. Therefore, it is not possible to identify general rules concerning the chemistry of the aging processes and the performance of the insulating material, even if the degradation mechanisms of the pure polymer are already known. Any experimental evidence obtained from materials actually used as insulations can help to understand the consequences of the aging processes on their properties.

Due to their composition, additives can strongly influence the electrical properties of the polymer. Especially during accelerated aging, processes like additive migration or diffusion could affect the material electrical properties, without compromising its integrity and function. Therefore, it is necessary to correlate the electrical property variation with other properties, which are actual aging indicators, i.e. EaB, OIT/OITp and density. The correlation between electrical aging markers and insulation physical/chemical properties is the aim of the following sections.

## 4.1 Cross-Linked Polyethylene

The cable consisted of a coaxial cross-linked polyethylene insulation, shielded by copper polyester tape and copper wire braids, housed in an EVA jacketing. The insulation was aged under the conditions given in Table 4.1.

Table 4.1. Accelerated aging experiments for XLPE insulation.

| **Exp. No.** | **Temperature** [°C] | **Dose Rate** [kGy/h] |
|---|---|---|
| 2 | 85 | 0.42 |
| 5 | 85 | 1.06 |
| 6 | 85 | 0.76 |
| 8 | 55 | 1.06 |
| 9 | 55 | 0.76 |

The accelerated aging was effective, because it caused significant changes in several measured properties over the aging time. The elongation at break, for example,

was reduced to less than 5% of the initial value for the most aged samples at all aging stress levels, with final EaB-values lower than 50% absolute. It should be noted that the reduction of the sample length for testing led to EaB values higher than what would be expected for XLPE. However, the relative changes between the samples are correct and possible relationships between mechanical and electrical data would also be maintained.

In order to estimate the life under different thermal-radiation stresses, an experimental data fitting is performed. Fig.4.1 shows a linear regression in log-log scale, thus using an inverse power law:

$$EaB = at^{b_1} \tag{4.1}$$

The fitting was performed in the interval [200,1000] h of aging, down to an EaB of 50% absolute. For specimens aged at 85°C and 0.42 kGy/h, the fitting was performed between 400 h and 1000 h, where the experimental data follow an inverse power law.

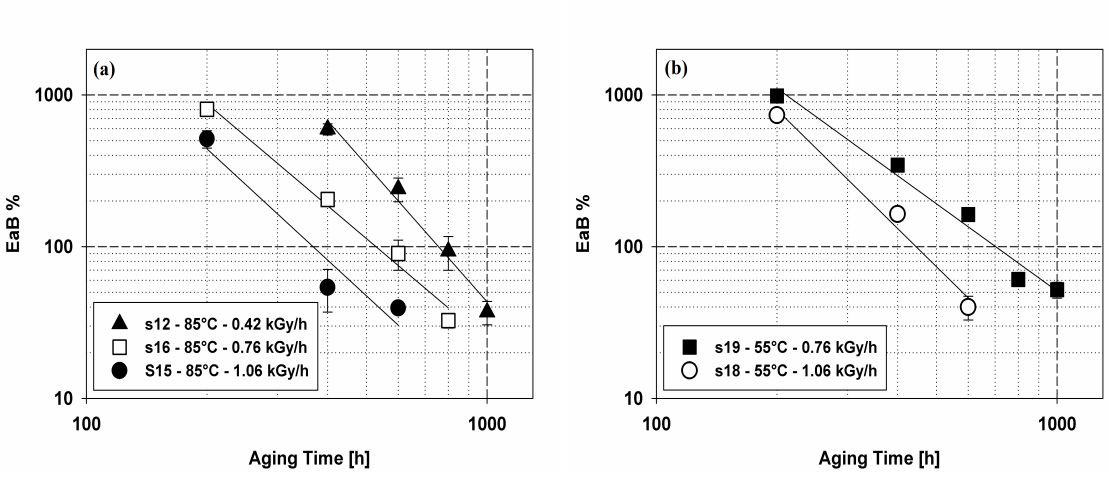


Figure 4.1. Elongation at break vs. aging time for XLPE samples aged at (a) 85°C and (b) 55°C. Experimental data fitting is performed using an inverse power law.

The dose rate effect can be quantified plotting the DED (dose required to reach an absolute EaB of 50%) as a function of the dose rate (Fig.4.2b). If dose rate effects are present, the DED usually increases with the dose rate (see section 1.4.1). In this case, the degradation of the surface causes the DED to decrease when the specimens are aged at 1.06 kGy/h, especially at 55°C. Fig.4.2a shows the cable life (also calculated using an elongation at break of 50% absolute as end-point) as a function of the dose rate and temperature. Observing specimens aged with a

dose rate above 1 kGy/h, the fast surface degradation of the specimens causes the EaB to drop below the 50% within 600 aging hours, making the effect of the aging temperature less important compared with specimens aged at 0.76 kGy/h.

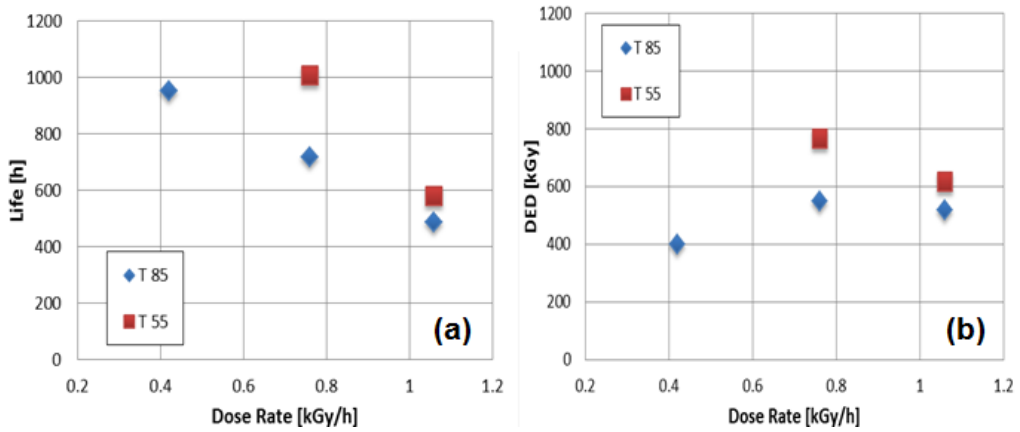


Figure 4.2. (a) Life and (b) DED vs. Dose Rate for XLPE samples aged at 85°C and 55°C.

Results from electrical measurements also showed significant changes with the aging time over the whole frequency range. Among the investigated properties, the most suitable electrical aging markers are located at the frequency where their relative variations are larger, i.e.:

- 0.1 Hz for $\epsilon'$;
- 100 kHz for $\epsilon''$.

Even if the imaginary part of permittivity at 50 Hz seems to be a good aging indicator (smooth exponential increase with aging time, which depends on the applied stress level), it was not selected for the comparison since at low dose rates and low temperatures its variation becomes significant only after 600 hours, whereas the EaB shows a remarkable drop from the beginning of the aging experiment. Crossplots of EaB vs. $\epsilon'$ at 0.1 Hz and vs. $\epsilon''$ at 100 kHz are shown in fig. 4.3a and 4.3b, respectively. The dose rate (in kGy/h) and temperature (in °C) are shown in the legend, next to the sample label. The same notation is used in the figures throughout this chapter.

Both the real and imaginary parts of permittivity for XLPE show similar behavior when compared to the elongation at break. From Fig.4.3, no clear relation between EaB and the investigated electrical properties can be found. Samples aged at lower dose rates ($\leq$ 0.76 kGy/h) and 85°C show a linear trend in the semi-log plot, whereas a different trend can be noticed for samples aged at 55°C, as well as at the highest dose rate (1.06 kGy/h).

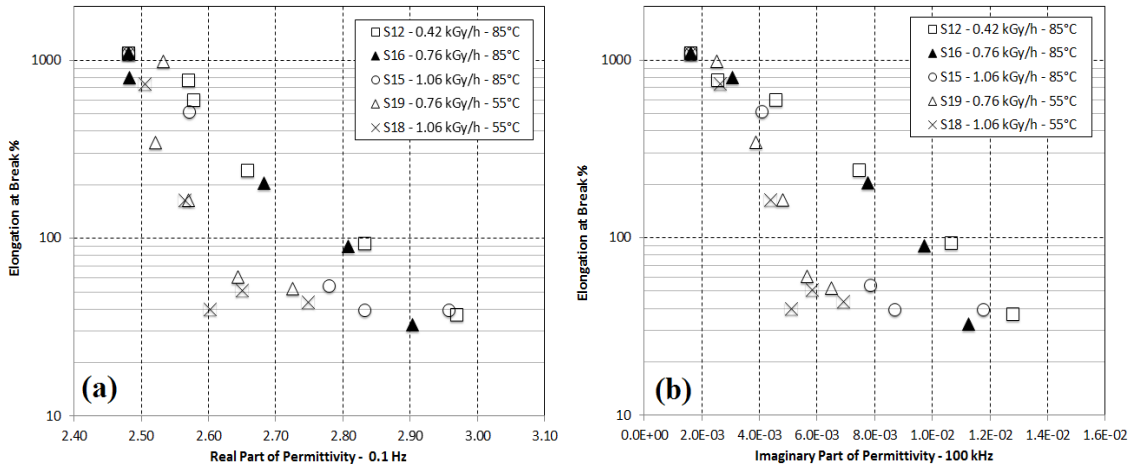


Figure 4.3. XLPE - Crossplots of EaB and (a) $\epsilon$' at 0.1 Hz, (b) $\epsilon$" at 100 kHz.

This discrepancy is caused by diffusion-limited oxidation (DLO), where the oxygen consumption rate is higher than the oxygen supply rate through diffusion. Elongation at break is strongly affected by the more oxidized layer near the surface (Fig.4.4), where cracks can be initiated and quickly propagate through the sample, whereas electrical measurements are averaged over the sample cross-section. This means that comparing EaB to electrical properties for samples where DLO-effects are present can result in comparing the worst aged part to that of the average, which does not necessarily behave in the same way.

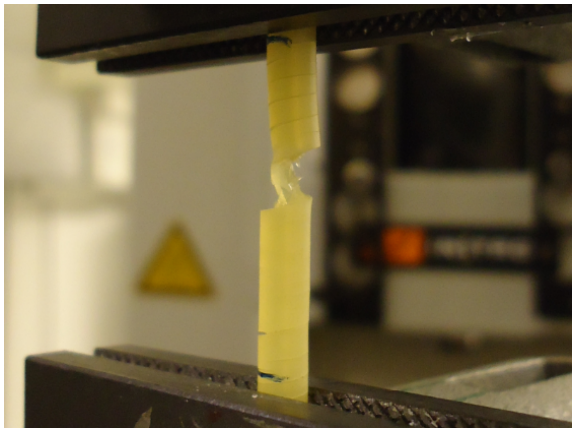

Figure 4.4. DLO causes surface cracks affecting tensile testing results.

The oxidation profiles, characterized by FTIR spectroscopy across the sample thickness are shown in Fig.4.5. The plots show the ratio between carbonyl peak and

$C - H_2$ stretch peak areas, after 1000 aging hours, for three samples aged under different dose rate-temperature stresses. The samples are located between $-300$ $\mu$m and 400 $\mu$m; the cable outer surface is on the left hand side (light blue region in Fig.4.5), whereas the inner part is on the right (dark violet in Fig.4.5). The brighter the colour, the higher the concentration of oxidation products, and a clear gradient can be seen between the surface in contact with air and the inside, which faces the conductor. This provides further proof that the samples are heterogeneously aged. The results from FTIR mapping further indicate that the total amount of oxidation is similar for samples aged at each temperature, but the distribution differs. This suggests that all the oxygen that diffuses through the sample surface is consumed, and because the rate of diffusion varies with the temperature, more oxygen can diffuse through the sample at the higher temperature. This, in turn, results in a higher total degree of oxidation for the higher temperature.

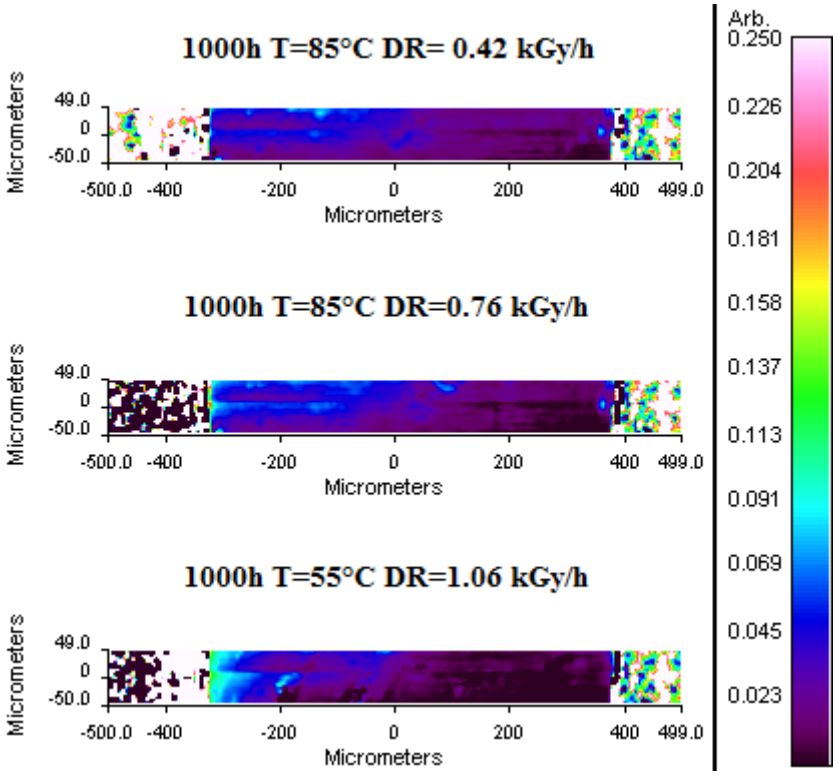


Figure 4.5. FTIR map over the sample thickness. The color scale represents the ratio of the areas of the carbonyl peak ($\approx 1720\ cm^{-1}$) and the $C-H_2$ stretch peak ($\approx 2900\ cm^{-1}$).

Hence, DLO effects make the comparison of EaB to electrical properties not appropriate, but the comparison with other thickness-averaged properties, such as

density of the whole cross-section, may yield better correlations. A crossplot of density and real part of permittivity at 0.1 Hz is shown in Fig.4.6a, while the correlation with $\epsilon''$ at 100 kHz is shown in Fig.4.6b.

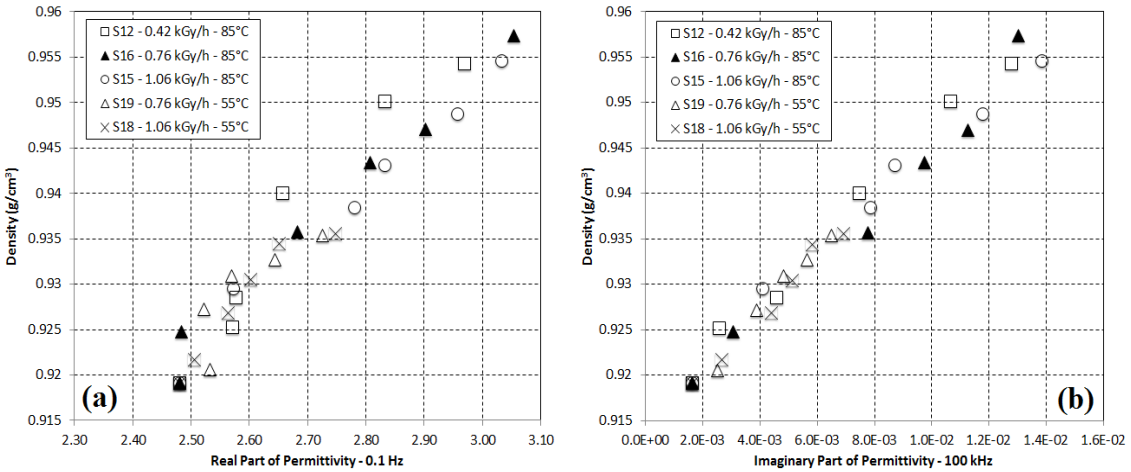


Figure 4.6. XLPE - Crossplots of density and (a) $\epsilon$' at 0.1 Hz, (b) $\epsilon$" at 100 kHz.

As the material ages, the density increases due to the introduction of oxygen into the polymer [24, 25, 86]. An increase in density can depend also on an increase in crystallinity, since the crystals have higher density than the amorphous parts, but DSC measurements did not show significant changes in crystallinity over aging time. Fig.4.6 shows a clear linear trend between density and the chosen electrical properties, particularly good with $\epsilon''$ at 100 kHz. This suggests that dielectric spectroscopy can give a good indication of the average level of oxidation in the sample, at least for almost pure polyethylene (only small amounts of additives, such as antioxidants, were found during the preliminary characterization). For a homogeneously aged sample, the oxidation can likely be correlated to the elongation at break, and dielectric spectroscopy is a viable option for the condition monitoring of this cable.

Literature confirms that dielectric response can be used as an indicator of aging processes occurring in polymer insulation [87, 88, 89]. The radiation-induced increase in the quantity of polar (mainly carbonyl) groups causes an increase in polarity, and thus the increase of the magnitude of dielectric relaxation processes can clearly be connected with the radiation-induced oxidation [90, 91]. In order to evaluate the possible application of dielectric spectroscopy as CM technique, and the reliability of $\epsilon''$ at 100 kHz as aging marker, the influence of the test temperature on its behavior with aging was investigated. These tests could also reveal the prevailing degradation mechanisms. Fig. 4.7 shows the behavior of $\epsilon$" at 100 kHz for specimens aged at 85°C and 55°C, with irradiation dose rate of 0.76 kGy/h, at

three different test temperatures, 25°C, 50°C, and 80°C. The test temperature does not affect the behavior $\epsilon$" with aging only for samples aged at 55°C. For samples aged at 85°C, an increase in the test temperature result in a smaller variation of $\epsilon$" with aging.

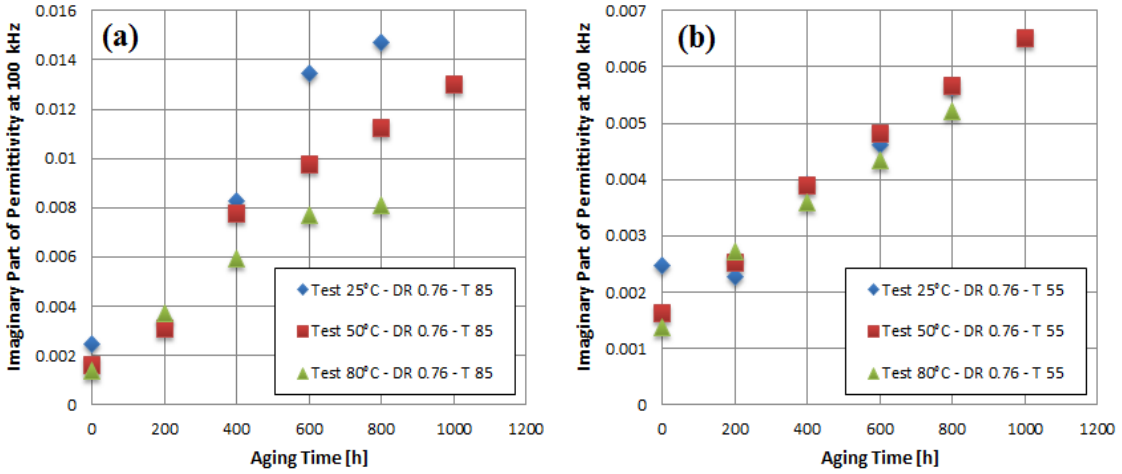


Figure 4.7. Influence of the test temperature on the values of $\epsilon$" at 100 kHz for specimens aged at (a) 85°C and (b) 55°C with irradiation dose rate of 0.76 kGy/h.

Two main effects can be evidenced when polyethyelene is subjected to ionizing radiation in air: crosslinking and oxidative degradation. In general, the dominating process is determined by material structural peculiarities and irradiation conditions. As previously mentioned in section 2.3.3, polyethylene displays three characteristic relaxations zones called $\alpha$, $\beta$ and $\gamma$ relaxations, in order of decreasing temperature. The $\alpha$ and $\beta$ relaxations are commonly attributed to the relaxation mechanisms in the crystalline and amorphous phases, respectively; the $\gamma$ relaxation, according to different authors, is due to the localized motions of chain ends or branches associated with the amorphous phase [92, 93, 94, 95].

The $\beta$-relaxation is attributed to the amorphous regions because its magnitude increases with decreasing crystalline fraction. The amount of polar groups increases with increasing absorbed dose, causing modification of the dielectric properties, especially dielectric $\beta$-relaxation; in the crystalline regions indeed, the macromolecules have very small mobility and oxygen is almost unable to diffuse. Because of that, oxidative degradation and crosslinking mostly take place in the amorphous phase [96] and on boundary layers (lamellae fold-surface interfaces) resulting in two main effects (Fig.4.8):

- polar groups introduced by oxidation cause the increment of the $\beta$-relaxation peak;

- crosslinking restricts the motion of macromolecules, resulting in a shift of the $\beta$ peak to higher temperatures with increasing absorbed dose.

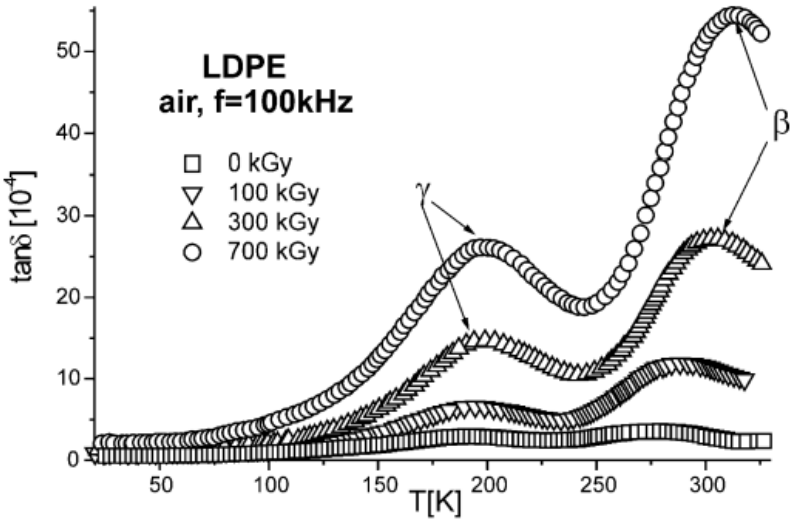


Figure 4.8. Dielectric loss tangent versus temperature of LDPE 0.3 mm thick samples irradiated in air (room temperature) with an irradiation dose rate of 9 kGy/h [93].

The independence of $\epsilon$" at 100 kHz from the test temperature indicates that in this temperature range the dielectric response exhibits a flat behavior; therefore, the results are probably obtained between $\beta$ and $\alpha$ relaxation peaks (truncated in fig. 4.8). Results reported in fig. 4.7b suggest that for samples aged at 55°C under gamma-irradiation, the increase of the $\beta$ peak with aging time related to oxidation leads to the variation of $\epsilon$" at 100 kHz. However, the influence of the test temperature on its increment is almost negligible. The $\beta$ peak increases also for samples aged at 85°C, but in this case, the effect of the test temperature becomes noticeable; this can be likely associated with the shift of the $\beta$ peak to higher temperatures, indicating a higher crosslinking degree. Further investigation, in particular soluble/gel fraction measurement, is required to prove this theory. However, dielectric spectroscopy performed at different temperatures confirmed the reliability of $\epsilon$" at 100 kHz as a cable insulation aging marker.

## 4.2 Ethylene-Propylene Rubber

The cable consisted of three EPR insulations contained within an inner sheath of CSPE filler, screened by mineral tape and metal sheaths and covered by a thin

CSPE outer jacket. The aging conditions for these samples are presented in Table 4.2. Samples are taken from a power cable, therefore, the diameter of the conductor is large and make the cable resistant to bending. Since a large amount of these samples would have filled up the thermobox, so only three different combinations of dose rate-temperature were applied.

Table 4.2. Accelerated aging experiments for EPR insulation.

| **Exp. No.** | **Temperature** [°C] | **Dose Rate** [kGy/h] |
|---|---|---|
| 2 | 85 | 0.39 |
| 5 | 85 | 1.58 |
| 9 | 55 | 1.58 |

The accelerated aging was effective, in that it caused significant changes in several measured properties over the aging time. The elongation at break, for example, was reduced to less than 100% absolute at all aging stress levels. For samples irradiated at 1.58 kGy/h, the final EaB values are close to the 50% absolute. The results of mechanical testing are reported in fig.4.9, as a function of the aging time. In order to estimate the life under different thermal-radiation stresses, a linear regression with the experimental data in log-log scale is performed, i.e. using an inverse power law (Fig.4.9):

$$EaB = at^{b_1} \tag{4.2}$$

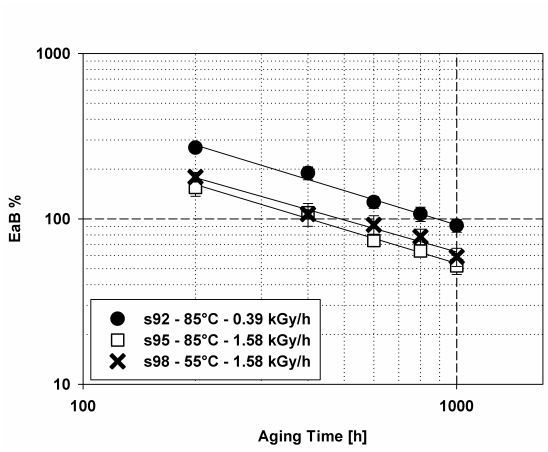


Figure 4.9. Elongation at break vs. aging time for EPR-based insulations. Experimental data fitting is performed using an inverse power law.

The effect of the dose rate becomes clear comparing samples aged at 85°C, with dose rates of 0.39 kGy/h and 1.58 kGy/h. As the dose rate increases, in fact, the

total dose required to reach the same level of degradation ($EaB = 50\%$) almost doubles. In addition, also the aging temperature affects the variation of mechanical properties with aging: for specimens aged at 55°C, the degradation is slightly slower, as confirmed by the life and DED values of fig.4.10.

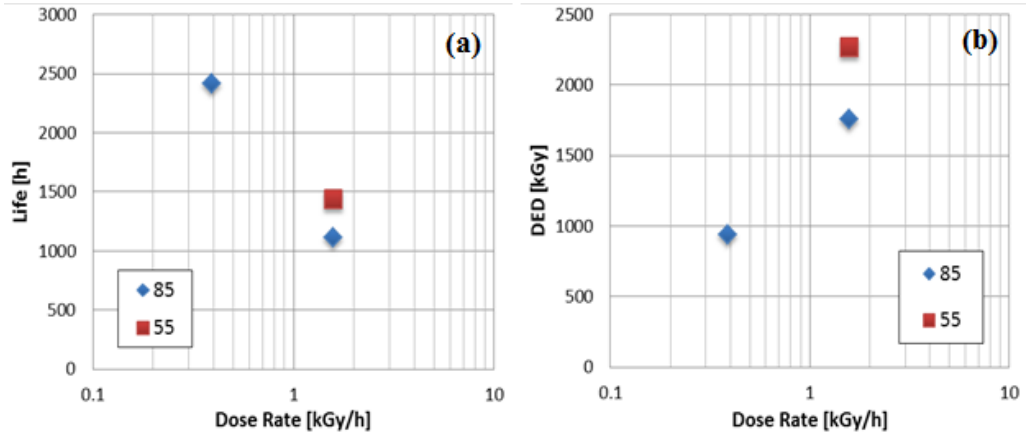


Figure 4.10. (a) Life and (b) DED vs. Dose Rate for EPR-based samples aged at 85°C and 55°C.

Also in this case, the results of electrical measurements showed significant changes with the aging time over the whole frequency range, and the behavior of the properties investigated by dielectric spectroscopy is similar to that shown by XLPE. The most suitable electrical aging markers are:

- 0.1 Hz for $\epsilon'$;
- 100 kHz for $\epsilon''$.

At low frequency, EPR insulation presents a sharper and more defined increase of $\epsilon''$ (figs. 3.34, 3.41 and 3.42); however this variation is not correlated with any of the investigated chemical/physical aging markers: depending on the applied stress level, each crossplot exhibits a particular trend. Similar considerations can be applied to the quantities extracted by FFT analysis of depolarization currents.

The crossplots of $\epsilon'$ (at 0.1 Hz) and $\epsilon''$ (at 100 kHz) with elongation at break, Young's modulus and density are shown in figs. 4.11-4.13. The imaginary part of permittivity at 100 kHz is the best aging indicator for EPR-based insulations. Fig.4.12a shows a considerable initial drop in elongation at break accompanied by moderate changes of $\epsilon''$. This means that dielectric spectroscopy may be inappropriate to monitor the initial part of degradation, but at longer times, before the samples reach 50% EaB, $\epsilon$" changes significantly and can be more effectively monitored.

Young's modulus increases with aging time, although the increase is more moderate. A crossplot of Young's modulus and $\epsilon$" at 100 kHz is presented in fig.4.12b.

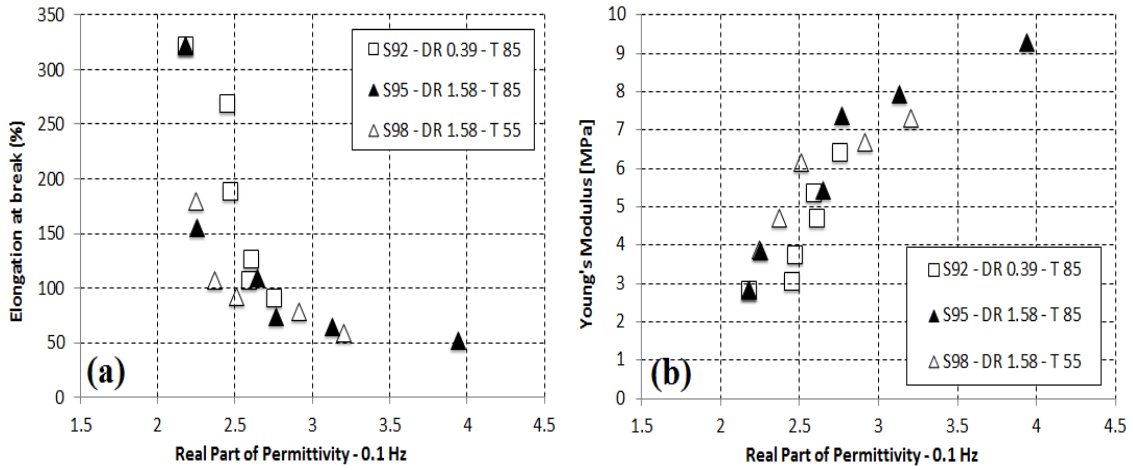


Figure 4.11. EPR - Crossplots of (a) EaB and (b) Young's Modulus with $\epsilon$' at 0.1 Hz.

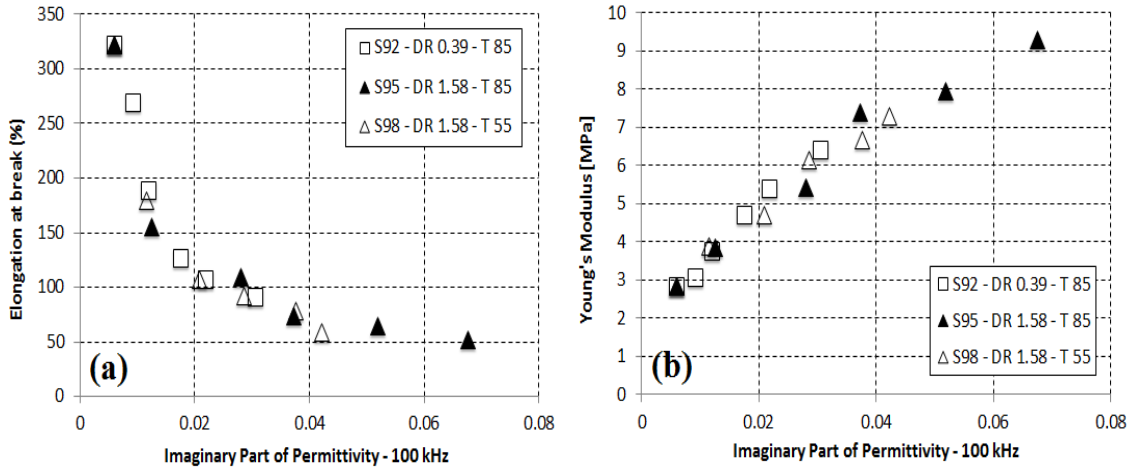


Figure 4.12. EPR - Crossplots of (a) EaB and (b) Young's Modulus with $\epsilon$" at 100 kHz.

The increase in modulus is well-correlated with the changes in $\epsilon$" at 100 kHz. Its increment is likely caused by a higher crosslinking degree. Due to the almost linear relationship between these two properties, it should be possible to evaluate Young's modulus from dielectric spectroscopy also for low levels of degradation.

The real part of permittivity at 0.1 Hz also shows a fairly good correlation with mechanical properties (Fig.4.11), whose trend resembles the previous one. However, especially at low dose rates, its variation is quite small even for samples which exhibit a remarkable reduction of EaB, limiting its application as aging indicator.

To further understand the nature of crosslinking, density measurements were carried out. Crossplots with $\epsilon'$ at 0.1 Hz and $\epsilon''$ at 100 kHz are shown in Fig.4.13. Also in this case, these results show a good correlation, with an almost linear relationship. It should be observed that $\epsilon$" at 100 kHz is still more sensitive to density variation than $\epsilon$' at 0.1 Hz. The increase in density is likely caused by the introduction of oxygen to the polymer chain, i.e. oxidation. Furthermore, loss of volatile parts, can be also the cause of the increasing density. Further investigation is required to understand the actual degradation process.

However, the degradation of this EPR-based insulation can be reasonably well monitored through dielectric spectroscopy, at least in aging conditions similar to those used for this work, using the imaginary part of permittivity at 100 kHz [97].

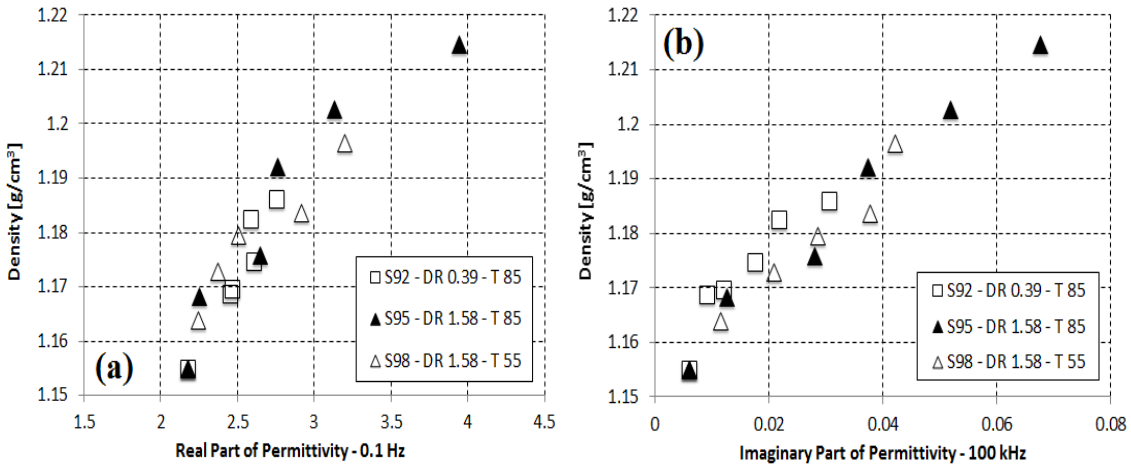


Figure 4.13. EPR - Crossplots of density with (a) $\epsilon$' at 0.1 Hz and (b) $\epsilon$" at 100 kHz.

## 4.3 Ethylene-Vinyl Acetate

The cable presented two EVA insulations with a high filler content (only the 42% wt of the insulation is actually a polymer) within an inner sheath of EVA/PE. This is shielded by a copper wire braid and covered by an outer sheath of EVA/PE. The aging conditions for this cable are given in Table 4.3.

Table 4.3. Accelerated aging experiments for EVA insulation.

| **Exp. No.** | **Temperature** [°C] | **Dose Rate** [kGy/h] |
|---|---|---|
| 2 | 85 | 0.42 |
| 5 | 85 | 1.50 |
| 6 | 85 | 0.94 |
| 8 | 55 | 1.50 |
| 9 | 55 | 0.94 |

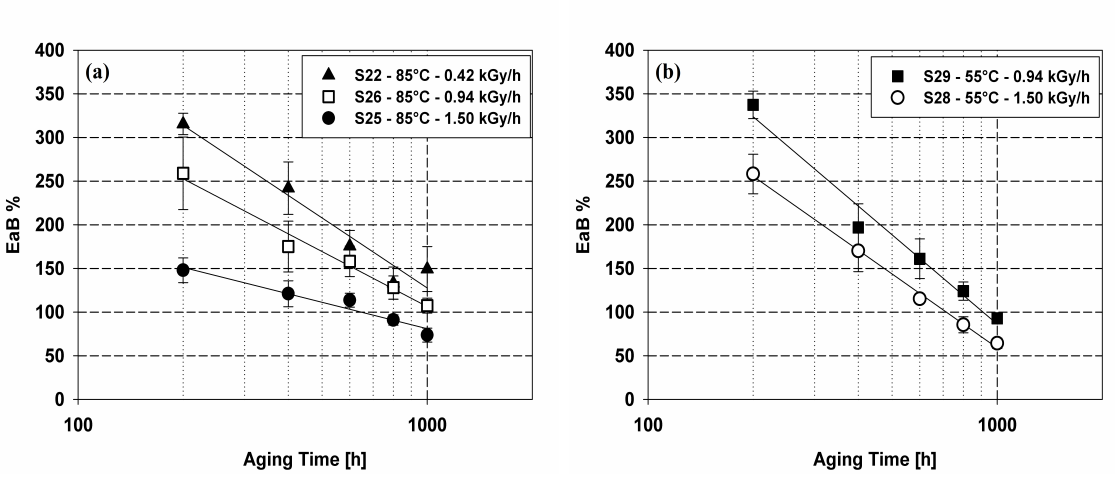


Figure 4.14. Elongation at break vs. aging time for EVA-based samples aged at (a) 85°C and (b) 55°C. Experimental data fitting is performed using a logarithmic function.

The aging of EVA-based samples clearly affected several insulation properties, and the aging was effective in that it reduced the elongation at break to around 50% for the most aged samples, i.e. those aged at 1.50 kGy/h. For samples which do not reach the end-point within 1000 hours, the trend is anyway well-defined and the extrapolation feasible. In order to estimate the life under different thermal-radiation

stresses, an experimental data fitting is performed. A logarithmic function was used, which corresponds to a linear regression in log-lin scale:

$$EaB = b_0 + b_1 log_{10} t \tag{4.3}$$

The insulation life based on the elongation at break is dose rate-independent in the range of dose rates investigated. Cables irradiated at 55°C present a steeper slope, which reduces their life and DED. The faster degradation of samples aged at lower temperature is found in literature as "inverse temperature" effect [31, 98, 99, 100] for semi-crystalline materials aged in the range of temperature where the crystalline phase melts. The DED remarkably increases with the dose rate, at least in the range here investigated, indicating the presence of physical or chemical dose rate effects. It should be noted that the steep decrease of EaB can be associated with both crosslinking and chain scission occurring during aging.

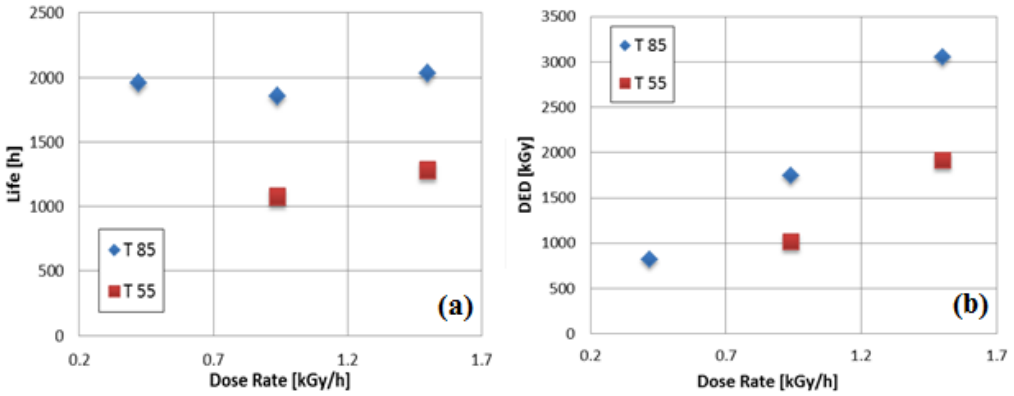


Figure 4.15. (a) Life and (b) DED vs. Dose Rate for EVA-based samples aged at 85°C and 55°C.

Fig.4.16 summarizes the results of OITp measurements performed on the unaged sample as well as on specimens aged at 55°C and 85°C. The thermogram revealed two broad endothermic peaks attributed to two types of crystallites of various size and lattice defects. It is reported in literature that EVA transition temperatures are usually located in two ranges; a lower transition temperature is located at $40-60$°C and a higher one in the range of $80-90$°C [101]. Generally, it is assumed that larger crystals with better-defined structure show higher melting temperatures; in fig.4.16 the transition at the highest temperature is indicated with $T_m$, and corresponds to 89°C for the unaged material. The low temperature transition is situated around 75°C, meaning that small crystallites characterized by low melting points are not present.

For the insulation aged at 55°C with dose rates of 0.94 and 1.50 kGy/h, the value of $T_m$ do not change with aging. The enthalpy of fusion determined from the

transitions (extended from 55°C to 100°C) increases from 22.3 J/g to about 28.2 J/g for the most severely damaged samples. When the transition peak shifts to higher temperatures, the effect is usually attributed to the increase in structural regularity and to the enhanced crystal thickness. For samples aged at 55°C, the variations of $T_m$ are situated in the narrow range of $89.5 - 91.3$°C. Furthermore, the intensity of the peak increases, contrary to the low-temperature one which almost disappears. It seems that the crystallites change structure and their population grows as might be concluded from the increase in the enthalpy of fusion ($\approx 30\%$). The last effect might be attributed to the radiation induced scission of tie macromolecules resulting in the growth of crystalline size and eventually in the increase of ordered phase contribution [102].

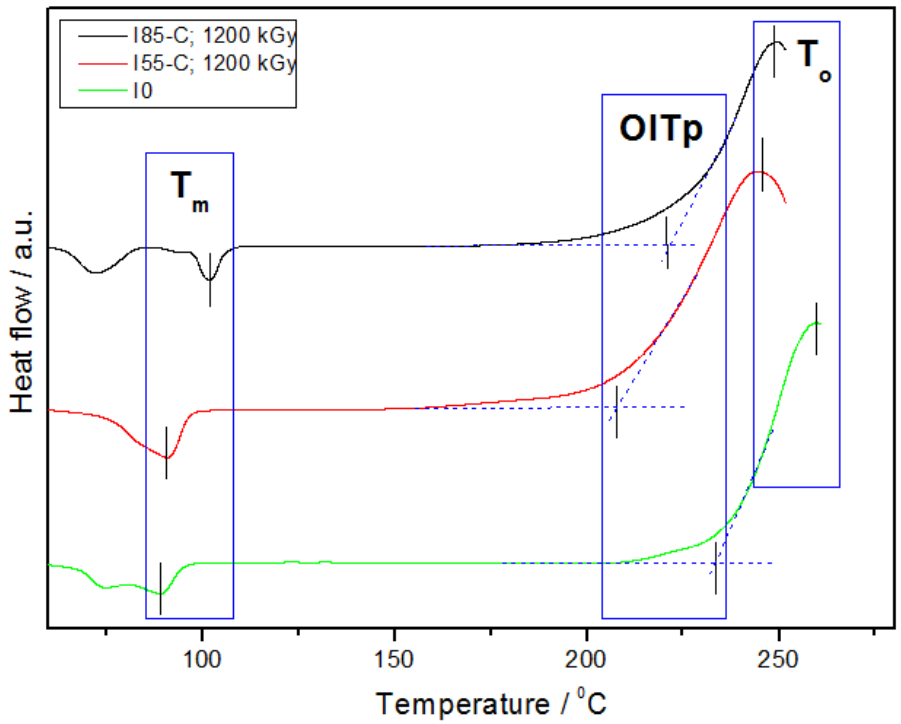


Figure 4.16. Examples of DSC-OITp thermograms obtained from EVA-based insulation before and after accelerated aging.

The thermograms substantially change when aging is performed at 85°C, i.e. at temperature corresponding to the melting state of a significant part of the crystalline phase. The endothermic high-temperature transitions are shifted towards higher temperatures, as $T_m$ becomes approximately 8°C higher. At 85°C, when thermal equilibrium is reached, all crystallites with melting points smaller than the annealing temperature are melted; afterwards, when cooling, they form new crystallites of melting point higher or lower than the annealing temperature[47]. Additionally,

under such conditions, the original crystals having melting temperature higher than 85°C continuously improve their structure in the reorganization process[103]. The phenomenon corresponds to the temperature dependent isothermal crystallization. In such circumstances, enthalpy of fusion should increase due to favorable environment for the formation of well defined, larger crystals. Nevertheless, simultaneously gamma-radiation induces scission of the polymer macromolecules, and for this reason, the resultant degree of crystallinity does not increase and a low temperature peak at 68°C is observed. Probably, the crystallites melted at 85°C, when exposed to ionizing radiation, are prone to crosslink due to intense conformational movements at this temperature. The effect was confirmed earlier for some other polymers, e.g. polytetrafuoroethylene [104].

Changes in OITp determined by accelerated aging are presented in Fig.4.17. The significant reduction of the values with increasing dose was confirmed for aging conducted both at 55°C and at 85°C; the OITp decreases by $\approx 30$°C in the first case and by $\approx 20$°C in the second one. Results suggest that the nature of the processes for dose rates situated in the range of $0.42 - 1.50$ kGy/h is generally the same.

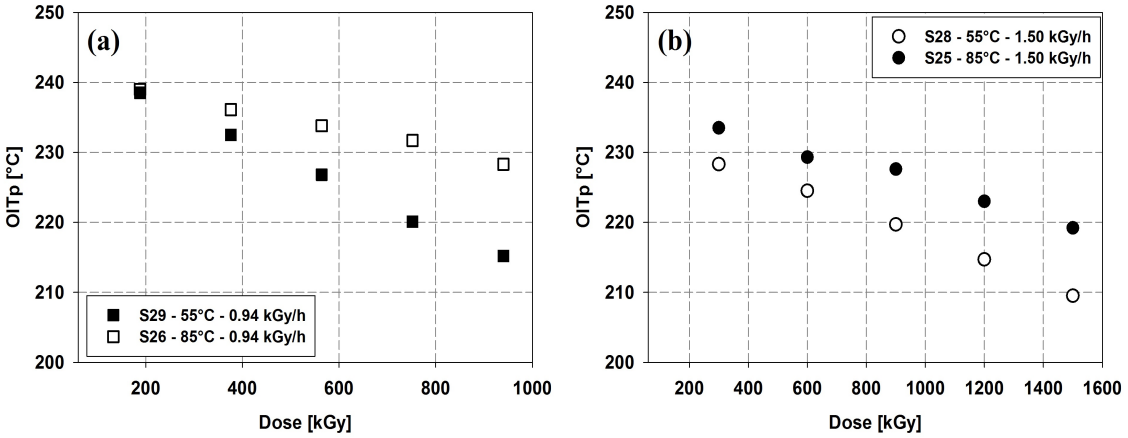


Figure 4.17. OITp vs. absorbed dose for EVA-based samples aged at (a) 0.94 kGy/h and (b) 1.50 kGy/h. Note that samples aged at lower temperature exhibit larger property variations.

Interestingly, as it is shown in Fig.4.17, the gradual reduction of OITp is strongly temperature dependent. For both dose rates, 0.94 and 1.50 kGy/h, the aging effect on OITp is much severe at 55°C than 85°C, confirming that radiation effects in the molten state are different than in crystallites, and that this difference results in abnormal behavior of the accelerated aged insulation. Crosslinking not only increases thermal stability, but also hinders diffusion of oxygen necessary for oxidative degradation. The inverse effect seems to be deeper for lower dose rate, i.e. at 0.94 Gy/h.

It seems that the generation of intermolecular bonds by ionizing radiation in the melted crystals results in hindering exothermic oxidative processes identified above 200°C on the thermograms.

As previously shown, the imaginary part of permittivity in the high frequency range is more sensitive to aging; its increment is associated with polar groups induced by radio-oxidation [74, 105]. The imaginary part of permittivity is therefore preferred for the crossplots rather than the real part, whose variation does not exceed 10%. This property provides a further confirmation of the results obtained by OITp and EaB measurements. Indeed, the effect of the dose rate is almost negligible in the range of doses investigated, while the "inverse temperature" effect is evidenced comparing samples aged at 0.94 kGy/h (Fig.4.18a) and 1.50 kGy/h (Fig.4.18b).

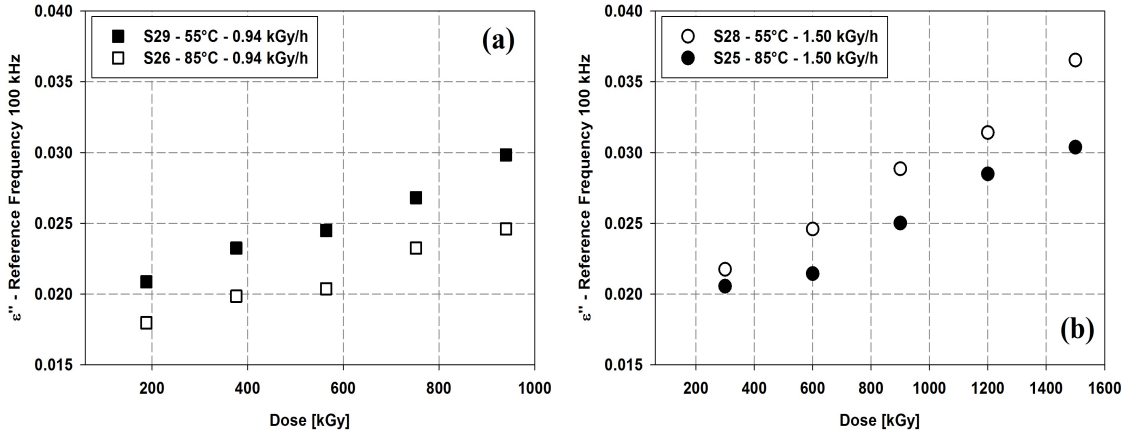


Figure 4.18. Imaginary part of permittivity at 100 kHz vs. absorbed dose for EVA-based samples aged at (a) 0.94 kGy/h and (b) 1.50 kGy/h. Note that samples aged at lower temperature exhibit larger property variations.

OITp, EaB and $\epsilon''$ at high frequency revealed the same phenomenon, i.e. the so-called "inverse temperature effect". In order to understand the correlation between these properties, crossplots of $\epsilon''$ (100 kHz, 1 MHz) and EaB are depicted in Fig.4.19. The best correlation is shown by $\epsilon''$ at 1 MHz; on the one hand, especially for samples aged at 0.42 kGy/h, the EaB shows a remarkable drop accompanied by moderate changes in $\epsilon''$, which limits the initial effectiveness of the selected quantity as aging indicator. On the other hand, the imaginary part of permittivity becomes more sensitive and better-correlated to EaB when the latter falls below 100% absolute, that can be advantageous for its application as CM method.

Crossplots of $\epsilon''$ (100 kHz, 1 MHz) and OITp are depicted in Fig.4.20. In this case, the best correlation is shown by $\epsilon''$ at 100 kHz. The linear trend of the correlation indicates that the investigated electrical property is sensitive also to small changes

in OITp. Observing the data reported in Fig.4.20a, the OITp associated with a precise value of $\epsilon''$ at 100 kHz can vary within a range of $\approx 5°C$, corresponding to the 15% of the total OITp decrease ($\approx 30°C$).

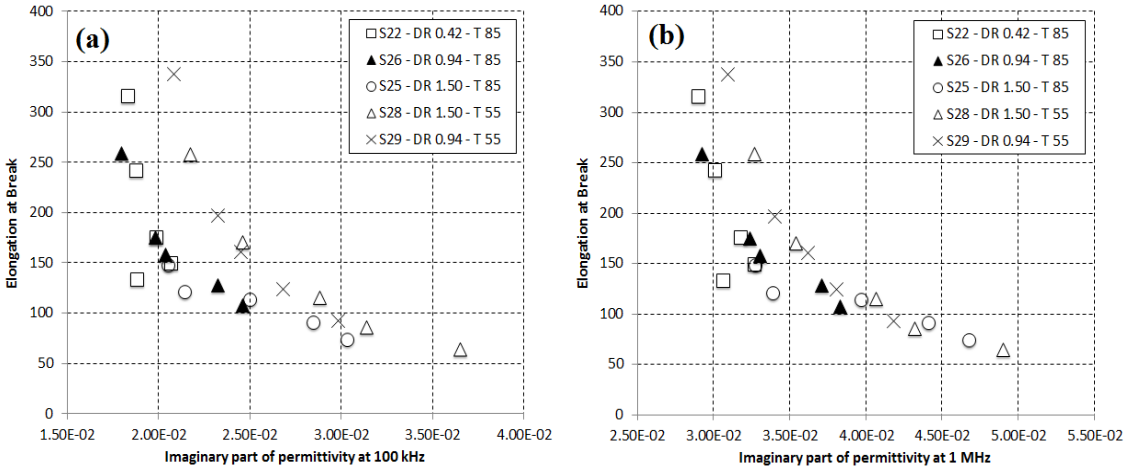


Figure 4.19. EVA - Crossplots of EaB and $\epsilon$" at (a) 100 kHz and (b) 1 MHz.

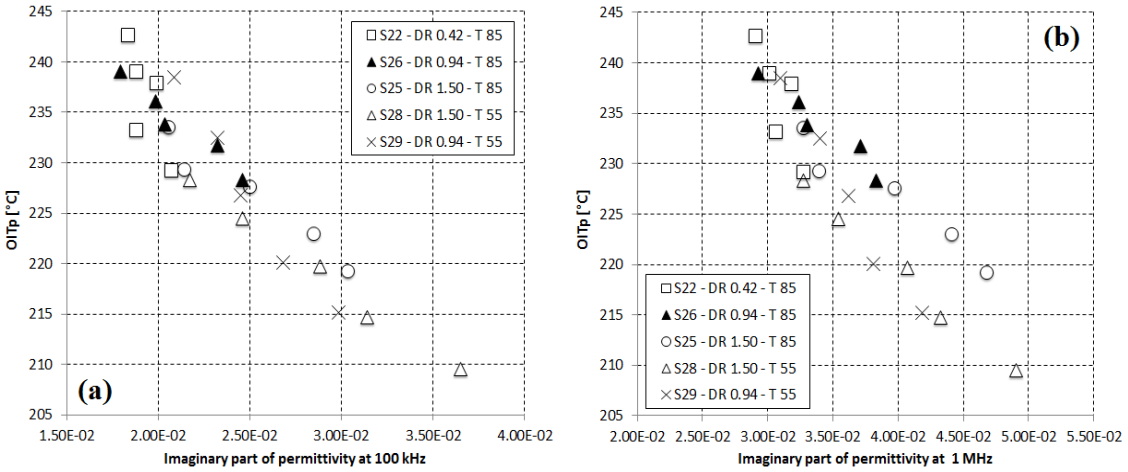


Figure 4.20. EVA - Crossplots of OITp and $\epsilon$" at (a) 100 kHz and (b) 1 MHz.

Other measurements did not provide further information. The changes in density are small, because its value is predominantly determined by the fillers. The uncertainties in the measurements are of a comparable magnitude, so conclusions based on density measurements are difficult to draw. FTIR and TGA results did

not reveal significant changes with aging. In addition, the presence of carbon black and a significant fraction of fillers in the system are believed to hide the aging effects revealed by infrared spectroscopy.

The dielectric response of EVA-based insulations is strongly influenced by the vinyl-acetate content, which usually determines degree of cristallinity and melting temperatures [73, 101, 106]. Results obtained from OITp measurements revealed the effect of the aging temperature on crystallite melting temperatures and peak intensity. Melting temperatures are located at relatively low temperature, thus the analysis of the test temperature influence on the behavior of $\epsilon''$ at high frequency is required to evaluate the reliability of the aging marker. Fig. 4.21 shows the behavior of $\epsilon$" at 100 kHz for specimens aged at 85°C and 55°C, with irradiation dose rate of 0.94 kGy/h, at three different test temperatures, 25°C, 50°C, and 80°C. The increasing test temperature reduces the absolute value of $\epsilon''$; however, its increment with aging is conserved as the trends are almost parallel. Furthermore, this behavior is observed at both aging temperatures, also by $\epsilon''$ at 1 MHz. These considerations make the high-frequency $\epsilon$" a suitable aging indicator for condition monitoring.

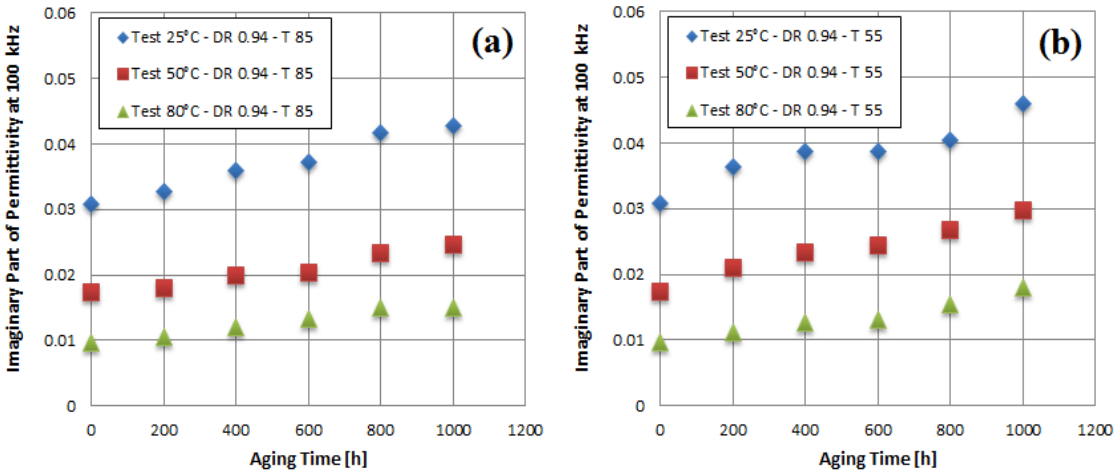


Figure 4.21. Influence of the test temperature on the values of $\epsilon$" at 100 kHz for specimens aged at (a) 85°C and (b) 55°C with irradiation dose rate of 0.94 kGy/h.

Some considerations can be made from the temperature behavior of $\epsilon$" at high-frequency. Ethylene-vinyl acetate copolymers exhibit intermediate properties between the two homopolymers, polyethylene and vinyl acetate (VA), depending on the proportion of both comonomers. These intermediate properties are consequences of the complex morphological architecture of these copolymers, which is in general composed of a crystalline phase (comprised of poly-methylenic units), an interfacial region (with both ethylenic and VA segments) and a complex amorphous phase (with

non-crystallized methylenic segments and VA units). EVA relaxation processes are very complex, the assignments in the literature are controversial and precise explanations for the relationship between the relaxation processes and the VA content are not well established. A complete study of phase transitions and relaxation processes of EVA copolymers is presented in [107]. Comparing the DSC thermograms presented in this paper with those of Fig. 4.16, the EVA-based insulation studied in this Ph.D. thesis presents likely a relatively low VA content, let say $\leq 20\%$. Since the dielectric spectroscopy performed at increasing test temperatures revealed a decrease of the high-frequency $\epsilon$", the experimental data are related to a polarization peak located at lower temperatures ($\leq 25°C$). This polarization peak is related to the $\alpha$ relaxation ($270 - 290$ K) involving preferentially the methylene interfacial units. It is thus associated with the motion of the chains in the interfacial region of the polymer matrix [107]. It is known that interfacial regions and tie molecules play a determinant role in the "inverse temperature" effect. Therefore, their relation with the high-frequency imaginary part of permittivity could explain how this electrical property is able to detect this particular degradation mechanism.

# Chapter 5

# Conclusions

Low-voltage electrical cables and their condition assessment are top research priorities for the nuclear industry. In the framework of the ADVANCE European project, a representative selection of safety-related cables was studied. This Ph. D. thesis focuses in particular on three different materials, i.e. XLPE, EPR-based and EVA-based insulations. Cable jackets were removed, and only the insulations were subjected to accelerated aging, under the simultaneous application of thermal and gamma-radiation stresses.

The impact of cable aging on the electrical parameters was monitored and characterized adapting and optimizing condition monitoring techniques developed mainly for HV and MV cables, i.e. dielectric spectroscopy, polarization-depolarization current measurements and space charge measurements. Insulation aging is defined as the irreversible process resulting in the variation of insulation structure (physical and/or chemical) and properties, compromising its function. A good condition indicator should present a monotone and remarkable trend with degradation. The aging marker should be sensitive to the effects of aging for the particular material at different stress levels and its variation must be irreversible.

Space charge measurements performed with PEA method did not reveal useful aging markers. Samples aged with low stress levels presented an almost negligible variation of the extracted quantities, e.g. the maximum stored charge density, and the interpretation of the results is often not easy. Similar considerations can be made for the trap-controlled mobility and trap depth distribution. Therefore, the application of space charge measurements to low-voltage NPP cables can give only a qualitative evaluation of material degradation, through the space charge density pattern. The main concerns consist in the low-voltage cable design: loose contacts, small thickness, dispersive materials (additives) blurs the results of HV tests like space charge measurements.

Polarization-depolarization current measurements provide other electrical quantities like conductivity and very-low-frequency dielectric response. Conductivity can

not be a suitable aging indicator. In general, after an initial variation, it usually fluctuates without a clear trend. The depolarization characteristics varies with aging only for XLPE and EPR-based insulations. The interfacial contribution to the real part of susceptibility and the dielectric losses of XLPE increases with aging, but their behavior is not clearly correlated with the applied stresses. EPR-based insulations presents a more remarkable increase of the very low frequency dielectric response. However, when these variations are correlated with elongation at break or density, the do not fit to the same curve. This means that the value of the electrical aging marker corresponding to the mechanical end-point (typically 50% absolute elongation) could change with the aging stress applied.

Dielectric spectroscopy is the most promising electrical condition monitoring technique among those investigated in this work. Between $10^{-2}$ Hz and $10^{6}$ Hz, both real ($\epsilon'$) and imaginary ($\epsilon''$) parts of permittivity of XLPE and EPR-based insulations increases over the whole frequency range. The variation of $\epsilon'$ is more evident at low frequency, while $\epsilon''$ increases remarkably also in the high frequency range. For EVA-based insulation, the aging strongly affects the dielectric losses only at high frequency, and the real part of permittivity presents almost negligible variations. From these observations it is possible to understand why electrical measurements at power frequency are commonly considered not useful for condition monitoring: dielectric spectroscopy revealed that at power frequency the variation of the cable electrical properties is very limited.

From the correlation of electrical quantities with mechanical properties and density, some important conclusions can be drawn. The real part of permittivity at 0.1 Hz and the imaginary part at 100 kHz are well-correlated with density. However, diffusion-limited oxidation (DLO) strongly affects the elongation at break: cable outer surface is more oxidized and cracks initiated and quickly propagated through the sample, whereas electrical measurements are averaged over the sample cross-section. This in turn means that comparing elongation to electrical properties for samples where DLO-effects are present can result in comparing the worst aged part to the average, which does not necessarily behave in the same way. The good correlation with density suggested that dielectric spectroscopy can give a good indication of the average level of oxidation in the sample. For a homogeneously aged sample, the oxidation can likely be correlated with the elongation at break, and dielectric spectroscopy is a viable option for the condition monitoring of this cable.

EPR-based insulation shows the best correlation between electrical aging markers, mechanical properties and density, especially considering $\epsilon''$ at 100 kHz which is related to oxidation. DLO is known to be lower on EPR-based materials, allowing the correlation of elongation with electrical aging markers. Also the real part of permittivity at 0.1 Hz could be used as aging indicator, even if data presented a larger scatter. Even if its variation is remarkable, the imaginary part of permittivity at 0.1 Hz does not correlate with elongation or density. Again, the best aging marker

is located at high frequency.

At high frequency, the imaginary part of EVA-based insulation correlates well with oxidation induction temperature, whereas the correlation with elongation became feasible only when this mechanical property value is already below 100% absolute. However, all properties reveal the same phenomenon, i.e. the so-called "inverse temperature effect", meaning that their variation was related to similar radio-oxidation degradation mechanisms.

Concluding, dielectric spectroscopy showed that the imaginary part of permittivity at high frequency could be used as aging indicator, at least for the materials investigated in this work, which are widely used as NPP low-voltage cable insulation. In the high frequency range, the increment of $\epsilon''$ is related to oxidation, i.e., the main degradation mechanism of cable insulations. However, it is necessary to prove the sensitivity of this aging marker at lower stresses, more similar to those found in NPP during operation. On the one hand, dielectric spectroscopy could be applied as non-destructive test on "pace" cables for ongoing qualification. On the other hand, its application as in-situ condition monitoring technique is limited to shielded cables, which presents a fixed ground reference.

# Bibliography


[1] Electrical Power Research Institute, "Low-voltage environmentally-qualified cable license renewal industry report," 1993.

[2] International Atomic Energy Agency, "Assessment and management of ageing of major nuclear power plant components important to safety: in-containment instrumentation and control cables," 2000.

[3] U. S. Nuclear Regulatory Commission, "Literature review of environmental qualification of safety-related electric cables," 1996.

[4] C. Kröhnke, *Polymer Science: A Comprehensive Reference.* Elsevier, 2012, vol. 8.14-Polymer Additives.

[5] International Atomic Energy Agency, "Pilot study on the management of ageing of instrumentation and control cables," 1995.

[6] Electrical Power Research Institute, "Integrated cable system aging management guidance - Low voltage cables," 2003.

[7] V. Plaček, T. Kohout, J. Kábrt, and J. Jiran, "The influence of mechanical stress on cable service life-time," *Polymer Testing*, vol. 30, pp. 709–715, 2011.

[8] International Atomic Energy Agency, "Management of life cycle and ageing at nuclear power plants - Improved I&C maintenance," 2004.

[9] Electrical Power Research Institute, "Initial acceptance criteria concepts and data for assessing longevity of low-voltage cable insulations and jackets," 2005.

[10] International Atomic Energy Agency, "Assessing and managing cable aging in nuclear power plants," 2012.

[11] Japan Nuclear Energy Safety Organization, "Final report of the project of assessment of cable aging for nuclear power plants," 2009.

[12] Electrical Power Research Institute, "Aging management guideline for commercial nuclear power plants - electrical cable and terminations," 1996.

[13] IEEE Std. 323-1974, "IEEE Standard for Qualifying Class 1E Equipment for Nuclear Power Generating Stations."

[14] IEEE Std. 323-1983, "IEEE Standard for Qualifying Class 1E Equipment for Nuclear Power Generating Stations."

[15] IEEE Std. 323-2003, "IEEE Standard for Qualifying Class 1E Equipment for Nuclear Power Generating Stations."

[16] IEEE Std. 383-1974, "IEEE Standard for Type Test of Class 1E Electric Cables, Field Splices, and Connections for Nuclear Power Generating Stations."

[17] IEEE Std. 383-2003, "IEEE Standard for Qualifying Class 1E Electric Cables and Field Splices for Nuclear Power Generating Stations."

[18] Electrical Power Research Institute, "Natural versus artificial aging of electrical components," 2000.

[19] K. T. Gillen and R. L. Clough, "Predictive aging results for cable materials in nuclear power plants," Sandia Laboratories, Tech. Rep., 1990.

[20] International Atomic Energy Agency, "Stability and stabilization of polymers under irradiation," 1997.

[21] H. Kudo, A. Shimada, A. Idesaki, T. Ohshima, K. Tamura, and T. Seguchi, "Degradation mechanisms of cable insulation materials during radiation-thermal ageing in radiation environment," in *Proceedings of the International Symposium on the Ageing Management and Maintenance of Nuclear Power Plants*, 2010, pp. 84–91.

[22] T. Seguchi, K. Tamura, T. Ohshima, A. Shimada, and H. Kudo, "Degradation mechanisms of cable insulation materials during radiation and thermal ageing in radiation environment," *Radiation Physics and Chemistry*, vol. 80, pp. 268–273, 2011.

[23] J. Wise, K. T. Gillen, and R. L. Clough, "Time development of diffusion-limited oxidation profiles in a radiation environment," *Radiation Physics and Chemistry*, vol. 49, no. 5, pp. 565–573, 1997.

[24] K. T. Gillen, R. L. Clough, and N. J. Dhooge, "Density profiling of polymers," *Polymer*, vol. 27, pp. 225–232, 1986.

[25] K. T. Gillen, M. Celina, and R. L. Clough, "Density measurements as a condition monitoring approach for following the aging of nuclear power plant cable materials," *Radiation Physics and Chemistry*, vol. 56, pp. 429–447, 1999.

[26] D. Corbin, "Etude de l'oxydation et de la tenue d'élastomères irradiés: conséquences sur l'intégrité des câbles électriques lors d'une situation accidentelle d'un réacteur à eau pressurisée," Ph.D. dissertation, Université de Caen, 2001.

[27] A. B. Reynolds, R. M. Bell, N. M. N. Bryson, T. E. Doyle, M. B. Hall, L. R. Mason, L. Quintric, and P. L. Terwilliger, "Dose rate effects on the radiation-induced oxidation of electric cables used in nuclear power plants," *Radiation Physics and Chemistry*, vol. 45, no. 1, pp. 103–110, 1995.

[28] V. Plaček, B. Bartoníček, V. Hnát, and B. Otáhal, "Dose rate effects in radiation degradation of polymer-based cable materials," *Nuclear Instruments and Methods in Physics Research B*, vol. 208, pp. 448–453, 2003.

[29] V. Plaček, "Assessment of parameters for simulation of thermal ageing of materials in nuclear power plants using DSC," *Journal of Thermal Analysis and Calorimetry*, vol. 80, pp. 525–528, 2005.

[30] International Electrotechnical Commission, "IEC 61244 - determination of long term radiation ageing in polymers. Part 2 - Procedures for predicting ageing at low dose rates," 1993.
[31] Sandia Laboratories, "Nuclear energy plant optimization (NEPO) - final report on aging and condition monitoring of low-voltage cable materials," 2005.
[32] Brookhaven National Laboratory, "Condition monitoring of cables," 2009.
[33] Electrical Power Research Institute, "Cable polymer aging and condition monitoring research at Sandia National Laboratories under the nuclear energy plant optimization (NEPO) program," 2005.
[34] IEC/IEEE 62582-3, "Nuclear power plants - Instrumentation and control important to safety - Electrical equipment condition monitoring methods. Part 3 - Elongation at break," 2012.
[35] IEC 60544-2, "Electrical insulating materials - Determination of the effects of ionizing radiation on insulating materials - Part 2 - Procedures for irradiation and test," 2012.
[36] ISO 527, "Plastics - determination of tensile properties."
[37] M. J. Jacobus and G. F. Fuerher, "Mechanical properties of cables exposed to simultaneous thermal and radiation aging," Sandia Laboratories, Tech. Rep., 1990.
[38] I. M. Ward and D. W. Hadley, *An Introduction to the Mechanical Properties of Solid Polymers.* Wiley, 1993.
[39] V. Shah, *Handbook of plastics testing and failure analysis.* Wiley, 2007.
[40] IEC/IEEE 62582-4, "Nuclear power plants - Instrumentation and control systems important to safety - Electrical equipment condition monitoring methods - Part 4 - Oxidation induction techniques," 2012.
[41] ISO 11357-1, "Plastics - Differential scanning calorimetry (DSC) - Part 1 - General principles."
[42] ISO 11357-6, "Plastics - Differential scanning calorimetry (DSC) - Part 6 - Determination of oxidation induction time (isothermal OIT) and oxidation induction temperature (dynamic OIT)."
[43] B. Bartoníček, V. Hnát, and V. Plaček, "Ageing monitoring of plastics used in nuclear power plants by DSC," *Journal of Thermal Analysis and Calorimetry*, vol. 64, pp. 571–576, 2001.
[44] Electrical Power Research Institute, "Reduction of oxidation induction time testing to practice as a life assessment technique for cable insulation," EPRI, Tech. Rep., 1996.
[45] B. Bartoníček, V. Hnát, and V. Plaček, "Life-assessment technique for nuclear power plant cables," *Radiation Physics and Chemistry*, vol. 52, pp. 639–642, 1998.
[46] K. T. Gillen, R. Bernstein, R. L. Clough, and M. Celina, "Lifetime predictions for semi-crystalline cable insulation materials: I. Mechanical properties and

oxygen consumption measurements on EPR materials," *Polymer Degradation and Stability*, vol. 9, pp. 2146–2156, 2006.

[47] J. D. Menczel and R. B. Prime, *Thermal analysis of polymers - Fundamentals and Applications*. Wiley, 2009.

[48] ISO 7111, "Plastics - thermogravimetry of polymers - temperature scanning method."

[49] ASTM 3850, "Test method for rapid thermal degradation of solid electrical insulation materials by thermogravimetric method (TGA)."

[50] International Atomic Energy Agency, "Management of ageing of I&C equipment in nuclear power plants," 2000.

[51] M. Beneš, N. Milanov, G. Matuschek, A. Kettrup, V. Plaček, and V. Balek, "Thermal degradation of PVC cable insulation studies by simultaneous TG-FTIR and TC-EGA methods," *Journal of Thermal Analysis and Calorimetry*, vol. 78, pp. 621–630, 2004.

[52] M. Beneš, V. Plaček, G. Matuschek, N. Milanov, A. A. Kettrup, W. D. Emmerich, K. Györyovà, and V. Balek, "Lifetime simulation and thermal characterization of PVC cable insulation materials," *Journal of Thermal Analysis and Calorimetry*, vol. 82, pp. 761–768, 2005.

[53] J. V. Gulmine and L. Akcelrud, "FTIR characterization of aged XLPE," *Polymer Testing*, vol. 25, pp. 932–942, 2006.

[54] U.S. Nuclear Regulatory Commission, "Assessment of environmental qualification practices and condition monitoring techniques for low-voltage electric cables," 2001.

[55] P. D. Blackmore, D. Birtwhistle, G. A. Cash, and G. A. George, "Condition assessment of EPDM composite insulators using FTIR spectroscopy," *IEEE Transactions on Dielectrics and Electrical Insulation*, vol. 5, no. 1, pp. 132–141, 1998.

[56] E. L. Leguenza, P. C. N. Scarpa, and D. K. Das-Gupta, "Dielectric behavior of aged polyethylene under UV radiation," *IEEE Transactions on Dielectrics and Electrical Insulation*, vol. 9, no. 4, pp. 507–513, 2002.

[57] A. Buttafava, A. Tavares, M. Arimondi, A. Zaopo, S. Nesti, D. Dondi, M. Mariani, and A. Faucitano, "Dose rate effects on the radiation induced oxidation of polyethylene," *Nuclear Instruments and Methods in Physics Research B*, vol. 265, pp. 221–226, 2007.

[58] EU Project ADVANCE, "Description of Work," 2010.

[59] L. A. Dissado and J. C. Fothergill, *Electrical Degradation and Breakdown in Polymers*. Peter Peregrinus for IEE, 1992.

[60] G. C. Montanari, "Relation between space charge and polymeric insulation ageing: cause and effect," *IEE Proceedings on Science, Measurement and Technology*, vol. 150, no. 2, pp. 53–57, 2003.

[61] ——, "Dielectric material properties investigated through space charge measurements," *IEEE Transactions on Dielectrics and Electrical Insulation*, vol. 11, no. 1, pp. 56–64, 2004.

[62] J. M. Alison, "The pulsed electro-acoustic method for the measurement of the dynamic space charge profile within insulators," in *Space Charge in Solid Dielectrics*. The Dielectrics Society, 1998, pp. 93–121.

[63] G. Mazzanti, G. Montanari, and J. M. Alison, "A space-charge based method for the estimation of apparent mobility and trap depth as markers for insulation degradation. theoretical basis and experimental validation," *IEEE Transactions on Dielectrics and Electrical Insulation*, vol. 10, no. 2, pp. 187–197, 2003.

[64] G. Mazzanti, G. Montanari, F. Palmieri, and G. Alison, "Apparent trap-controlled mobility evaluation in insulating polymers through depolarisation characteristics derived by space charge measurements," *Journal of Applied Physics*, vol. 94, no. 9, pp. 5997–6004, 2003.

[65] G. Chen, A. E. Davies, and H. M. Banford, "Influence of radiation environments on space charge formation in gamma-irradiated LDPE," *IEEE Transactions on Dielectrics and Electrical Insulation*, vol. 6, no. 6, pp. 882–886, 1999.

[66] G. Mazzanti, G. C. Montanari, and F. Palmieri, "Quantities extracted from space-charge measurements as markers for insulation aging," *IEEE Transactions on Dielectrics and Electrical Insulation*, vol. 10, no. 2, pp. 198–203, 2003.

[67] A. K. Jonscher, *Dielectric relaxations in solids*. Chelsea Dielectric Press, 1983.

[68] R. J. Young, *Introduction to Polymers*. Chapman & Hall, 1981.

[69] D. K. Das-Gupta, "Polyethylene: structure, morphology, molecular motion and dielectric behavior," *Electrical Insulation Magazine*, vol. 10, no. 3, pp. 5–15, 1994.

[70] P. C. N. Scarpa, A. Svatik, and D. K. Das-Gupta, "Dielectric spectroscopy of polyethylene in the frequency range of $10^{-5}$ Hz to $10^{6}$ Hz," *Polymer Engineering and Science*, vol. 36, no. 8, pp. 1072–1080, 1996.

[71] G. C. Montanari and D. K. Das-Gupta, "Polarization and space charge behavior of unaged and electrically aged crosslinked polyethylene," *IEEE Transactions on Dielectrics and Electrical Insulation*, vol. 7, no. 4, pp. 474–479, 2000.

[72] D. K. Das-Gupta and P. C. N. Scarpa, "Polarization and dielectric behavior of AC-aged polyethylene," *IEEE Transactions on Dielectrics and Electrical Insulation*, vol. 3, no. 3, pp. 366–374, 1996.

[73] A. M. Henderson, "Ethylene-Vinyl Acetate (EVA) copolymers - A general review," *Electrical Insulation Magazine*, vol. 9, no. 1, pp. 30–38, 1993.

[74] Chung Lee, Ki-Yup Kim, and Boo-Hyung Ryu, "Radiation effects on electrical and mechanical properties of LDPE/EVA Blends," in *Conference Record of the 2006 IEEE International Symposium on Electrical Insulation*, 2006, pp. 261–264.

[75] S. Yamanaka, T. Fukuda, G. Sawa, M. Ieda, M. Ito, and W. Kawakami, "Degradation mechanisms of cable insulation materials during radiation and thermal ageing in radiation environment," *IEEE Transactions on Electrical Insulation*, vol. 27, no. 6, pp. 1073–1082, 1992.

[76] S. Yamanaka, T. Fukuda, G. Sawa, M. Ieda, M. Ito, and T. Seguchi, "Electrical conduction and dielectric properties of gamma-irradiated EPR," in *Proceedings of the 4th International Conference on Properties and Applications of Dielectric Materials*, vol. 1, 1994, pp. 83–86.

[77] S. Bernier, J. L. Parpal, E. David, D. Jean, and D. Lalancette, "Dielectric response of laboratory aged PE cables," in *Conference Record of the 2008 IEEE International Symposium on Electrical Insulation*, 2008, pp. 83–86.

[78] L. Boudou, J. Guastavino, N. Zouzou, and J. M. Vega, "Conductivity of polyethylene - role of antioxidant and crosslinking by-products," in *Proceedings of the 2001 IEEE 7th International Conference on Solid Dielectrics*, 2001, pp. 245–247.

[79] M. A. Dakka, A. Bulinski, and S. S. Bamji, "On-site diagnostics of medium-voltage underground cross-linked polyethylene cables," *Electrical Insulation Magazine*, vol. 27, no. 4, pp. 34–44, 2011.

[80] ——, "Correlation between DC polarization and failure characteristics of XLPE and EPR aged with AC voltage in a wet environment," *IEEE Transactions on Dielectrics and Electrical Insulation*, vol. 12, no. 4, pp. 700–708, 2005.

[81] European Standard EN 50393, "Test methods and requirements for accessories for use on distribution cables of rated voltage 0,6/1,0 (1,2) kv," 2006.

[82] W. L. McLaughlin, "ESR dosimetry," *Radiation Protection Dosimetry*, vol. 47, no. 1, pp. 255–262, 1993.

[83] O. Bocchi, "Analysis of the dielectric response for the assessment of low-voltage cable insulation used in nuclear power plants," Master's thesis, University of Bologna, 2011-2012.

[84] M. Bernabé, "Space charge and dielectric response measurements to assess insulation aging of low-voltage cables used in nuclear power plants," Master's thesis, University of Bologna, 2011-2012.

[85] P. Bizzarri, "Study of the impact of radiation-thermal ageing on the electrical parameters of low-voltage cables used in nuclear power plants," Master's thesis, University of Bologna, 2011-2012.

[86] A. Motori, F. Sandrolini, and G. C. Montanari, "A contribution to the study of aging of XLPE insulated cables," *IEEE Transactions on Power Delivery*,

vol. 6, no. 1, pp. 34–42, 1991.

[87] A. Motori, F. Sandrolini, G. C. Montanari, and M. Loggini, "Electrical properties for detection of thermal aging in XLPE cable models," *Proceedings of the 3rd International Conference on Properties and Applications of Dielectric Materials*, vol. 2, pp. 761–764, 1991.

[88] R. A. Fouracre, S. J. MacGregor, M. Judd, and H. M. Banford, "Condition monitoring of irradiated polymeric cables," *Radiation Physics and Chemistry*, vol. 54, no. 2, pp. 209–211, 1999.

[89] C. Kim, Z. Jin, P. Jiang, Z. Zhu, and G. Wang, "Investigation of dielectric behavior of thermally aged XLPE cable in the high-frequency range," *Polymer Testing*, vol. 25, no. 4, pp. 553–561, 2006.

[90] S. Nakamura, F. Murabayashi, K. Iida, G. Sawa, and M. Ieda, "Degradation of dielectric properties of polyethylene by combined $\gamma$-irradiation and thermal stresses," *IEEE Transactions on Electrical Insulation*, vol. 22, no. 6, pp. 715–720, 1987.

[91] D. Kostoski, E. Suljovrujić, J. Dojčilović, and L. Novakovic, "Effects of charge trapping in gamma irradiated and accelerated aged low-density polyethylene," in *Proceedings of the 2004 IEEE International Conference on Solid Dielectrics*, vol. 1, 2004, pp. 379–382.

[92] A. Motori, G. C. Montanari, and S. Gubanski, "Investigation of relaxation processes in thermally-aged XLPE cable models," in *Conference on Electrical Insulation and Dielectric Phenomena - Annual Report*, vol. 2, 1993, pp. 751–756.

[93] D. K. E. Suljovrujić and J. Dojčilović, "Charge trapping in gamma irradiated low-density polyethylene," *Polymer Degradation and Stability*, vol. 74, no. 1, pp. 167–170, 2001.

[94] P. Frübing, D. Blischke, R. Gerhard-Multhaupt, and M. S. Khalil, "Complete relaxation map of polyethylene: filler-induced chemical modifications as dielectric probes," *Journal of Physics D: Applied Physics*, vol. 34, no. 20, pp. 3051–3057, 2001.

[95] E. Suljovrujić, "Dielectric study of post-irradiation effects in gamma-irradiated polyethylenes," *Radiation Physics and Chemistry*, vol. 79, no. 7, pp. 751–757, 2010.

[96] ——, "Dielectric studies of molecular $\beta$-relaxation in low density polyethylene: the influence of drawing and ionizing radiation," *Polymer*, vol. 43, no. 22, pp. 5969–5978, 2002.

[97] Chung Lee and Kang-Bok Lee, "Radiation effects on dielectric properties of ethylene propylene rubber," *Journal of Industrial and Engineering Chemistry*, vol. 14, pp. 473–479, 2008.

[98] M. Celina, K. T. Gillen, and R. L. Clough, "Inverse temperature and annealing

phenomena during degradation of crosslinked polyolefins," *Polymer Degradation and Stability*, vol. 61, no. 2, pp. 231–244, 1998.

[99] M. Celina, K. T. Gillen, J. Wise, and R. L. Clough, "Anomalous aging phenomena in a crosslinked polyolefin cable insulation," *Radiation Physics and Chemistry*, vol. 48, no. 5, pp. 613–626, 1996.

[100] S. G. Burnay and J. Dawson, "Reverse temperature effect during radiation ageing of XLPE cable insulation," in *Proceedings of the International Conference on Ageing studies and life extension of materials*, 1999.

[101] X. M. Shi, J. Zhang, D. R. Li, and S. J. Chen, "Effect of damp-heat aging on the structures and properties of ethylene-vinyl acetate copolymers with different vinyl acetate contents," *Journal Applied Polymer Science*, vol. 112, no. 4, pp. 2358–2365, 2009.

[102] Z. D. Kostoski, "Radiation-induced crystallinity changes and melting behavior of drawn isotactic polypropylene," *Polymer Degradation Stability*, vol. 47, no. 3, pp. 353–356, 1995.

[103] W. Stark and M. Jaunich, "Investigation of ethylene/vinyl acetate copolymer (EVA) by thermal analysis DSC and DMA," *Polymer Testing*, vol. 30, no. 2, pp. 236–242, 2011.

[104] T. Seguchi, "New trend of radiation application to polymer modification - Irradiation in oxygen free atmosphere and at elevated temperature," *Radiation Physics and Chemistry*, vol. 57, no. 3-6, pp. 367–371, 2000.

[105] Chung Lee, Ki-Yup Kim, Boo-Hyung Ryu and Kee-Joe Lim, "Electrical and mechanical properties of $\gamma$-ray irradiated LDPE/EVA blends," in *8th International Conference on Properties and applications of Dielectric Materials*, 2006, pp. 447–450.

[106] L. Gao, S. Wu, D. Tui, and K. C. Kao, "The correlation between properties and structure of ethylene-vinyl-acetate (EVA) copolymers," in *Proceedings of the Twenty-First Symposium on Electrical Insulating Materials*, 1988, pp. 59–63.

[107] S. Yamaki, E. A. Prado, and T. D. Z. Atvars, "Phase transitions and relaxation processes in ethylene-vinyl acetate copolymers probed by fluorescence spectroscopy," *European Polymer Journal*, vol. 38, no. 9, pp. 1811–1826, 2002.